MEDICAL IMAGE PROCESSING: APPLICATIONS IN OPHTHALMOLOGY AND TOTAL HIP REPLACEMENT

by

Nesreen Ahmad Tofeeq Otoum

A doctoral thesis
submitted in partial fulfilment of the requirements
for the award of

Doctor of Philosophy

Department of Computer Science

Loughborough University

December 2012

Supervisors: Prof. Eran A. Edirisinghe
Prof. Alastair G. Gale

ABSTRACT

Medical imaging tools technologically supported by the recent advances in the areas of computer vision can provide systems that aid medical professionals to carry out their expert diagnostics and investigations more effectively and efficiently. Two medical application domains that can benefit by such tools are ophthalmology and Total Hip Replacement (THR). Although a literature review conducted within the research context of this thesis revealed a number of existing solutions these are either very much limited by their application scope, robustness or scope of the extensiveness of the functionality made available. Therefore this thesis focuses on initially investigating a number of requirements defined by leading experts in the respective specialisms and providing practical solutions, well supported by the theoretical advances of computer vision and pattern recognition.

This thesis provides three novel algorithms/systems for use within image analysis in the areas of Ophthalmology and THR. The first approach uses Contourlet Transform to analyse and quantify corneal neovascularization. Experimental results are provided to prove that the proposed approach provides improved robustness in the presence of noise, non-uniform illumination and reflections, common problems that exist in captured corneal images. The second approach uses a colour based segmentation approach to segment, measure and analyse corneal ulcers using the HVS colour space. Literature review conducted within the research context of this thesis revealed that there is no such system available for analysis and measurement of corneal ulcers. Finally the thesis provides a robust approach towards detecting and analysing possible dislocations and misalignments in THR X-ray images. The algorithm uses localised histogram equalisation to enhance the quality of X-ray images first prior to using Hough Transforms and filtered back projections to locate and recognise key points of the THR x-ray images. These key points are then used to measure the possible presence of dislocations and misalignments. The thesis further highlights possible extensions and improvements to the proposed algorithms and systems.

Nesreen Otoum, December 2012

To my beloved Parents
(Es'af Ogdeh & Ahmad Tofeeq Otoum)

ACKNOWLEDGEMENT

This thesis is the end of my journey in obtaining my Ph.D. It has been a great privilege to spend several years in the Department of Computer Science at Loughborough University. The best and worst moments of my doctoral journey have been shared with many people and I have worked with a great number of people whose contribution in assorted ways to the research and the making of the thesis deserved special mention. It is a pleasure to convey my gratitude to them all in my humble acknowledgment.

The chain of my appreciation begins with name of Almighty Allah (s.w.t), the Most Gracious, and the Most Merciful who has blessed me always in every situation, to get the courage and knowledge to accomplish my tasks.

My first debt of gratitude must go to my supervisor, Professor Eran A. Edirisinghe for taking me under his supervision. This work would not have been possible without his guidance, support and encouragement. And he has always been available to advise me. His wide knowledge and logical way of thinking have been of great value to me. His detailed and constructive comments, technical and editorial advice was essential to the completion of this thesis. Above all, and the most needed, I am very grateful for his patience, motivation, enthusiasm, and immense knowledge. I am indebted to him more than he knows.

I shall also like to express my deep and sincere gratitude to my second supervisor Professor Alastair G. Gale for his time, encouragement and suggestions. I would also like to add a special thanks to Professor Chris Hinde for his financial support, for his kindness, helpful advices and I owe him my heartfelt appreciation.

I shall also like to thank my DIRG colleagues, who shared their knowledge, provided useful feedback on my work, and for providing a friendly and helpful

atmosphere for my study. I shall like to thank to Dr. Dhammike Wickramanayake, Dr. Iffat Zafar, Dr. Fatima Abri, Dr.Usman Zakir, Dr. Muhammad Athar Ali, Mr. Andrew Leonce , Mr. Niraj Doshi Mr. M. Akramshah Ismail, Ms. Sara Saravi, Ms. Giounona Tzanidou. I would also like to thank Ms. Christine Bagley for her invaluable support and encouragement. I am also thankful to the technical and clerical staff members of the Department of Computer Science, Loughborough University.

Special thanks to my best friend, Anoud Bani-Hani for making this journey enjoyable and memorable. Her friendship, support and assistance through the good and bad times have meant more to me than I could ever express.

Where would I be without my family? My parents deserve special mention for their unconditional, inseparable support, prayers and endless love. Their love was my driving force. I owe them everything and wish I could show them just how much I love and appreciate them. My Father Ahmad Tofeeq Otoum, in the first place is the person who has always been supportive of me I will always be indebted to him for the kindness and care he has shown me since my birth and his endless support in every aspect of my life. For this, there is no replacement. My Mother, Esa'f Ogdeh is the one who sincerely raised me with her caring and gentle love and prayed day and night for my success. Her blessing has been with me at every step, words can't describe her place in my life. My special gratitude to my beloved brothers: Abdullah, Yousef, Mohammad, Yahia, and Anas. To my beloved sisters: Reem and Fatima, to my brother and sisters in law, my nieces and nephews. Thank you all for being supportive, loving and caring during my entire life. I would not have made it this far without your support and encouragement.

Nesreen Otoum   *18th December 2012*

TABLE OF CONTENTS

LIST OF FIGURES AND TABLES

FIGURES

ABBREVIATIONS AND NOTATIONS

ABBREVIATIONS

ROI	Region Of Interest
THR	Total Hip Replacement
DWT	Discrete Wavelet Transforms
RGB	Red, Green, Blue
HSV	Hue, Saturation, Value
DCE	Differential Contrast Enhancement
NIH	National Institutes of Health
2D	2 Dimensional
ROC	Receiver Operating Characteristics
FCM	Fuzzy C-Means
3D	3 Dimensional
CT	Computed Tomography
ASM	Active Shape Model
LP	Laplacian Pyramid
DFB	Directional Filter Bank
POI	Pixels Of Interest
LHE	Local Histogram Equalization
SPECT	Single Photon Emission Computed Tomography
PET	Positron Emission Tomography

NOTATIONS

y_α	Non-linearity function
m	Determines the degree of nonlinearity
s	Introduces dynamic range Compression
a	Normalization parameter

K_m	Normalization parameter
M_a	Maximum Contourlet coefficient
L_1 , L_2	Templates
M	Noise estimation operator
σ_n	Standard deviation
f	Image
W and H	Represent the width and height of image f
p	Pixel
$x_1, x_2, \ldots x_8$	Pixels
$min(R, G, B)$	Minimum value of red, green, blue
$max(R, G, B)$	Maximum value of red, green, blue
$F_A(D_A)$	Cumulative probability of the original image
N	Number of image pixels
n_k	The number of pixels at intensity level k or less.
a	Represents the slope
b	Represents the intercept parameter

CHAPTER 1

An Overview

1.1 Introduction

The need for medical imaging systems that aid medical experts to make decisions has substantially increased in recent years. This is partly due to the growth in population, advances in image capture and display systems and thus the need for the medical experts to be efficient in performing image analysis tasks. This has resulted in the development of a large number of computer vision and pattern analysis based imaging systems that have been proposed and implemented supporting either automatic and/or semi-automatic operation of advanced functionality.

Due to the need for taking quick and accurate decisions in the diagnosis and treatment of some of the life threatening diseases and medical conditions medical professionals welcome any help that the latest imaging technology can provide. To this effect, medical imaging systems capable of diagnosis and analysis of various medical conditions are already being used in hospitals, clinics and other health care practices. Of particular interest to the research context of this thesis is medical imaging systems that are based on segmenting a given region of interest (ROI) and performing further image analysis aimed at more detailed diagnosis.

The cornea of an eye is a thin, transparent membrane that covers the iris and the pupil of the eye. Any injuries that occur on the surface of the cornea can subsequently be infected with bacteria, virus or fungi that will lead to the formation of a Corneal Ulcer, which is an increasingly common reason for visual impairment and blindness in patients. Further a normal cornea is devoid of both blood and lymphatic vessels. This vascularity is highly conserved evolutionarily to maintain transparency and visual acuity. Nonetheless, due to a variety of severe inflammatory diseases, the cornea can become invaded by pathologic blood and lymphatic vessels. Pathologic corneal neovascularization not only reduces the quality of being able to see objects through the cornea (also called corneal transparency) but also is a

major risk factor for corneal transplantation. In addition, host corneal neovascularization (both before as well as after surgery) is one of the most significant risk factors for subsequent immune rejections after replacing the damaged cornea with a clear cornea (corneal grafting). Thus timely and effective treatment of corneal neovascularization and corneal ulcers is important. However, unfortunately, the manual inspection and quantification of the above conditions by inspecting images taken with a basic camera, becomes an extremely tedious, time consuming task, prone to human error. Thus the medical experts involved in the area of Ophthalmology can be supported by automatic/semi-automatic imaging systems that can be used to aid their decision making process.

In Orthopaedics, the most common causes of Total Hip Replacement (THR) failure are due to prosthesis debris, which can include: stainless steel, bone, cement, polyethylene and other implant components and particles. Further any of the implanted components could move or dislocate from their original positions. The key technical issue is to accurately determine the various measurements concerning the implant, polyethylene, joint cement and joint bone structures from radiographic hip images and to monitor them to be maintained within acceptable tolerances.

Thus the development of computer vision systems which will automatically/semi-automatically and validly assess radiographs of patients who have had THR, as part of their postoperative monitoring, with the purpose of providing early identification of potential implant failure, can save medical experts time to take appropriate corrective actions in time to save patients from having to go through painful experiences. In this thesis our focus is the computer vision based identification of dislocation and misalignment in THR x-ray images.

1.2 Research Motivation

The motivation for research covering the context of the investigations carried out by the research presented in this thesis was a direct result of request and feedback received from medical experts in the areas of Ophthalmology and Total Hip

Replacement attached to the University Hospitals of Nottingham (Queen's Medical Centre) and Leicester (The Leicester Royal Infirmary). These medical experts who are world leaders in the treatment of patients suffering from eye ulcers, corneal neovascularization and complications that have resulted after total hip replacement provided the practical cases and the lack of any existing aid to help analyse and quantify the above complications. This shortage of technology provided the basic research motivation to seek solutions that utilise computer vision and pattern recognition based algorithms to develop total, end-to-end solutions to the identified practical problems.

The above motivations to conduct research to close gaps in the three identified practical application domains initiated a comprehensive literature review to seek the state-of-art in existing solutions. These investigations revealed that the following:

1. Although solutions have been proposed to quantify corneal neovascularization, the most effective solution based on the use of Discrete Wavelet Transforms (DWT) to analyse the corneal images, suffered from the DWT's inability to approximate lines in multiple-directions. The initial investigations revealed the ability of Contourlet Transforms to resolve this problem and hence provide a more robust solution.

2. Although in literature, research has been conducted and widely published in the area of segmenting and analysing general purpose skin ulcers, no work has been conducted in the specific segmentation and analysis of eye ulcers. Nevertheless a practical need exists to provide an automatic analysis approach to replace the inefficient and ineffective manual inspection and measurement approaches at present adopted by medical professionals. However our initial investigations revealed that the treatment of eye ulcers for subsequent image capture and manual inspection requires any automatic or semi-automatic alternative approaches to follow very specific colour based segmentation approaches and subsequent automated measurement or quantification.

3. Our literature review since the identification of the practical medical need via the consultations carried out with the medical experts revealed that the

computer vision based analysis of Total Hip Replacement x-ray images are mainly limited to the analysis of complications other than dislocations and misalignments. Only one paper focused on providing a solution to the above problem areas. That two was limited in its application and solution scope [see Chapter-5]. A need for a simple, robust but accurate computer vision based tool was thus identified.

The above research motivations led to the following aim and objectives.

1.3 Aim and Objectives

Aim: To design and develop robust, efficient computer vision based algorithms for monitoring the treatment process of corneal ulcers, the quantification the corneal neovascularization and detecting and identifying the dislocation and misalignment in THR X-ray images, giving rise to imaging systems that will be able to enhance the fool proof nature and the accuracy of manual medical diagnosis.

The specific objectives of this research are listed below:
- To identify and investigate the possible research gaps and development needs of existing medical imaging devices used in ophthalmology and orthopaedics.
- To investigate the current-state-of-art in segmenting the corneal area either based on fully automatic or semi-automatics approaches.
- To compare and investigate the effectiveness of using different colour spaces (e.g., RGB, HSV) in segmenting corneal ulcers.
- To propose an approach for the quantification or a corneal ulcer area, that can be used as a tool to continuously monitor progress of any treatment process being followed.
- To propose a method to quantify corneal neovascularization based on mathematical transforms.

- To propose a robust localised histogram equalisation based enhancement technique to enhance THR X-ray images that normally appear noisy and low in contrast.

- To select the mark points of interest in THR X-ray images that can be subsequently used for assessing and quantifying the Dislocation and Misalignment of components.

- To identify the limitations of the proposed algorithms and outline the future directions of research.

1.4 Contributions of Research

The original contributions made by this thesis are briefly presented in this section and are further detailed in Chapters 3-5. The research findings of this thesis have been published as conference proceedings and journal papers. The full details of associated conference and journal proceedings can be found in Appendix [A].

1.4.1 Quantification of Corneal Neovascularization

In chapter 3, a novel approach to the quantification of corneal neovascularization is proposed using Contourlet Transforms [43] to enhance the blood vessels prior to their segmentation. A special feature of the approach is that it is robust to different levels of noise that is present in corneal images. Experimental results have been provided to analyse the proposed algorithm's robustness in the presence of noise, non-uniform illumination and reflections. In addition, the enhanced image is finally thresholded and undergoes thinning to produce the final binary image that is used to quantify a measure of blood vessels. For a database of corneal neovascularization images consisting of images with different levels of noise, contrast and other illumination artefacts, an accuracy of 91% was obtained with the proposed approach.

The above work was presented at two international conferences [79][80] and

subsequently resulted in the publication of an invited journal paper [81]. The conference paper won the Best Paper Award.

1.4.2 Application of Computer Vision Approaches to Evaluating the Effectiveness of Treatment of Corneal Ulcers.

In chapter 4, an efficient computer aided colour based segmentation approach to segmenting, detecting and quantification of corneal ulcers is presented. In the proposed approach the corneal images are first analysed in the HSV colour space. Initially the removal of potential reflections from the affected areas is carried out by making a logical comparison between the output results of the colour segmentation algorithm. Subsequently a semi-automated approach to extract the corneal area by initially registering an ellipse to the candidate corneal boundary detected via edge detection and allowing the user to modify the boundary to overlap with the boundary of the ulcer being observed is adopted. Although this step makes the approach semi-automatic, it removes the impact of breakages of the corneal boundary due to occlusion, noise, image quality degradations. Experimental results are provided to prove the use and the accuracy of this approach in monitoring the treatment process of corneal ulcers indicating a gradual reduction of size of the ulcer over a period of time. For this purpose real test data obtained from medical professionals have been used.

The above work resulted in the publication of a conference paper [82]. Subsequently this system was developed as a software supported hardware system and is at present being developed into an application that will shortly be clinically tested by medical experts at the Queens Medical Centre, Nottingham. If successful the idea is for the device to be made commercially available. At the time of publication of this thesis discussions are being held to support the commercial exploitation activities.

14.3 Total Hip Replacement

In chapter 5, a novel approach toward detecting dislocations and misalignments in total hip replacement X-ray images is presented. The algorithm initially applies localised histogram equalisation [62] to bring back detail in any over or under exposed areas of the original x-ray image. Hough transform and Filtered Back Projection have been using to determine and identify the mark points in the X-ray image. These mark points have been used to calculate and measure the cases of dislocation and misalignment in total hip replacement.

This work is currently being prepared as a paper for submission to the 9th International Conference on Computer Vision Systems (ICVS) 2013. An extended version of the paper will be subsequently submitted to the SPIE Medical Imaging, Journal.

1.5 Organization of Thesis

This thesis has been organized into six chapters as summarized below.

Chapter 1 provides an overview of the Ophthalmology and total hip replacement applications domain providing a summary of problems, research motivation and proposed solutions. The chapter also provides the research aims, objectives and original contributions of this thesis.

Chapter 2 provides existing and related literature on corneal neovascularization, analysis of corneal ulcers and total hip replacement (THR), identifying research gaps in these application domains where computer vision based approaches can provide useful solutions.

Chapters 3, 4, and *5* present the original contributions of this thesis, i.e., three computer vision based solutions for aiding the analysis and measurement processes in the application areas of Ophthalmology and total hip replacement. These chapters

include specifically the novel methodologies of the approaches adopted, experimental setup used, design details, results and analysis of experiments carried out and suggestions for further improvement.

Chapter 6 concludes the research presented in this thesis with an insight into the future directions and enhancements.

CHAPTER 2

Literature Review

2.1 Introduction

This chapter introduces existing literature in the three application domains in which research has been conducted and presented in this thesis, namely, processing of corneal images for quantification of neovascularization , the analysis of the healing process of ulcers and in analysing total hip replacement images for determining defects in dislocation and orientation. The literature review provided in the following sections provide a clear indication of the novelty of application areas focused within this thesis and provides inspiration and ideas for the research presented in the rest of this thesis.

For clarity of presentation the chapter is divided into several sections. Section 2.1 provides a detailed literature review of using computer vision approaches for the quantification of corneal neovascularization and the state-of-the-art in related research. Section 2.2 provides a review of literature on analysing corneal ulcers using computer vision approaches and the state-of-the-art in related research. Section 2.3 provides a number of state-of-the-art computer vision techniques used in analysing total hip replacement images. Finally section 2.4 summarises, drawing up conclusions that leads to the definition of research problems addressed in this thesis.

2.2 Quantification of corneal neovascularization

The existing literature on quantification of Corneal Neovascularization focuses entirely on the clinical analysis aspects of the medical condition. Some of these papers present clinical analysis processes that utilise basic image processing tools [1-8] such as noise removal, contrast adjustment, image thresholding, to provide

medical professionals with better quality and easy to analyse images. On the other hand some promising approaches have been developed for the enhancement of blood vessels in retinal imaging [9-13]. Details of a number of these key approaches are presented below.

P.Feng, Y.Pan, B.Wei, W.Jin, D.Mi [9]

In this paper Contourlet Transform is used to initially provide a local, flexible multi-resolution and directional image decomposition of a retinal image. It is shown that the directional nature of Contourlet Transforms allows for a more accurate representation of contours, allowing their subsequent processing/enhancement to be done more efficiently. The algorithm presented in this thesis for the segmentation and subsequent quantification of corneal neovascularization is inspired by this work.

C. Cursiefen, F. Bock, F. K. Horn, F. E. Kruse, B. Seitz, V. Borderie, B. Früh, M. A. Thiel, F. Wilhelm, B. Geudelin, I. Descohand, K. Steuhl, A. Hahn, D. Meller [14]

This paper focuses on developing a technique to detect corneal neovascularization in animal eyes. In this technique images taken with the use of a standard corneal slit-lamp are modified using appropriate filters for shading adjustment and to balance inhomogeneous illumination. Subsequently simple pixel thresholding is used detect only the blood vessels and make them available for further manual medical analysis.

F. Bock, J. Onderka, D. Hos, F. Horn, P. Martus, C. Cursiefen [15]

In this paper a method to quantitatively analyse the corneal area (of animals) covered by blood vessels (for animal use) is presented which is based on the detection of a grey value ranges present in the images. The original digital grey

value images go through four stages of filtering, first before detecting the blood vessels so as to avoid the detection of other objects and to enhance the disclosure of the vessels. These filters include, a DCE (Differential Contrast Enhancement) filter that increases the sharpness of the images, an Erosion filter which is used to remove punctual noise, a Gradient filter which is a combination of the Erosion filter, a Dilatation operation and an Arithmetic subtraction: to erase final interferences and to carry off the outer rim of the vessels. Finally by ignoring 3% of the brightest and 3% of the darkest pixels and spreading the intensity range of the remaining pixels linearly to the maximal possible range, an image with better contract is produced. Finally the vessels are detected using a threshold setting and the corneal area is outlined by using the innermost vessel of the limbal arcade as the border.

A. D. Proia, D. B. Chandler, W. L. Haynes [16]

In this paper a method for quantifying corneal neovascularization has been proposed and applied to corneal images obtained from rats. The area of the cornea and blood vessels are independently determined by analysing the digitised data as discrete values of varying shades of grey (grey-scale analysis). The area and grey scale of the injury and its distance from the corneoscleral limbus is measured to determine variability of location and intensity of the injury in different animals.

D. R. Anijeet, Y. Zheng, A. Tey, M. Hodson, H. Sueke, S. B. Kaye [17]

To quantify the corneal neovascularization in this paper the first step used is to measure the corneal diameter in pixels, manually, by identification of limbus of the cornea. A sub-image containing all corneal vessels is subsequently defined manually and this area is enhanced through the use of a Gaussian filter to remove noise, followed by the application of selective enhancement filters to the smoothed image to enhance all potential vessels as linear structures. Finally, based on a selected threshold value the enhanced image is converted to a binary image. The binary image is further cleansed by removing objects smaller than 10 pixels.

S. Amano, R. Rohan, M. Kuroki, M. Tolentino , A. P. Adamis [18]

In this paper a set of standardized illumination, contrast, and threshold settings were used to capture and analyse corneal images. The entire cornea is initially outlined manually, and a conversion factor is calculated based on the actual area of the cornea in square millimetres relative to it is displayed on the computer screen used for displaying the image for analysis. This conversion factor is used to calculate the true value of the area of neovascularization, which is measured by outlining an isosceles triangle with its apex at the centre of the cornea and its 3-mm base (actual size) tangential to the limbus. This way a line drawn from the apex orthogonally to the base would pass through the pellet. The area of the isosceles triangle is used to serve as a standardised area within which neovascularization is quantified. The area of neovascularization is then manually outlined and calculated.

M. P. Holzer, K. D. Solomon, D. T. Vroman, H. P. Sandoval, P. Margaron , T. J. Kasper, C. E. Crosson [19]

In this paper the NIH Image Tool [20], a public domain image processing and analysis tool, is used to help determine the area of corneal neovascularization. A number of slit-lamp images with a standardized magnification are initially captured after suture placement. Images are subsequently digitised, and the neovascularized area (in square millimetres) determined using standard NIH Image tool functions.

In the algorithms presented in [14-19] attempts have been made to segment blood vessels in corneal neovascularization based on very basic approaches grey level image segmentation. These trivial approaches have been introduced and used by medical specialists unaware of the recent trends in imaging processing and have been based on basic commercial software packages that are used for general purpose image enhancement applications. No attempts have been made to eliminate non-uniform illumination or noise and reflection/highlight removal. Further no attempt has been made to enhance images after segmentation to improve contrast of blood vessels prior to quantification. In our analysis of these approaches it was

observed that the above pre and post processing stages form vital elements of the imaging pipeline that will result in improved accuracy of final results. Hence the approaches proposed in this thesis address these issues.

2.3 Corneal Ulcers

Automatic computer vision based analysis of corneal images for evaluating the effectiveness of a treatment process being followed by medical professionals is a new application area where research can be conducted. Our literature review revealed that no prior research exists in using Computer Vision approaches for Corneal Ulcer area detection. The closest research relates to the detection of ulcers and wounds in human skin [21-27]. However this research is irrelevant to corneal ulcer area detection as the background (cornea area) and the foreground (ulcer area treated with a luminous liquid) are unique compared to detecting skin ulcers, in detecting corneal ulcers.

However the quantification of corneal ulcers requires the accurate identification of the corneal area, thus the corneal boundary, as this is used to calculate the ratio used for the quantification, i.e ulcer area to corneal area. Even though within the research context of this thesis the corneal area is determined following a semi-automatic process, vision based methods exist in the literature where corneal boundary is fully automatically detected. One such area is the research field of Iris Recognition. The following section discusses the state-of-art in iris recognition, as Chapter-6 suggests the inclusion of a fully automatic corneal area detection algorithm as a future possible improvement to the research proposed in this thesis.

2.3.1 Iris Recognition.

The Iris recognition has been used in a number of application areas recently, especially in areas related to biometric identification. The iris area segmentation is one of the most important steps in an iris recognition system. In this section we

present a number of key iris area segmentation approaches proposed in the literature,

A. E. Yahya and M. J. Nordin [28]

In this paper the authors proposed an iris segmentation method that employs Chan-Vese active contour method [29] to extract the iris from its surrounding structures. In this study the image of the eye is pre-processed by filling in the segmented reflections based on image inpainting technique [30] [31]. Then an AdaBoost-Cascade Detector [32] [33] is adopted to detect the iris region in the eye image and to determine and confirm that the eye is not closed. After the abovementioned stages the authors have used the Chan-Vese active contour method to find the inner and outer boundaries of iris.

G. Annapoorani, R. Krishnamoorthi, P. G. Jeya, S. Petchiammal [34]

In this paper the proposed approach comprises of specular reflection removal, pupil localization, iris localization and eyelid localization. For the part of iris localization or segmentation, a gradient based heuristic approach is devised to detect the iris boundary within the image of the eye. After the pupil area has been segmented, starting from the pupil centre two regions are identified to look for jumps in grey scale level and based on the heuristic that there will only be two important gradients in the region (i.e. at pupil – iris, iris – sclera boundaries). The pixels belonging to the pupil area are the darkest, the pixels belonging to the iris area are of intermediate in greyscale colour and the pixels belonging to the sclera area will be the lightest. Following the above analysis the second gradient is identified and is considered to be the estimated boundary of the iris.

A. Zaim [35]

A fast, automatic and effective real-time algorithm for localizing and segmenting the iris and pupil boundaries of the eye from camera images is presented in this

paper. Circular region growing is first used to localize the eye's centroid. Then several geometrical features of the shape of the eye are utilised to constraint a model built in the polar image space. The model employs knowledge of anatomical attributes as well as gradient information to extract the iris boundaries.

Further the occluding eyelashes are removed by the application of morphological closing. Next, the centre of the pupil is localized by fist applying the Split and Merge algorithm to detect connected regions of uniform intensity and then growing a circular template to distinguish the pupil from other potential circular or semicircular objects. A model-based algorithm is subsequently` applied in the polar-sampled space and an edge linking scheme is used to detect the horizontally-mapped boundaries of the iris. Results have demonstrated 92% accuracy rate with a relatively rapid execution time.

P. Yao, J. Li, X. Ye, Z. Zhuang , B. Li [36]

The Iris segmentation algorithm utilised in this work is based on a modified version of the Log-Gabor filter [37] though complex 2D Gabor filters have been successfully used in many applications, they are not perfectly suitable to encode the iris texture as the real parts of the filters are not strictly bandpass. The advantage of a Log- Gabor filter over complex Gabor filter is that the former is strictly bandpass filter and the latter is not. The property of strictly bandpass makes the Log-Gabor filters more suitable to extract the iris phase features regardless of the background brightness. So the algorithm presented in this paper which is based on modified Log-Gabor filters, can overcome the limitation of the complex 2D Gabor filters.

2.4 Total Hip Replacement (THR).

The literature in this section focuses on existing work on automatically detecting complications (e.g. dislocations, misalignments, wear, looseness, subsidence and infections) in THR x-ray images. It is noted that the vast majority of papers that presents research into analysing THR x-ray images focuses on manual inspection and subsequently carrying out detailed clinical analysis. These papers are of a

clinical importance rather than of an importance to scientists and medical professionals interested in knowing how Computer Vision can aid in the detailed analysis process of THR x-ray images. This section focuses only on research papers presenting original research on the use of Computer Vision approaches to analyse THR x-ray images. The literature review carried out within the research context of this thesis revealed that the majority of such papers focus on automatically or semi-automatically identifying complications such as wear, looseness, subsidence and infections in THR x-ray images. Research that focuses of detecting possible dislocation and/or misalignment in THR X-ray images is very limited and hence the focus of the research presented in Chapter-5.

A. Oprea, C. Vertan [38]

The research presented in this paper focuses on segmenting the most important clinically relevant parts: prosthesis, bone (femur) and soft tissue part, in a total hip replacement x-ray image. The paper investigates the use of several classical adaptive region segmentation techniques, using either the initial pixel luminance space (adaptive histogram thresholding), or an extended feature space (Fuzzy C-Means) and evaluates the segmentation quality, by using the standard detection error and ROC (Receiver Operating Characteristics) curves. It is concluded that the FCM segmentation provides superior performance for the segmentation of all image components and can be reliably used.

L. Florea and C. Vertan [39]

This paper describes two methods for automatic analysis of THR x-ray images. First method is based on histogram based segmentation of image components, while the second method uses an edge oriented segmentation followed by a 3D modelling of the femoral bone. These methods are first used to evaluate the measurement of the prosthesis fit inside the medullar bone and the secondly to measure the percentage of pixels that are simultaneously placed on the prosthesis border and on the medullar channel border.

M. Komeno, M. Hasegawa, A. Sudo, A. Uchida [40]

In this paper the proper position of the cup and the stem of a THR system, after total hip arthroplasty, were determined by measuring the cup and stem ante-version using computer tomography (CT). Cup ante-version was measured as the angle between the line connecting the anterior edge with the posterior edge of the cup and the vertical line against the line connecting the posterior portions of the pelvis in the slice passing through the centre of the cup. The Stem ante-version was measured as the angle between the line connecting the posterior portions of the femoral condyles and the axis of the stem superimposed sequentially. The sum of cup and stem ante-version in posterior dislocated hips was significantly less than that in non-dislocated hips and the sum in anterior dislocated hips was significantly greater than that in non-dislocated hips.

T. M. Barker, W. J. Donnelly [41]

In this paper a new technique for the measurement of subsidence of the femoral components was proposed. The method relies on the implantation of two ball markers around the femoral stem. Dimensions of the stem are used to correct for magnification and out-of-plane rotations resulting from radiographic positioning. To measure the subsidence the authors determined the relative position of the hip implant and the location of the circular shape (prosthesis head). Hough transform based techniques were used in recognising shapes.

R. Smith and K. Najarian [42]

As in paper [41] this paper uses the Hough transform to detect and segment the pelvic bone structure of THR in x-ray images. The paper provides a hierarchical method for segmentation of three key structures from pelvic x-ray images: the ilium, the left and right acetabulums, using a hierarchical approach that combines directed Hough transform and active shape models. First, directed Hough transform

is used to detect the femur shafts and thus correctly determine the patient's horizontal position within the image. Hough transform is then combined with Active Shape Model (ASM) to detect the femur - and in turn, the acetabulum. The position of the femurs is used to initialize ASM for pelvic ring detection, and the location of the pelvic ring is then used to direct Hough transform for detection of the iliac crests.

2.5 Summary and conclusion.

In this chapter, we have briefly introduced and analysed the existing and related work for the 3 areas of research investigated in this thesis (see Chapters 3, 4 and 5). It is evident that research gaps exist in each of these areas, which are presented in more detail within the individual chapters. Considering these research gaps and analysing the practical relevance of needing solutions, a number of novel approaches to resolving these outstanding research problems are proposed in chapters 3-5. The research motivation behind each approach has been presented in the relevant chapters.

CHAPTER 3

Quantification of Corneal Neovascularization

The healthy cornea is devoid of both blood and lymphatic vessels. This vascularity (also termed the angiogenic privilege of the cornea) is highly conserved evolutionarily to maintain transparency and visual acuity. Nonetheless, because of a variety of severe inflammatory diseases, the cornea can become invaded by pathologic blood and lymphatic vessels. Pathologic corneal neovascularization (the excessive ingrowth of blood vessels from the limbal vascular plexus into the cornea, i.e., angiogenesis) not only reduces the quality of being able to see objects through the cornea (also called corneal transparency) but also is a major risk factor that may result in the need of a corneal transplantation. In addition, host corneal neovascularization (both before as well as after surgery) is one of the most significant risk factors for subsequent immune rejections after replacing the damaged cornea with a clear cornea (corneal grafting). Thus timely and effective treatment of corneal neovascularization is important.

Quantification of corneal neovascularization provides the means to monitor the effectiveness of a treatment process. To this effect many corneal imaging devices utilised at present are capable of providing medical experts with high quality images that can be manually inspected and quantified. However, in severe cases of corneal neovascularization, manual inspection and quantification becomes an extremely tedious, time consuming task prone to human error. A solution exists in using automated and/or semi-automated computer/machine vision approaches to carry out this task. However, the literature review presented in chapter 2 revealed that only a limited amount of research [14-20] has being carried out towards providing computer vision based solutions to segmenting and quantifying corneal neovascularization. The focus of this chapter is to present a novel approach to the

segmentation of blood vessels and hence the quantification corneal neovascularization.

For clarity of presentation, this chapter is divided in to several sections. In addition to this section that introduces corneal neovascularization and the importance of its treatment, Section 3.1 introduces the reader to the research problem and the need for a solution. Section 3.2 introduces the reader to the fundamental concepts, theories and techniques on which the proposed algorithms are based on and define relevant terms used. Section 3.3 discusses the proposed method. Section 3.4 provides experimental results and a comprehensive analysis of the performance of the proposed method. Finally Section 3.5 summarises and concludes the chapter.

3.1 Introduction

The first step of a corneal blood vessel detection algorithm is the segmentation of the corneal area. As discussed in chapter 2, a number of automatic and semi-automatic corneal segmentation algorithms have been utilised in unrelated application [28][34][35][36] areas. We have specifically used a semi-automatic approach, as it removes the chances of a broken corneal boundary that may result from occlusion, noise, low image quality etc. Further for medical professionals engaged in this activity, this provides a level of engagement leading to building confidence in the subsequent automatic stages, i.e. the segmentation of blood vessels and their quantification.

This chapter presents a Contourlet transform based approach to segmentation of corneal blood vessels (Corneal Neovascularization). The novelty of this work is the use of a computer aided approach that helps the medical practitioners in quantifying corneal neovascularization. In order to perform a successful segmentation of blood vessels, an image pre-processing stage that removed non-uniform background illumination that originates from the shiny nature of the cornea, was utilised. Further two stages of image pre-processing and enhancement, i.e. contrast enhancement

(performed in the Contourlet Domain) and noise reduction was also performed, prior to the application of Contourlet Transforms.

3.2 Research Background.

Blood vessel segmentation algorithms proposed in this chapter attempts to overcome the limitations of the existing approaches and provide practical solutions. This section will introduce the reader to the fundamental concepts, theories and techniques on which the proposed algorithms are based and defines the relevant terms used.

3.2.1 Contourlet Transform

The main challenge in exploring geometry in an image comes from the discrete nature of the data. The Contourlet Transform [43] starts with a discrete-domain construction and then studies it is convergence to an expansion in the continuous domain. Although the Contourlet Transform uses multi scale and time-frequency-localization properties of wavelets, in addition it offers image representation at multi- resolution, high degree of directionality and anisotropy. Figure 3.1 illustrates the comparison of performance of Wavelet and Contourlet Transform approximations near smooth contours.

The application of Contourlet Transform consists of two filtering stages named as Pyramidal Filtering and Directional Filtering. The Pyramidal Filtering is constructed based on a Laplacian Pyramid (LP) [44] which helps to obtain the multi-scale decomposition of the image. The LP decomposition at each level generates a down sampled lowpass version of the original and the difference between the original and the prediction, resulting in a band-pass image. Figure.3.2 illustrates this decomposition process.
 The LP has the distinguishing feature that each pyramid level generates only one band-pass image (even for multidimensional cases), and this image does not have

'scrambled' frequencies. This frequency scrambling happens in the wavelet filter bank when a highpass channel, after downsampling, is folded back into the low frequency band, and, thus, its spectrum is reflected. In the LP, this effect is avoided by downsampling the lowpass channel only

Wavelet Transform representation   **Contourlet Transform representation**
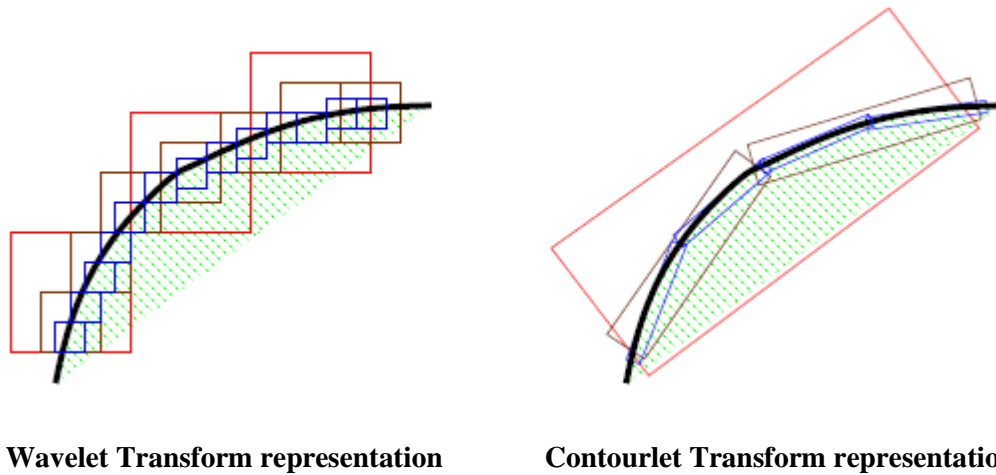
Figure 3.1: Illustrating Wavelet and contourlet transform performance near smooth contours to capture linear segments of contours [43].
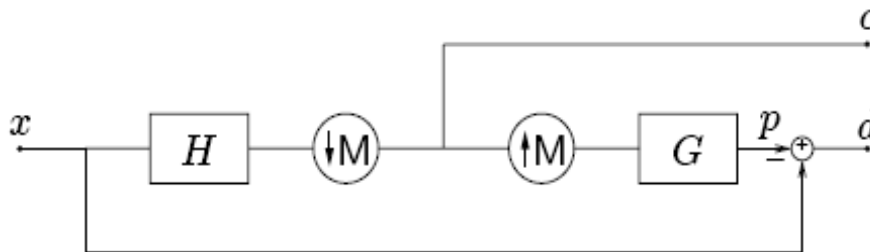
Figure 3.2: LP: One level of decomposition. The outputs are a coarse approximation c[n] and a difference d[n] between the original signal and the prediction. H and G are called (lowpass) analysis and synthesis filters respectively and M is a sampling matrix [43].

The Directional Filter consists of a Directional Filter Bank (DFB) [45], which helps in obtaining the wedge-shaped frequency decomposition.

The DFB utilises tow building blocks. The first block is a two-channel quincunx filter bank [46] with a fan filter (see figure 3.3) to obtain the horizontal and vertical direction frequency information. The second block of DFB uses a shearing operator to obtain the angular information. The decomposition pyramid can create 2^n sub-bands, where n represents the number of levels. For example n = 3 produces eight band pass images by utilising the selected filter. In the construction of band pass images the DFB fan filter can adaptively be utilised to extract any particular directional information such as horizontal, vertical or both sides. Figure 3.4 illustrates the evolution of support sizes of a contourlet function that satisfies the parabolic scaling [43].

Figure 3.3:Two-dimensional spectrum partition using quincunx filter banks with fan filters. The black regions represent the ideal frequency supports of each filter. Q is a quincunx sampling matrix [43].

Figure 3.4: Illustrating the evolution of support sizes of contourlet functions that satisfy the parabolic scaling [43]

3.3 Proposed Method.

The methodology presented in this section explains the procedure that has been followed to quantify the corneal neovascularizations. Figure 3.5 illustrates the block diagram of the proposed method.

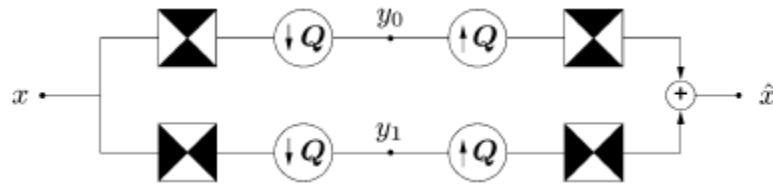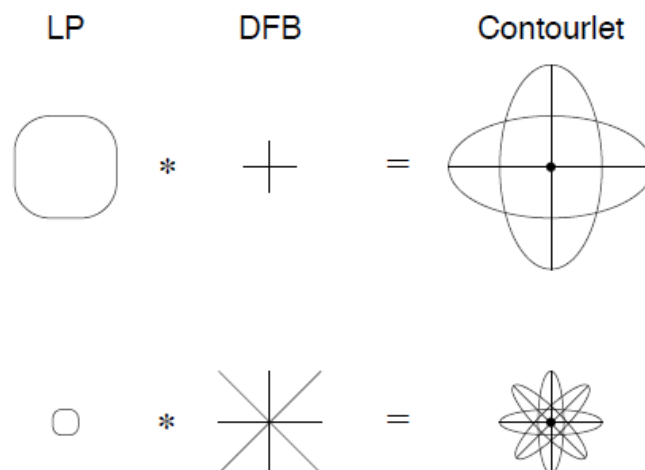### 3.3.1 Corneal Area Segmentation.

Although a number of automated corneal area segmentation algorithms have been proposed in literature (see chapter 2) under the present context of our research which focuses more on the accuracy of segmentation of blood vessels [47][28][34][35][36], it was decided to use a semi-automatic, and hence accurate, corneal boundary segmentation approach, as the potential users (i.e. Ophthalmologists) seek the highest possible accuracy. Thus in the approach adopted, an initial elliptic contour automatically placed approximately closer to the corneal boundary is adjusted manually by the user to register with the boundary of the cornea. Although this step requires manual intervention the process is straightforward and is worth the effort due to the difficulty of automatically detecting the complete contour of a corneal boundary using any existing image processing approach.

Figure3.6 illustrates the steps that are followed in the semi-automated segmentation of the cornea. In the initial stage an ellipse is drawn which has dimensions along the minor and major axes, approximately equal to half of the radius of circular edge (determined by a Canny edge detector with appropriate threshold settings) of the cornea. The system then allows the user to move the boundary and the entire elliptical shape, to enable its boundary's best alignment with that of the corneal boundary.

Once the corneal image is segmented as described above it undergoes a number of stages of processing as illustrated by figure 3.7.
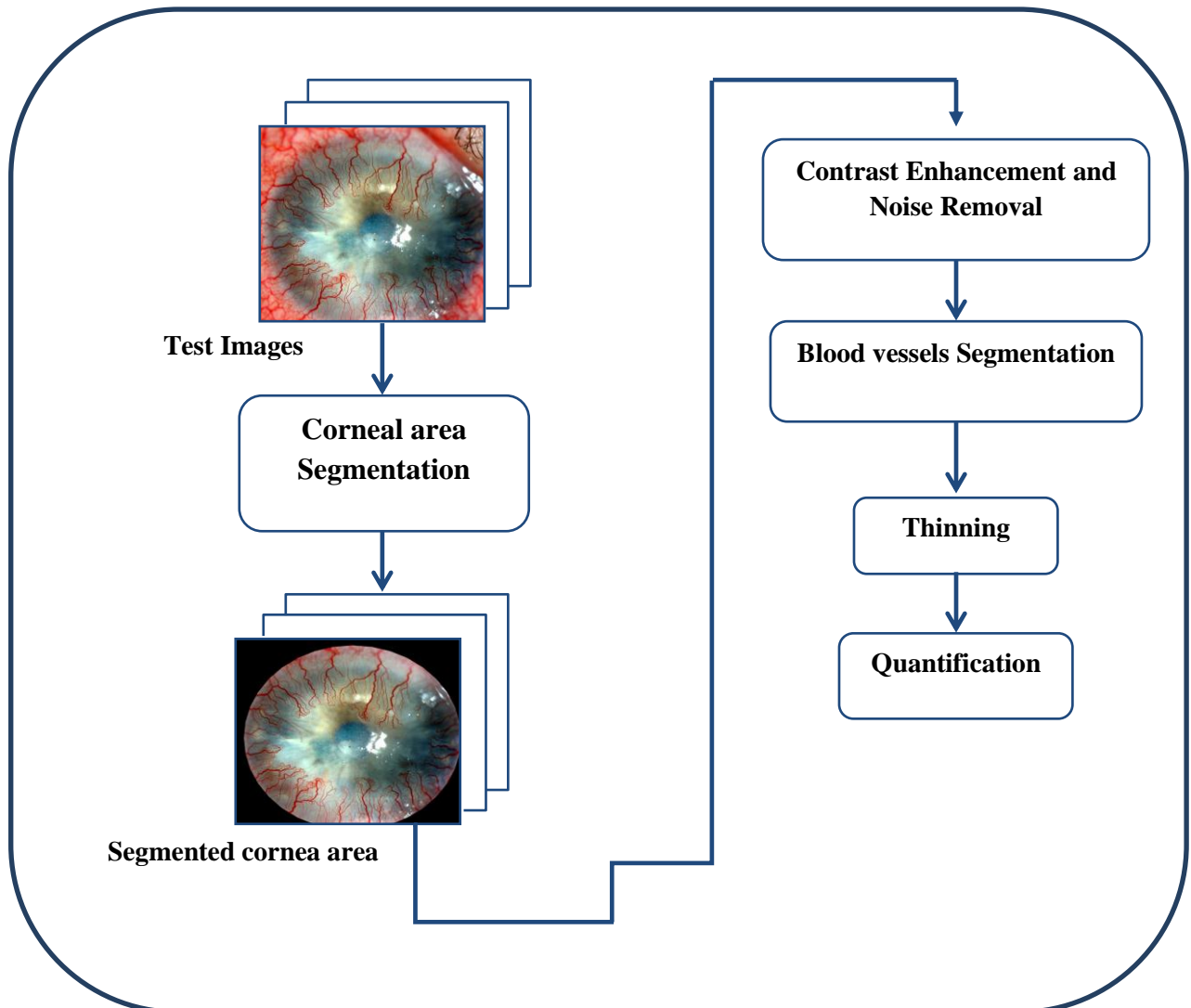
Figure 3.5: Proposed method for quantification of corneal blood vessels.

3.3.2 Contrast Enhancement and Noise Removal

The contrast enhancement and noise removal are both done within a Contourlet Transform domain processing procedure described in this section. As a result of this stage the contrast of the blood vessels of the corneal image is enhanced. Further noise and non-uniform background illumination is minimized. This allows the simple thresholding based blood vessel extraction algorithm to perform accurately. Figure.3.7 illustrates a detailed block diagram of the stages involved within this

phase of the proposed method. The subsequent sections provide more details of each important sub-stage.

<div align="center">(a)   (b)</div>
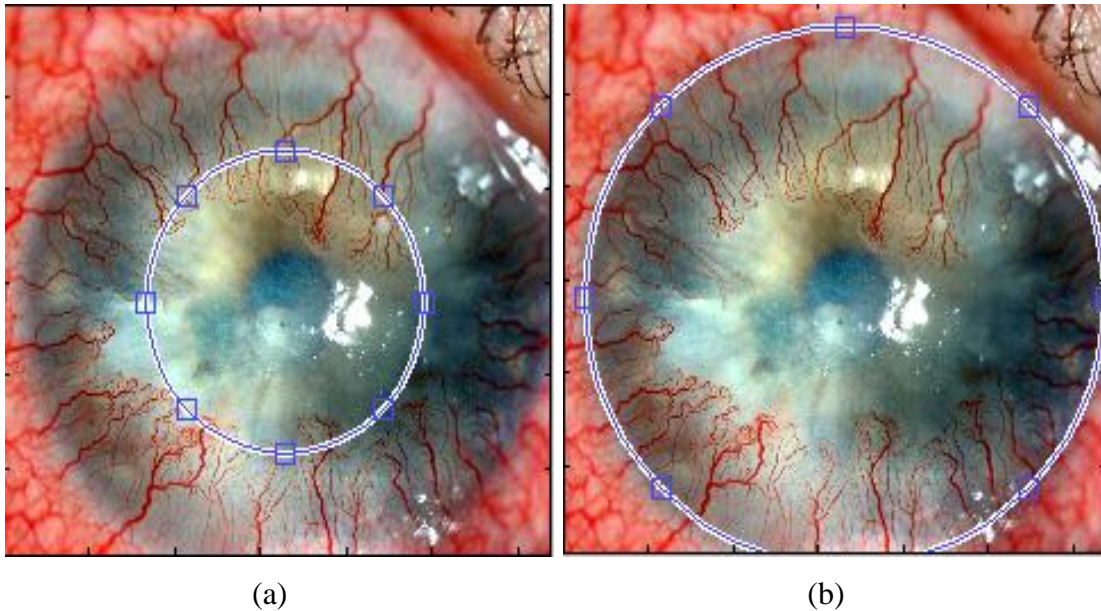
Figure 3.6: Semi-automated Segmentation of the Cornea (a) initial ellipse automatically drawn within the cornea (b) manually adjusted ellipse to coincide with the corneal boundary.

3.3.2.1 Pre-processing - Removal of non-uniform illumination:

Our investigations with the three colour planes revealed that either the difference between the red and green plane or the difference between the red and blue planes enables the removal of non-uniform background illumination, a major obstacle for the subsequent blood vessel segmentation stages.
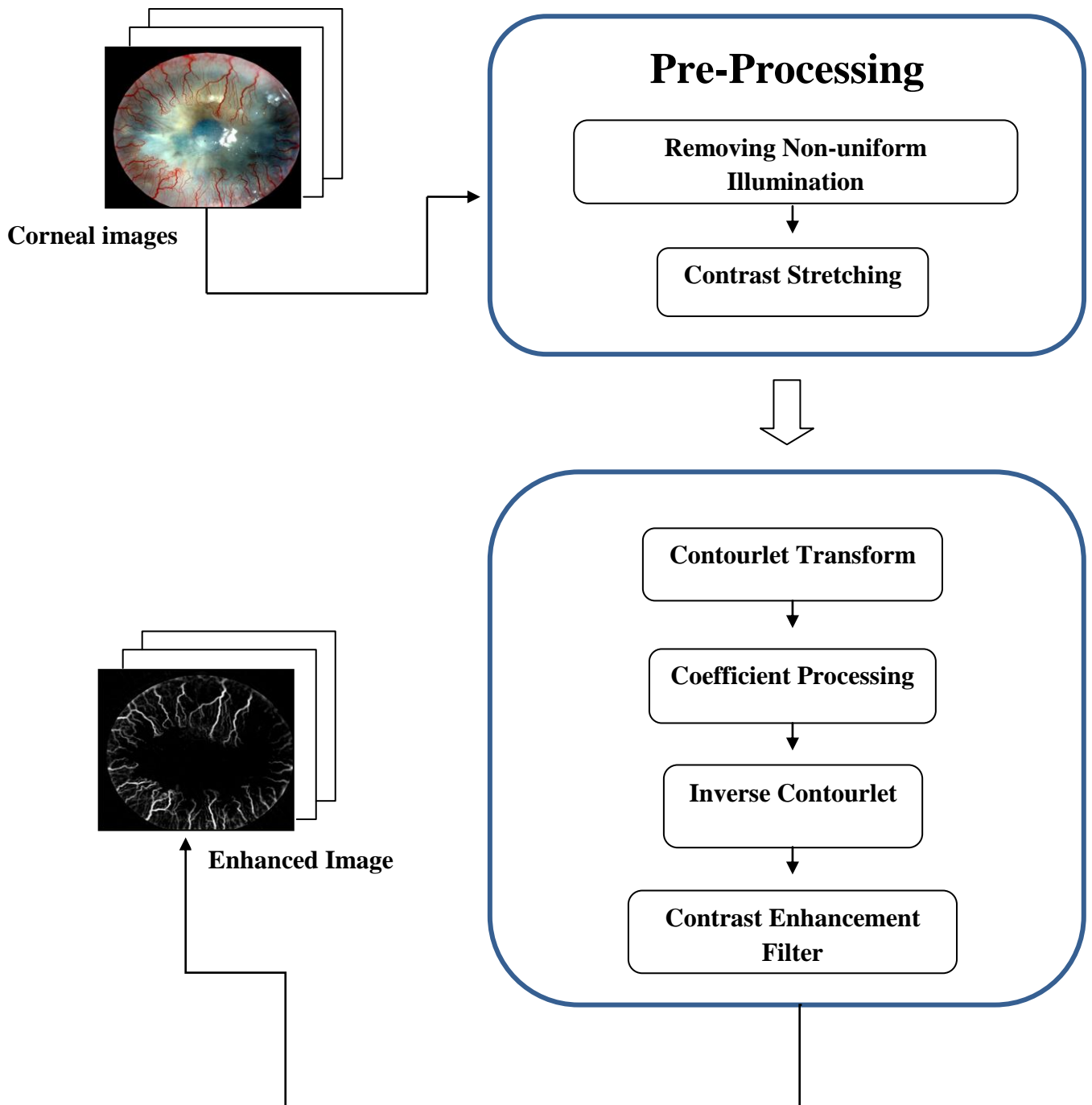
Figure 3.7: Illustrates the stages involved within the Contrast Enhancement and Noise Removal phase of the proposed method to the quantification of corneal neovascularization.

Figure 3.8 (d) illustrates that the highlighted areas have been removed in the difference image between the red and green component images.

(a)

(b)

(c)

(d)
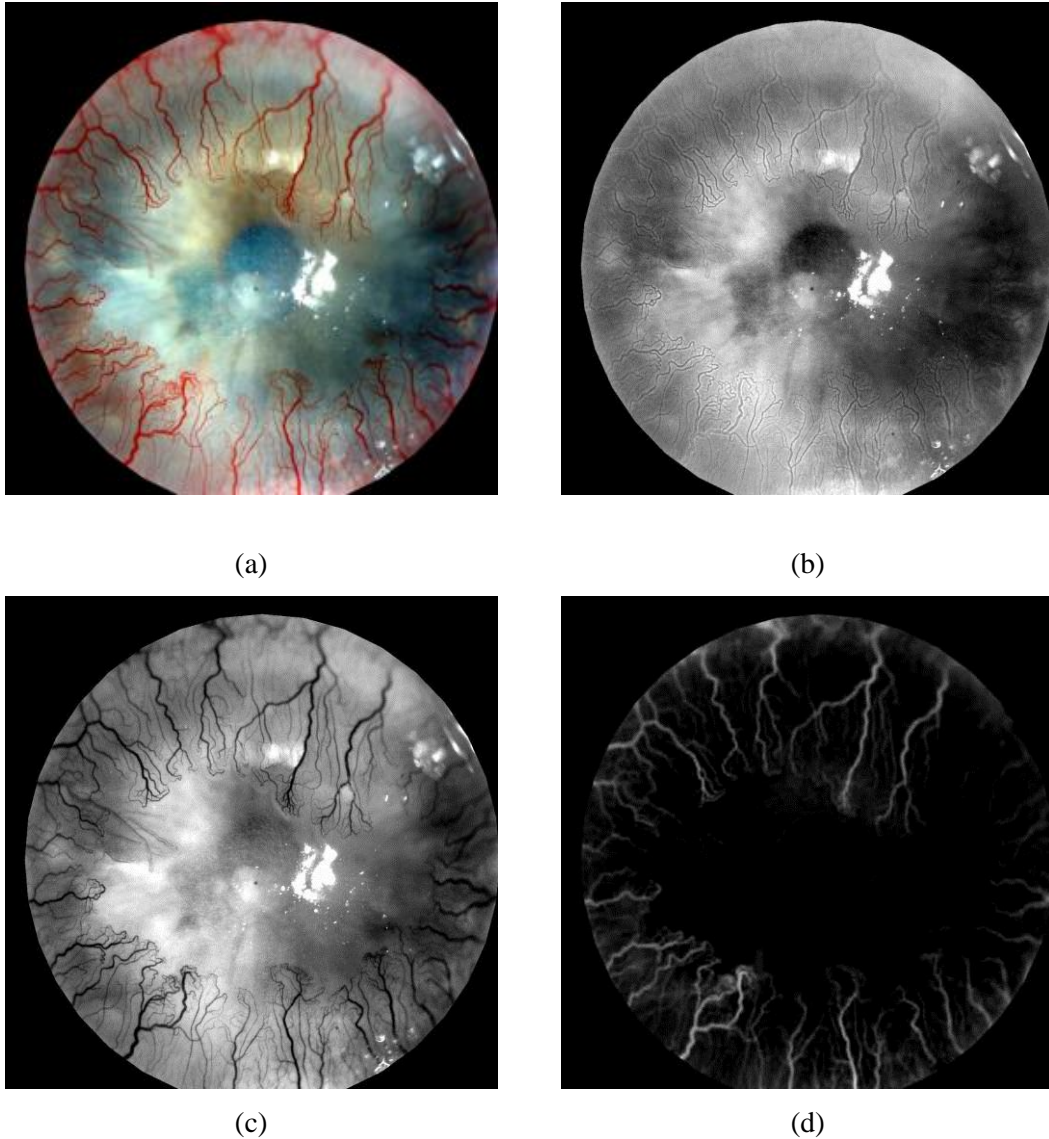
Figure 3.8: Removal of non-uniform illumination (a) original colour image (b) red component image (c) green component (d) red-green component image.

Subsequent to the formation of the difference image contrast stretching can be used to improve the contrast further. This involves the determination of the highest pixel value and re-mapping it to 255 and the determination of the lowest pixel value and re-mapping it to 0.

3.3.2.2 Contourlet transform:

As explained in section 3.2.1 generally the application of Contourlet Transform to an image involves two stages. A Laplacian pyramid is first used to capture point discontinuities followed by the application of a directional filter bank to link point discontinuities into a linear structure (see equation 3.2 and equation 3.3 section 3.3.2.4).

The overall result is thus an image expansion using basic elements such as contour segments and is hence named a Contourlet. Figure 3.9 illustrates the Contourlet decomposition [43] of a typical corneal image with neovascularization. The specific decomposition illustrated represents a two level decomposition with the first level illustrating four directions and the second level illustrating eight directions. It is noted that blood vessels are represented in their parts within the various sub-bands of decomposition.

Figure 3.9: Two level, 8 band Contourlet decomposition of a corneal image.

Our experiments revealed that at 2 levels of decomposition we were able to obtained sufficient details to segment blood vessels. Further our investigations revealed that at higher levels of decomposition the more detailed sub-bands formed, consisted mostly of noise that biased the segmentation process to produce less accurate results.
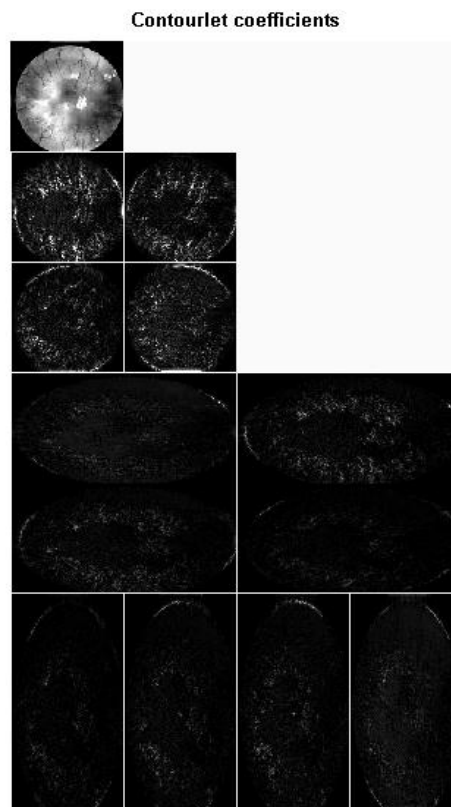
3.3.2.3 Contourlet based image enhancement:

A closer look at the difference image between the red and the green colour plains reveals blood vessels of different luminosity. The vessels having high contrast to the background (bright) are easy to detect but the vessels having low contrast to the background will be more difficult to segment. The approach proposed attempts to soften the stronger edges and amplify the faint edges so that the slim vessels will become visible. This is done as follows: After the decomposition of the image into Contourlet coefficients (i.e. the values that result from the transformation of pixel values, when a Contourlet Transform is applied to the corneal image) they are modified via a non-linearity function y_α defined below.

Note that taking noise into consideration we have adopted a noise standard deviation σ in the equation (see section 3.3.2.4).

$$
\begin{aligned}
&y_a(x,\sigma) = 1 &&\text{if } x < a\sigma \\
&y_a(x,\sigma) = \frac{x - a\sigma}{a\sigma}\,(\frac{m}{a\sigma})^p + \frac{2a\sigma - x}{a\sigma} &&\text{if } a\sigma \leq x < 2a\sigma \\
&y_a(x,\sigma) = (\frac{m}{x})^p &&\text{if } 2a\sigma \leq x < m \\
&y_a(x,\sigma) = (\frac{m}{x})^s &&\text{if } x \geq m
\end{aligned}
\tag{3.1}
$$

In the above equations, m determines the degree of nonlinearity. s introduces dynamic range compression. Using a nonzero s will enhance the weaker edges and soften the stronger edges. a is a normalization parameter. Parameter m is the value

under which coefficients are amplified. It is obviously dependent on the values of pixels. There are two possible options to derive the value of m,

• $m = K_m \sigma$, which m is derived from the noise standard deviation by using parameter K_m .

Note that K_m is independent of the Contourlet coefficient values and is not difficult to be set. When $\sigma =3$, $K_m =10$, all coefficients can be amplified between 3 and 30.

• $m = lM_a$, which m is derived from the maximum Contourlet coefficient M_a of the relative sub-band. l must be less than 1. In this case, choosing for instance $a=3$, $l=0.5$, we amplify all coefficients with an absolute value between 3^{σ} and half the maximum absolute value of the sub-band.

The first option allows the user to define the coefficients to be amplified as a function of their signal to noise ratio, while the second choice gives a general and easy way to fix the parameter m independently of the range of the pixel values.

The images we have captured for analysis have being obtained using optical devices that are known to produce noise with a 'normal distribution'. Such details are provided by the manufacturers of the camera and we have therefore used this assumption in our work.

3.3.2.4 Estimation of noise standard deviation σ:

Estimation of the amount of noise is crucial in many algorithms for digital image analysis. This enables an algorithm to adapt to the noise instead of following fixed thresholds. There are a number of standard approaches one can use to estimate the noise variance. Since image structures like edges have strong second order differential components, a noise estimator should be insensitive to the Laplacian of an image. One of the estimation methods is to suppress the image structure by Laplace masks [48].

The Laplacian of an image f can be defined as follows:

$$\nabla^2 f = \frac{\partial^2 f}{\partial x^2} + \frac{\partial^2 f}{\partial y^2} \qquad (3.2)$$

$$\nabla^2 f = f(x+1, y) + f(x-1, y) + f(x, y+1) + f(x, y-1) - 4f(x, y) \qquad (3.3)$$

Immerker in [49] suggests using the difference between two templates L_1 and L_2, approximating the Laplacian of an image in discrete format. The two masks are as follows:

$$L_1 = \begin{bmatrix} 0 & 1 & 0 \\ 1 & -4 & 1 \\ 0 & 1 & 0 \end{bmatrix} \qquad L_2 = \frac{1}{2}\begin{bmatrix} 1 & 0 & 1 \\ 0 & -4 & 0 \\ 1 & 0 & 1 \end{bmatrix} \qquad (3.4)$$

The noise estimation operator M is represented by the difference between the two masks above:

$$M = 2(L_2 - L_1) = \begin{bmatrix} 1 & -2 & 1 \\ -2 & 4 & -2 \\ 1 & -2 & 1 \end{bmatrix} \qquad (3.5)$$

which has zero mean and variance

$$(4^2 + 4.(-2)^2 + 4.1^2)\sigma_n^2 = 36\sigma_n^2 \qquad (3.6)$$

Assuming that the noise at each pixel has a standard deviation σ_n. Assume $f(x, y)$ * M denotes the value of applying the mask M at position (x, y) in the image f.

Computing the variance of the output of the M operator applied to the image f, will give an estimate of $36\sigma_n^2$ at each pixel, which can be averaged over the image f or local neighbourhoods to give an estimate of the noise variance σ_n^2. The variance of the noise in f can be obtained as,

$$\sigma_n^2 = \frac{1}{36(W-2)(H-2)} \sum_{image\ f} (f(x, y) * M)^2 \qquad (3.7)$$

Where *W* and *H* represent the width and height of image *f*, * is the time domain convolution.

To obtain the absolute deviation from the variance above, assuming a Gaussian distribution with zero mean and variance σ^2, the deviation is

$$\int_{-\infty}^{\infty} |t| \ \frac{1}{\sqrt{2\pi\sigma}} \ \exp\left(\frac{-t^2}{2\sigma^2}\right)dt = \sqrt{\frac{2}{\pi}} \ \sigma \qquad (3.8)$$

Then,

$$\sigma = \sqrt{\frac{\pi}{2}} \int_{-\infty}^{\infty} |t| \ \frac{1}{\sqrt{2\pi}\ \sigma} \ \exp\left(\frac{-t^2}{2\sigma^2}\right) dt \qquad (3.9)$$

From above, we can obtain σ_n, which is the standard deviation of noise from the variance σ_n^2

$$\sigma_n = \sqrt{\frac{\pi}{2}} \ \frac{1}{6(W-2)(H-2)} \sum_{image\ f} |f(x,y) * M| \qquad (3.10)$$

3.3.2.5 Inverse Contourlet transform:

Once the coefficients have been modified following the above procedure the Inverse Contourlet Transform is used to obtain the enhanced image. Figure 3.10 illustrates a typical example.

<center>(a)   (b)</center>
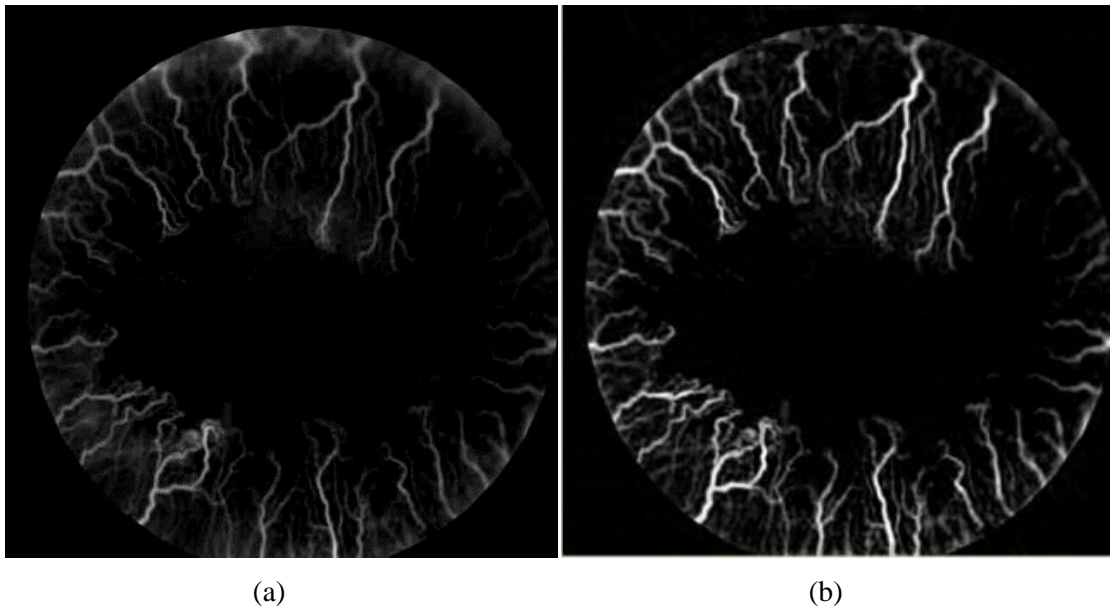
Figure 3.10: The difference between the red and green component images (a) before application (b) after application, of contourlet based enhancement.

3.3.2.6 Contrast enhancement filter:

The sharpening filtering can be used to make edges in an image sharper and more clearly defined. The idea of unsharp masking is to subtract a scaled "unsharp" version of the image from the original. In practice, we can achieve this effect by subtracting a scaled blurred image from the original [50]. Figure 3.11 illustrated schema for unsharp masking.
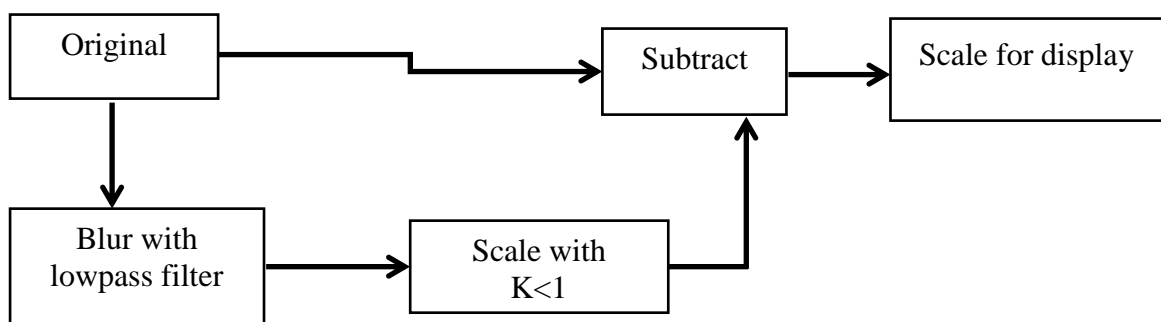
Figure 3.11 illustrated schema for unsharp masking.

The following unsharp contrast enhancement filter was applied on the output of the previous step (Inverse Contourlet Transform). This filter created from the negative of the Laplacian filter with parameter a controls the shape of the Laplacian [50][51].

$$\frac{1}{(a+1)}\begin{bmatrix} -a & a-1 & -a \\ a-1 & a+5 & a-1 \\ -a & a-1 & -a \end{bmatrix} \qquad (3.11)$$

3.3.3 Segmentation.

After the images have been enhanced following the procedure described in 3.3.2 we use a simple threholding based approach to segment the blood vessels (Note – experimental selection of threshold that results in the best perceptual results). In doing so we create a binary image with 0 (black) representing pixel values outside the blood vessels and 255 (white) representing pixel values belonging to the blood vessels.

Fig.3.12 illustrates the resulting blood vessel segmentation obtained by following the contrast enhancement procedure described in 3.3.2

(a)   (b)
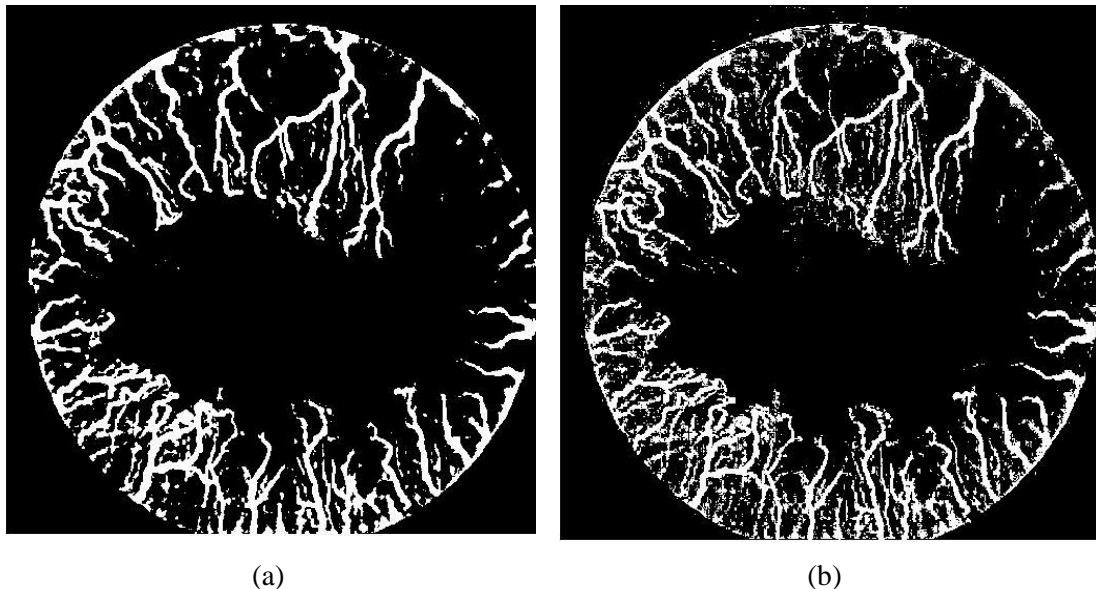
Figure 3.12: The segmentation result (a) before application (b) after application, of Contrast enhancement filter.

3.3.4 Thinning.

We applied a thinning approach [52][53][54] to make the blood vessels more analogous to the ones on the original image. The algorithm can be described as follows:

this thinning approach is a modification of the algorithm proposed in [53] to thin 8-connected skeletons and retain diagonal lines and 2x2 squares depends on a number of conditions (G1, G2 and G2 defined below) and iterations.

After dividing the image into two distinct subfields, in the first sub-iteration, if and only if conditions G1, G2 and G3 are all satisfied pixel p would be deleted from the first subfield.

In the second sub-iteration, if and only if conditions G1, G2 and G3' are all satisfied pixel p would be deleted from the second subfield. [52]

Where are the pixels $x_1, x_2, \ldots x_8$ Stand for the 8-neighbours of p and are collectively denoted by $N(p)$.

Condition G1:

$$X_H(P) = 1 \tag{3.12}$$

Where

$$X_H(P) = \sum_{i=1}^{4} b_i$$

$$\tag{3.13}$$

$$b_i = \begin{cases} 1, \text{if } x_{2i-1} = 0 \text{ and } (x_{2i} = 1 \text{ or } x_{2i+1} = 1) \\ 0, \text{otherwise} \end{cases}$$

Condition G2:

$$2 \leq \min\{n_1(P), n_2(P)\} \leq 3 \tag{3.14}$$

Where

$$n_1(P) = \sum_{k=1}^{4} x_{2k-1} \vee x_{2k}$$

$$n_2(P) = \sum_{k=1}^{4} x_{2k} \vee x_{2k+1}$$

(3.15)

Condition G3:

$$(x_2 \vee x_3 \vee \overline{x}_8) \wedge x_1 = 0$$

(3.16)

Condition G3':

$$(x_6 \vee x_7 \vee \overline{x}_4) \wedge x_5 = 0$$

(3.17)

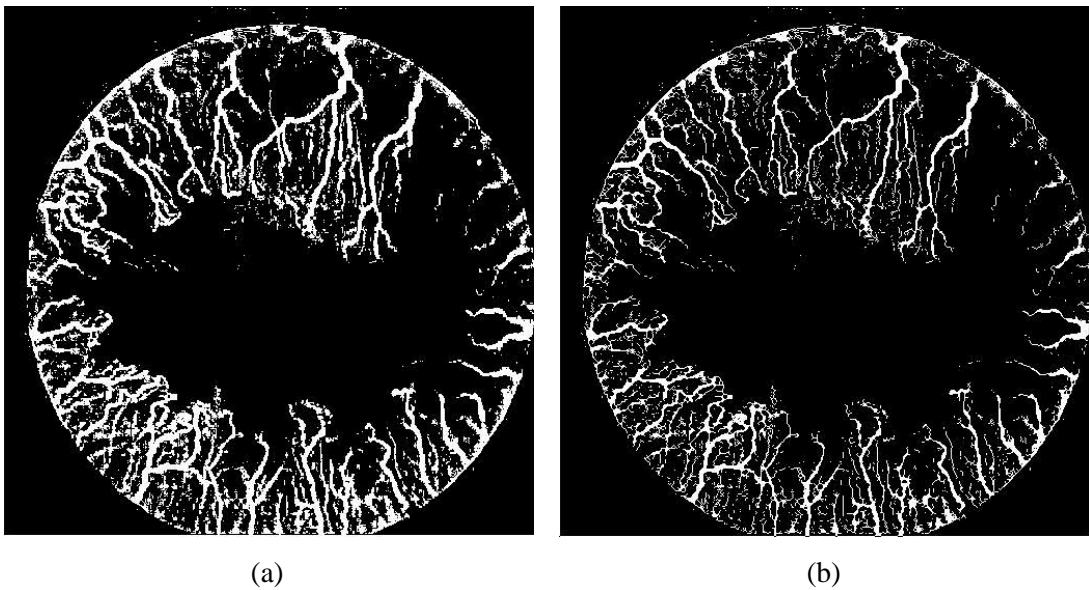(a)   (b)

Figure 3.13: The segmentation result (a) before application (b) after application, of the Thinning algorithm.

3.3.5   Quantification.

For each image the total amount of pixels belonging to the entire corneal area and the total amount of pixels belonging to the blood vessels are calculated. The first figure is calculated by adding up the number of pixels within the corneal boundary, regardless of its colour and the second figure is calculated by totalling up the white pixels within the boundary of the image. The percentage ratio between the total number of pixels located within the corneal blood vessels and the cornea is finally calculated.

3.4   Experimental Results and analysis.

Experiments were performed on a set of forty images with various degrees of corneal neovascularization. All algorithms were implemented with MATLAB. The results for six test images are illustrated in figure3.14. The images in figure3.14 have been arranged in descending order of the degree of corneal neovascularization. The results illustrate the capability of the proposed approach to enhance the blood vessels before segmentation, making the quantifications more accurate.

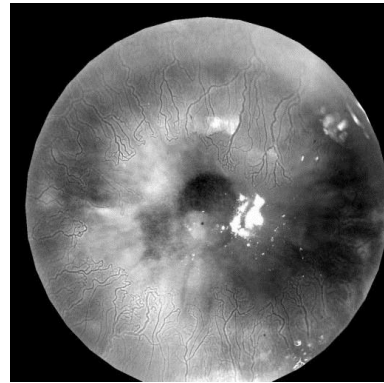|	Image 1	Image 2	Image 3	Image 4	Image 5	Image 6
Threshold	35	39	40	35	70	135
Cornea area	196022	190582	195034	197199	186190	157139
Vessel area	72491	60734	55448	51138	42728	13374
Ratio%	36.9	31.9	28.4	25.9	22.9	8.5

Table 3.1: Quantification results.

Figure 3.14 illustrate experimental results, where (a) is the original image, (b) is the red component image, (c) is the green component image ,(d) is the difference

between the red and green component images, before enhancement, (e) is the difference between the red and green component image after contourlet based enhancement, (f) is the result after applying the contrast enhancement filter, (g) is the binary image after segmentation that was used in the quantification. (h) is the result after the thinning algorithm is applied.

Image 1

(a)

(b)

(c)
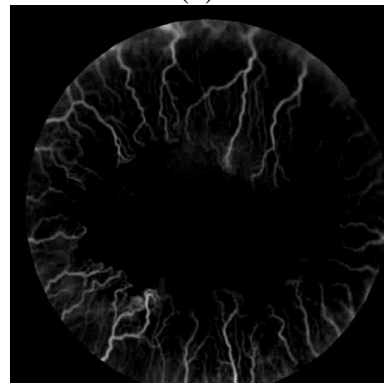
(d)
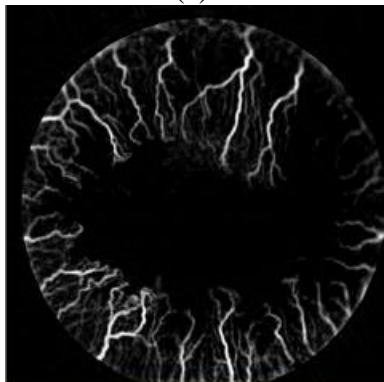
(e)
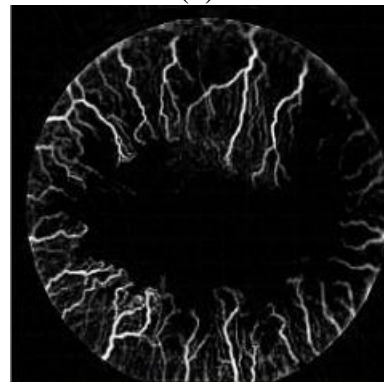
(f)
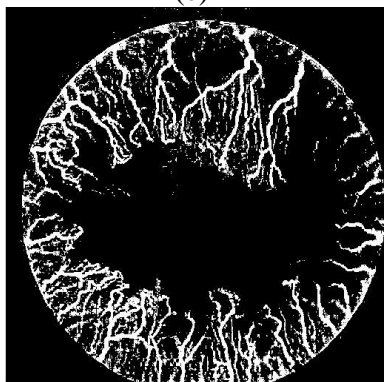
(g)
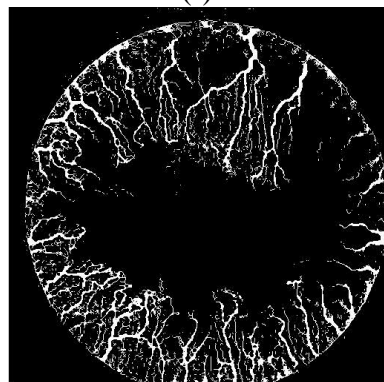
(h)

Image 2
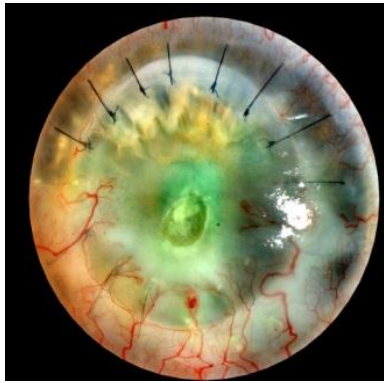
(a)
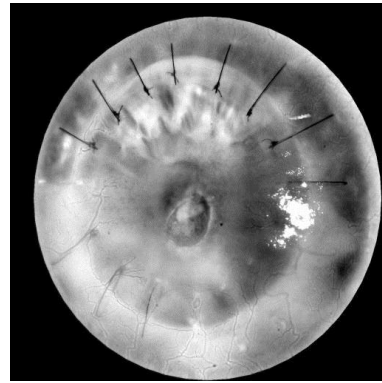
(b)
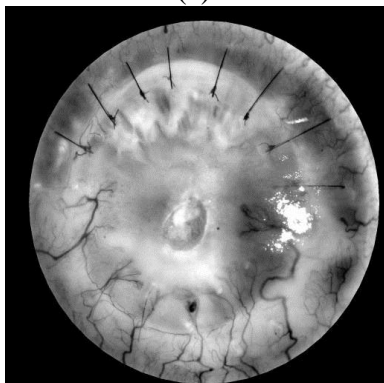
(c)
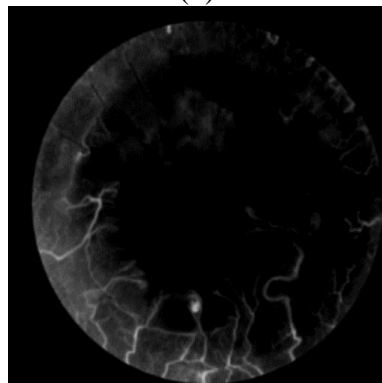
(d)
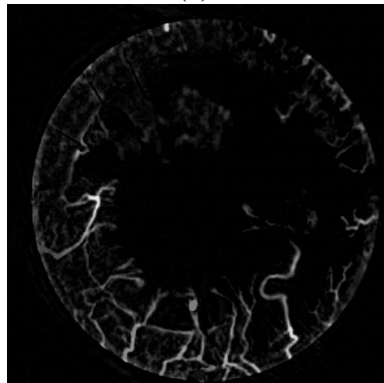
(e)
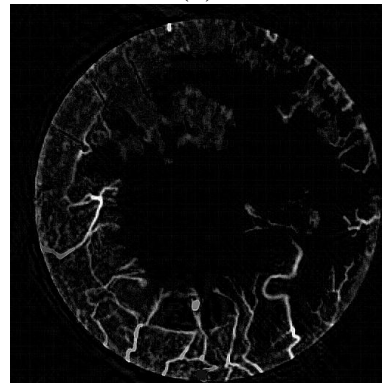
(f)
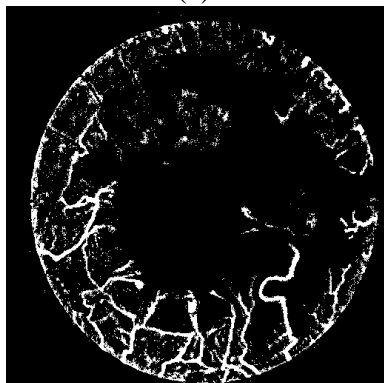
(g)
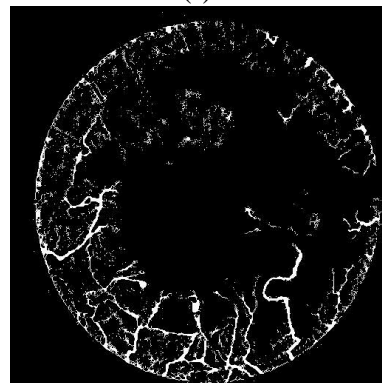
(h)

Image 3

(a)

(b)

(c)

(d)

(e)

(f)

(g)

(h)

Image 4

(a)

(b)

(c)

(d)

(e)

(f)

(g)

(h)
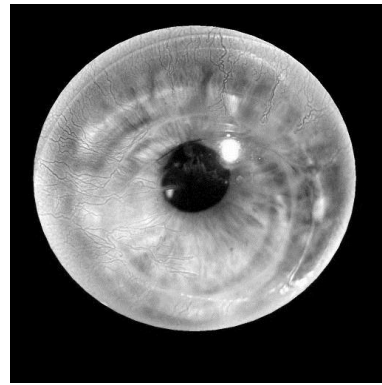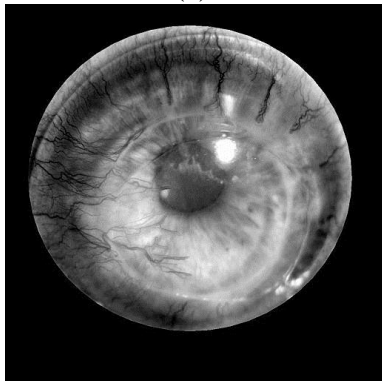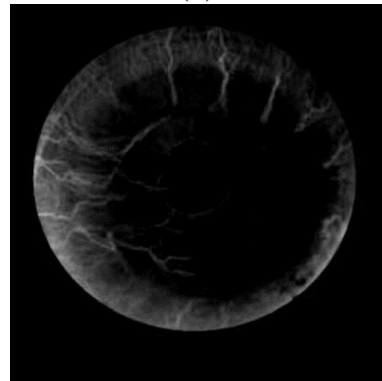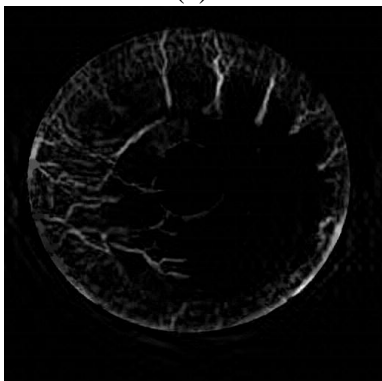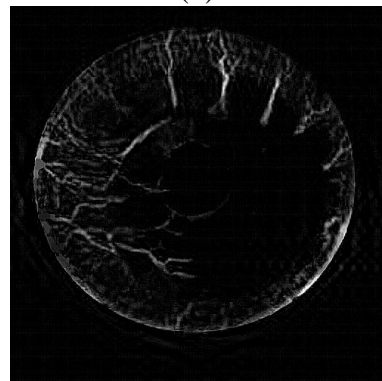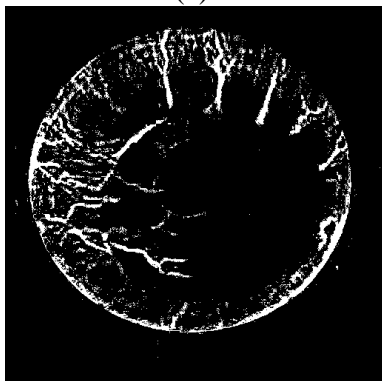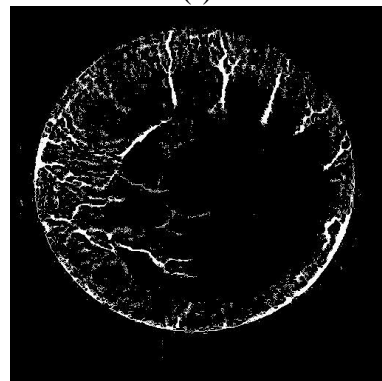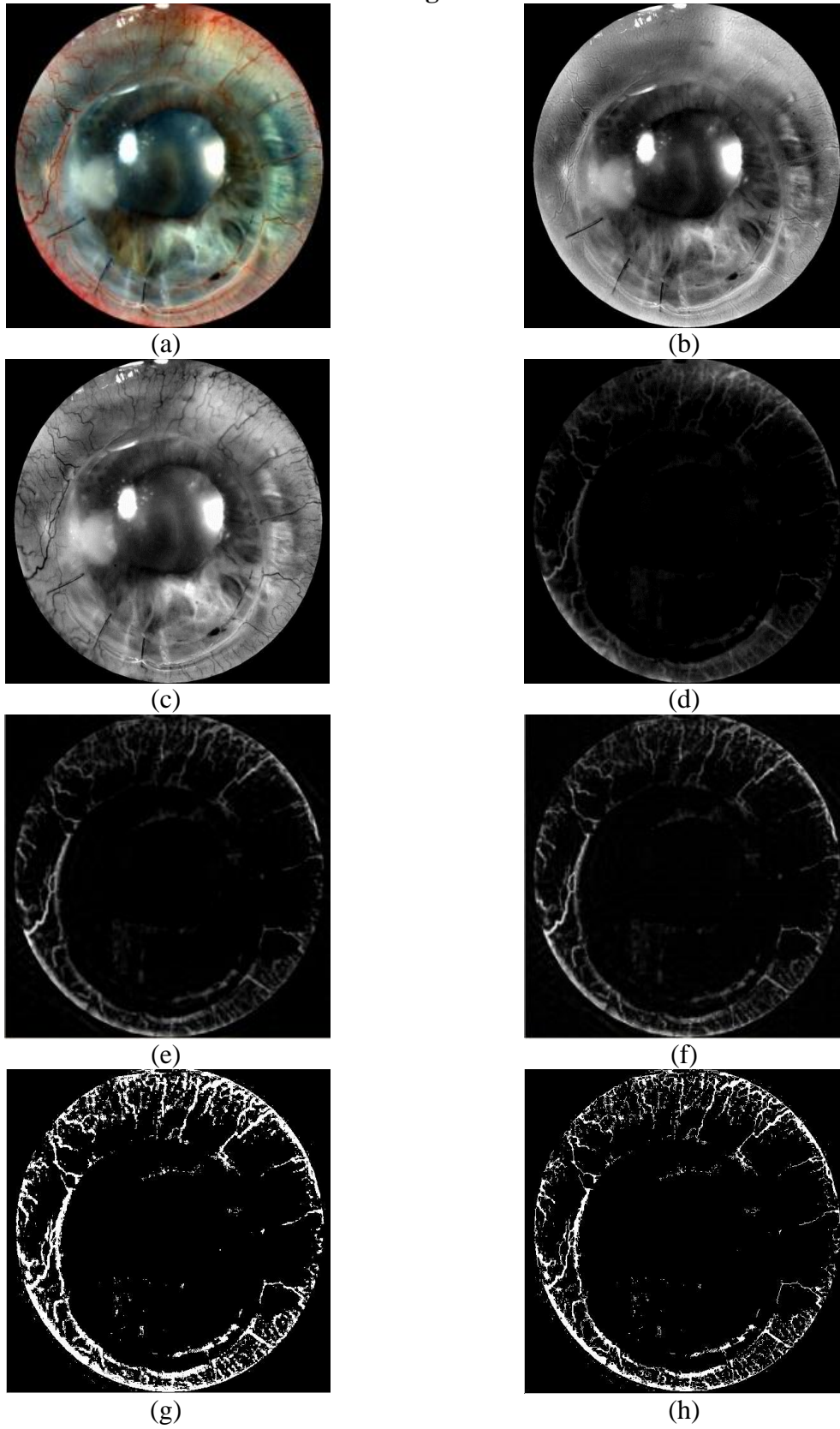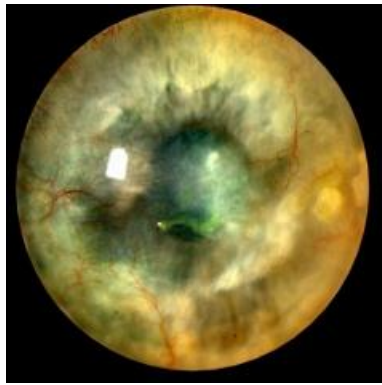
Image 5

(a)
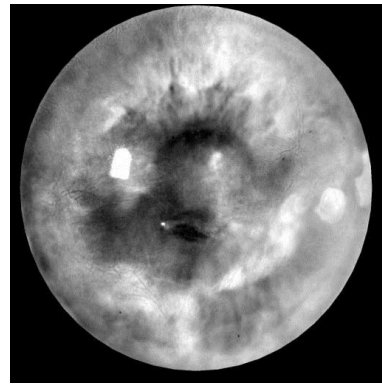
(b)
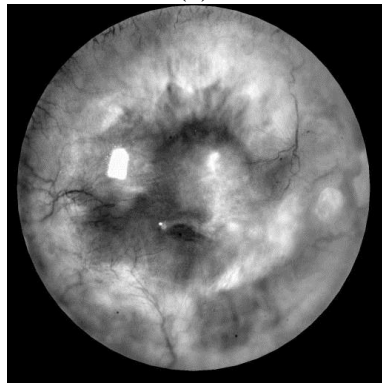
(c)
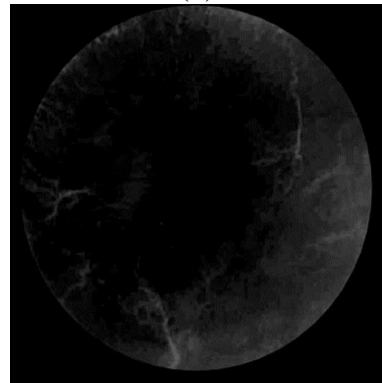
(d)
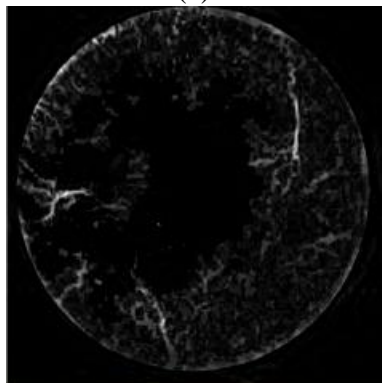
(e)

(f)

(g)

(h)

Image 6

(a)

(b)

(c)

(d)

(e)

(f)

<center>(g)   (h)</center>
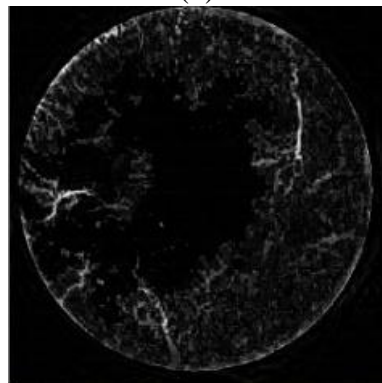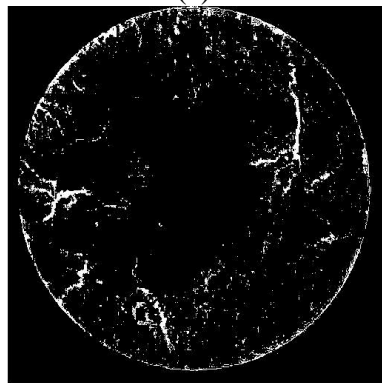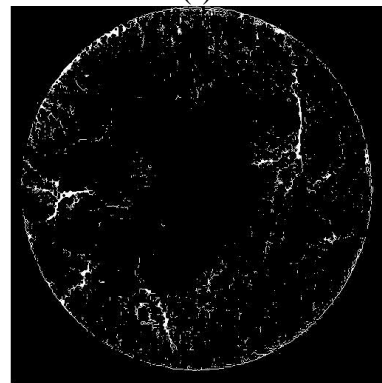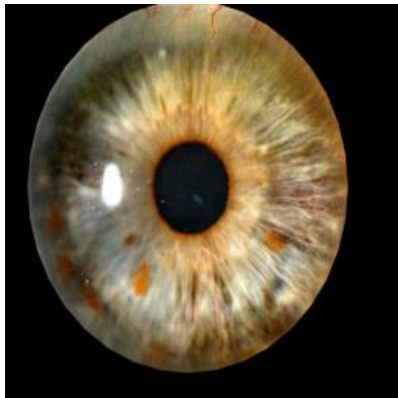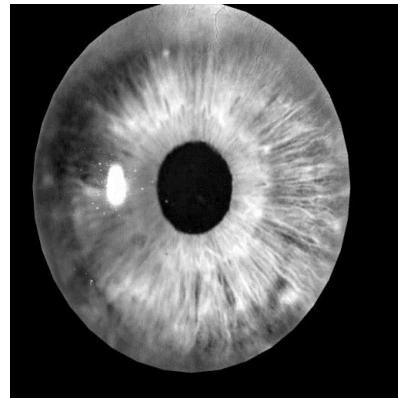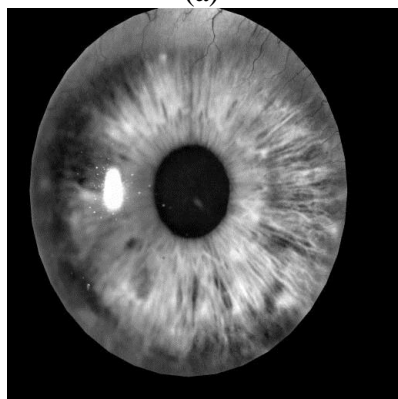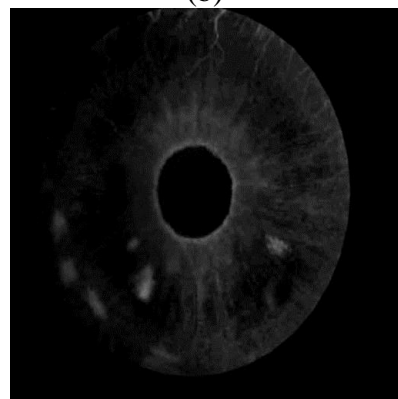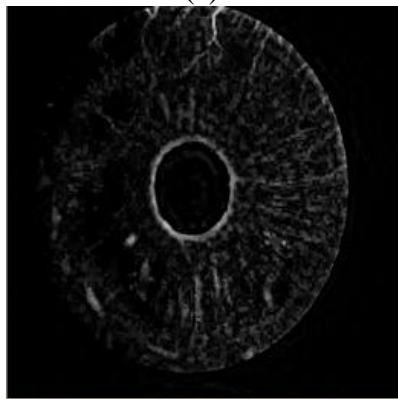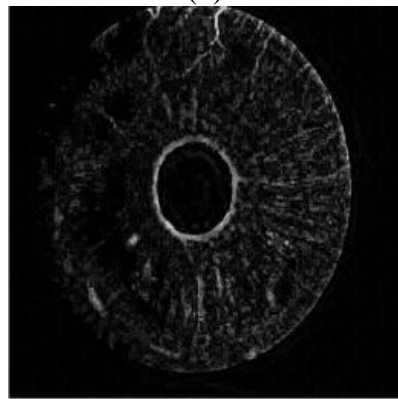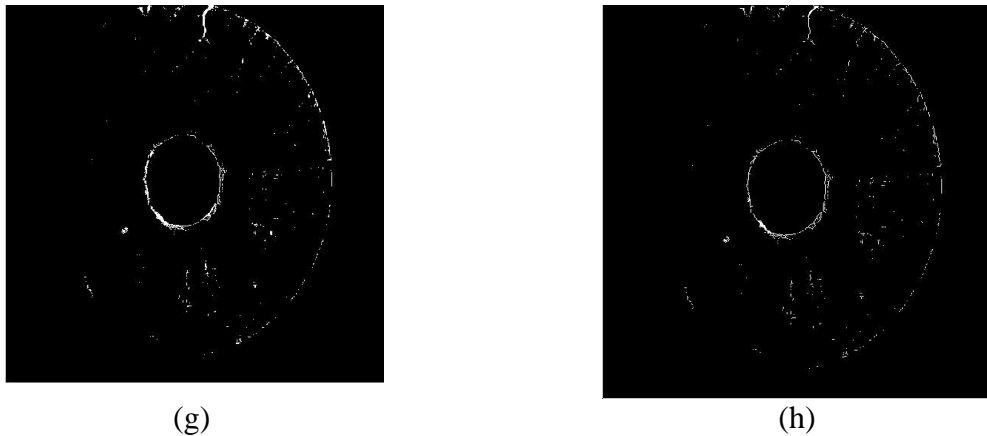
Figure 3.14: Experimental Results (a) original colour images (b) red component images (c) green component images (d) The difference between the red and green component image, before enhancement (e) The difference between the red and green component image after contourlet based enhancement (f) result after applying the contrast enhancement filter (g) binary images after segmentation that was used in the quantification. (h) Result after the Thinning algorithm is applied.

To investigate the practical usefulness of the proposed quantification approach, further experiments were performed on corneal images of two patients, one who had undergone corneal grafting and another who has been undergoing medical treatment, over a period of time. For the initial case the data was recorded over a three year period and for the latter case the data recording took over a period of seven months. Figure3.16 illustrates sequential images for the patient who had undergone corneal grafting and figure 3.17 illustrates sequential images for the patient who has been undergoing medical treatment. Charts 3.1 and 3.2 illustrate graphs demonstrating the healing progression for the patients. The progression of healing is well demonstrated by the graphs. This information will be vital to medical experts in monitoring patient care and evaluating the effect of different ways of treating corneal neovascularization.

A closer investigation of the test image (2) and (4) of figure3.14 illustrates that the proposed approach is also able to remove the consideration of suture marks that are present in the original image due to surgical intervention. Further, the approach has been able to perform remarkably well in the presence of significant effects of non-uniform illumination and reflections. As illustrated in figure 3.15.

(a)

(b)

(c)
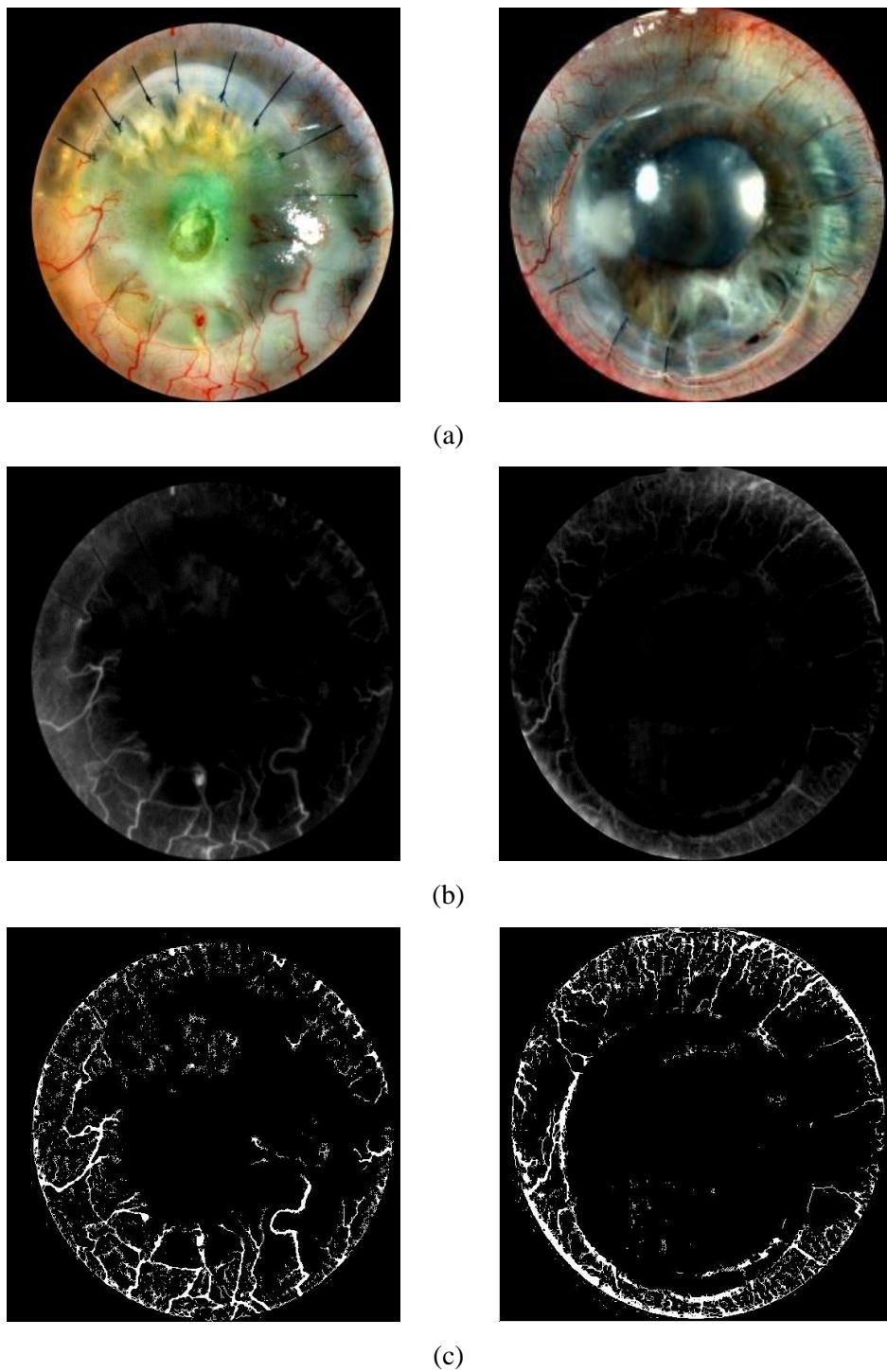
Figure 3.15: illustrated the proposed approach is also able to remove the consideration of the suture marks.

2007

2009

2010

(a)   (b)
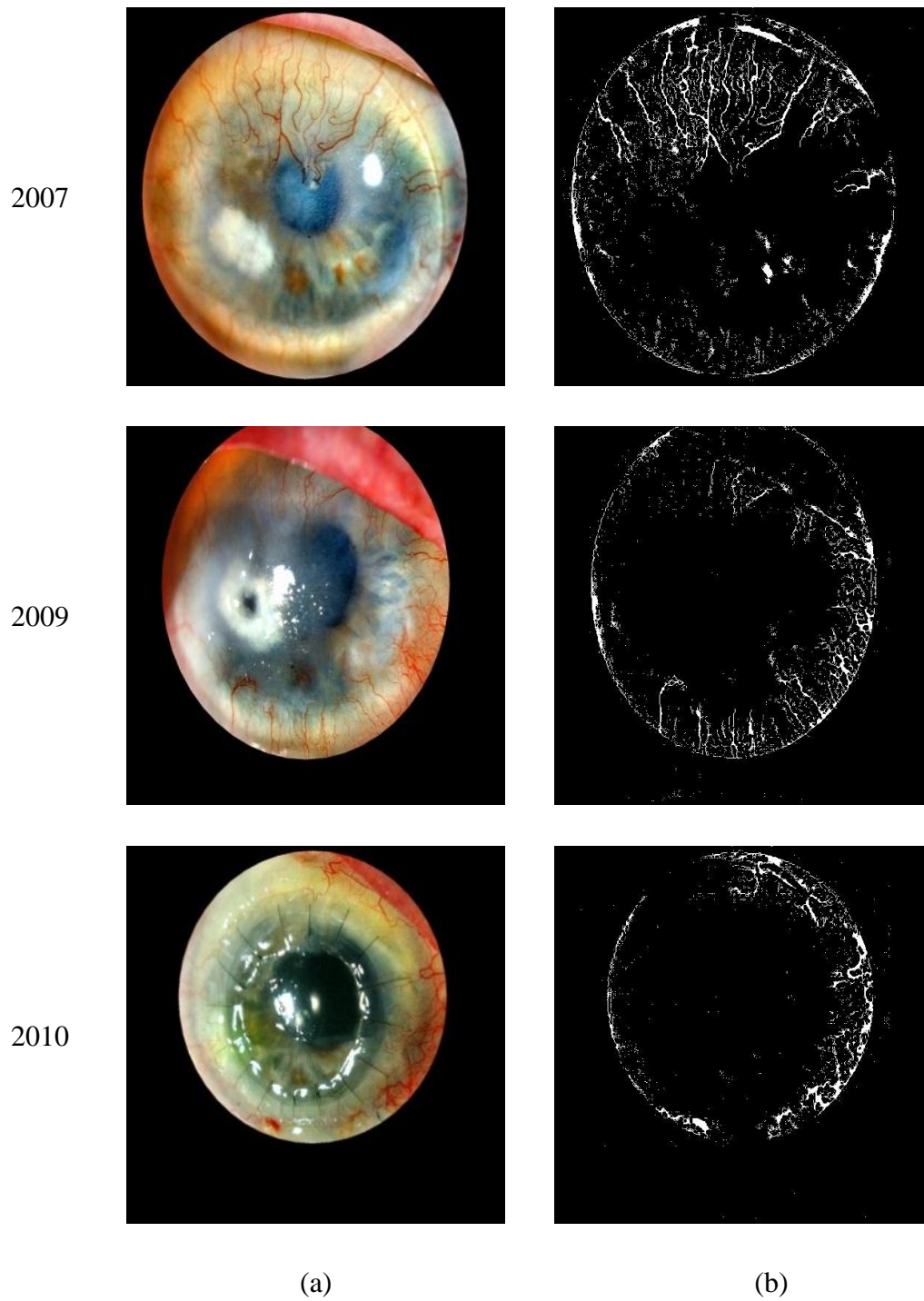
Figure 3.16: Results for a patient who has undergone corneal grafting. (a) Original Images. (b) Binary images after segmentation.
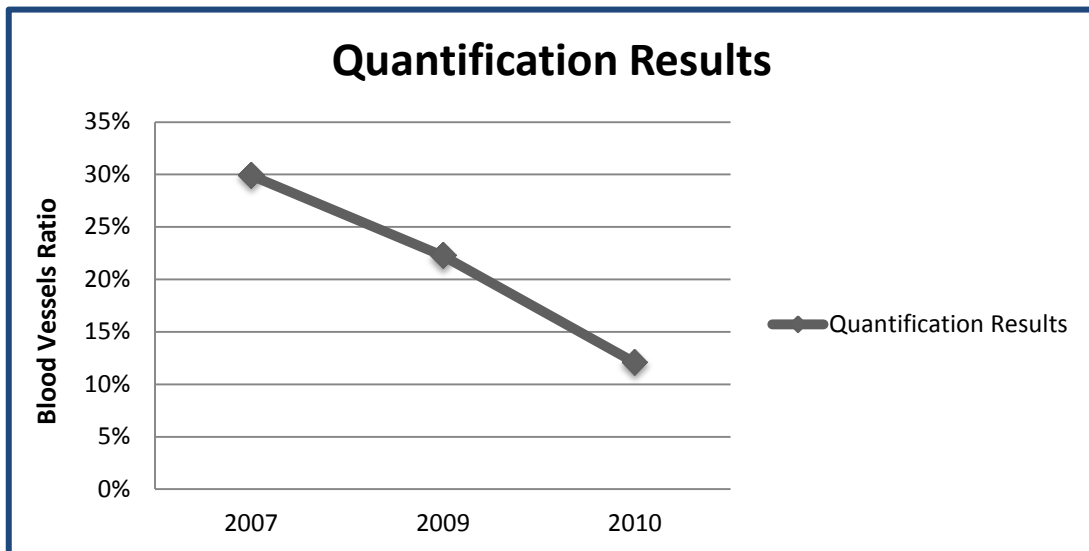
Chart 3.1: The healing progression of the cornea of the patient who had undergone corneal grafting. Refer to table 3.1.

May 2010

June 2010

December
2010

| (a) | (b) |
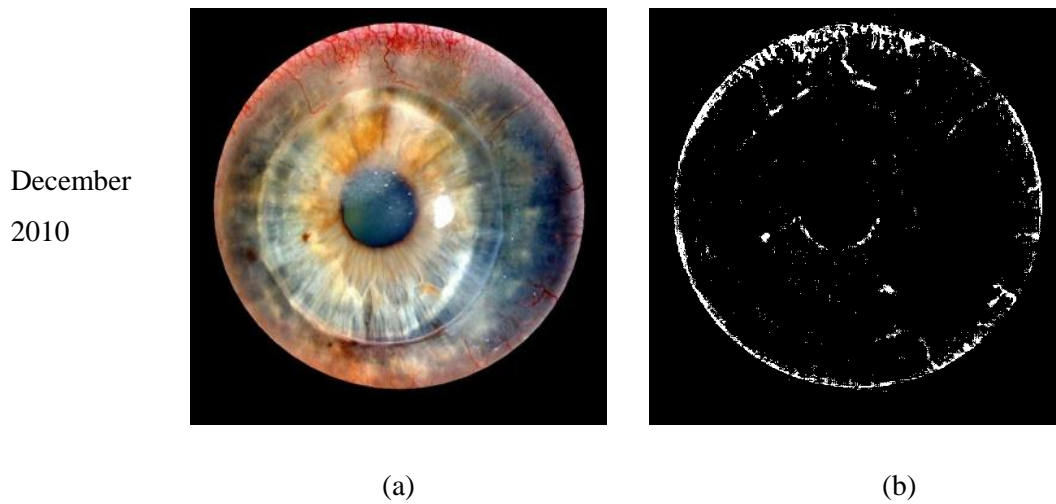
Figure3. 17: Results for the patient who has been undergoing medical treatment. (a)
Original Images (b) binary images after segmentation.
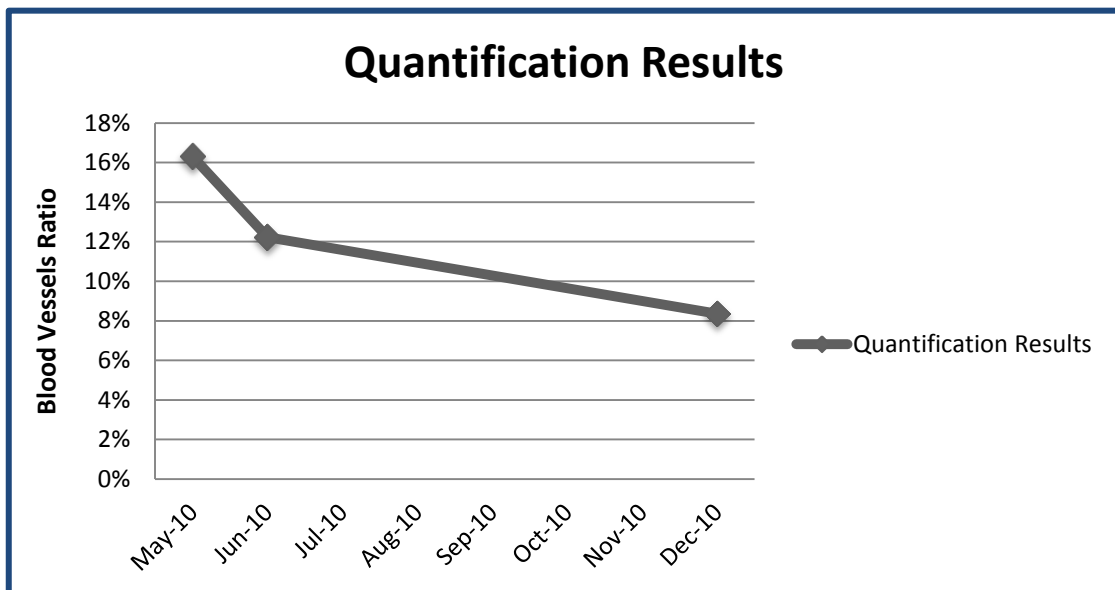
Chart 3.2: The healing progression of the cornea of the patient who had been
undergoing medical treatment. Refer to table 3.1.

3.5 Summary and Conclusion.

We have proposed an efficient computer aided approach to the quantification of corneal neovascularization. The approach is based on the use of Contourlet Transforms to enhance the blood vessels before their segmentation is carried out. A special feature of the approach is that it is robust to different levels of noise that may be present in corneal images. We have shown that the proposed approach is capable of performing effectively in the presence of noise, non-uniform illumination and reflections.

Quantifications experiments were done on six corneal images and the performance of the algorithms were analysed at various stages

CHAPTER 4

Application of Computer Vision Approaches to Evaluating the Effectiveness of Treatment of Corneal Ulcers.

Computer vision algorithms have been used in detecting ulcer areas in human skin, providing medical specialists with additional tools for investigating the treatment and recovery processes. A detailed literature review carried out by us revealed that this work is limited to the analysis of skin ulcers. Ulcers formed in eyes are a further medical condition that can benefit from using computer vision techniques for detailed diagnostics. In this chapter we present an approach for evaluating the effectiveness of treatment of corneal ulcers.

For clarity of presentation, this chapter is divided in to several sections. Section 4.1 introduces the reader to the research problem and discusses the need for a practical solution. Section 4.2 introduces the reader to the fundamental concepts, theories and techniques on which the proposed algorithms are based on and defines relevant terms used. Section 4.3 discusses the proposed method explaining a number of different algorithms used at different stages. Section 4.4 provides experimental results and a comprehensive analysis of the performance of the proposed method. Finally section 4.5 summarises and concludes the chapter.

4.1 The Research Problem.

The cornea is a thin, transparent membrane that covers the iris and the pupil of an eye. Any injuries that occur on the surface of the cornea can subsequently be

infected with bacteria, viruses or fungi that will lead to the formation of a Corneal Ulcer. Such a corneal ulcer known as an infectious ulcerative keratitis is an increasingly common reason for visual impairment and blindness. [55][56]

Segmenting corneal ulcers and finding the ratio between infected areas and the corneal areas provides the means to monitor the effectiveness of any treatment process being followed. To this effect many imaging devices exists (e.g. the popular 'slit lamp') that are capable of providing medical experts with high quality images that may be manually inspected and monitored (i.e. measuring the width and the height of a corneal ulcer from an image and calculating an estimated area of the ulcer). However, in most cases of corneal ulcers, manual monitoring of the healing process becomes an extremely tedious, time consuming task and is prone to human error.

The specialists treating corneal ulcers usually add a fluorescent dye to the eye to aid in manual medical diagnosis. Once the eye is treated with the dye, any ulcer areas that are present will appear in green (note: the exact colour depends on the dye being used) whilst the rest will appear blue. It is observed that the shape of an ulcer is rather complicated and the measurement of its area based on the measurement of its width and height only, will not provide an accurate answer. To this effect the automated or semi-automated computer aided inspection and measurement provides a quicker and more accurate alternative approach to the medical officials allowing their valuable time to be utilized in more important medical diagnosis related issues.

4.2 Research Background.

The automatic corneal ulcer segmentation algorithm proposed in this chapter attempts to overcome the limitations of the existing manual approaches and provide a practical solution. This section will introduce the reader to the fundamental concepts, theories and techniques on which the proposed algorithm is based and defines relevant terms used.

Note: Literature surveys carried out as a part of the research presented in this chapter revealed that no attempt has been previously made to segment and quantify corneal ulcers based on computer vision algorithms/techniques.

4.2.1 Colour Spaces.

This section introduces the key colour spaces used within this thesis to represent colour pixel values and the mathematics related to inter-colour space conversion. It presents two popular colour spaces, RGB and HSV. Preliminary experiments showed that it is difficult to segment the ulcer area in the original RGB colour space due to the difficulty of sensitively selecting the threshold for segmenting. However it was found that segmenting the ulcers in the HSV colour space is much easier and the selected thresholds will be more robust. Therefore in the following sections we describe the RGB and HSV colour spaces and conversion from the RGB space to HSV space

4.2.1.1 The RGB colour space.

The **RGB** (Red, Green, and Blue) colour space is the basic colour space widely used in the digital representation of colour picture elements, i.e. pixels. It is represented in the form of a cube in the Cartesian coordinate system in which the x, y and z axes are respectively represented by R, G and B colour components [57]. For a given digital colour image C, separate R, G, B vectors are used to represent each pixel (x, y) as defined in equation 4.1.

$$C(x, y) = (R(x, y), G(x, y), B(x, y))^T = (R, G, B)^T \qquad (4.1)$$

$(R, G, B)^T$ is an explicit combination the three vector values representing one particular colour in the RGB colour space.
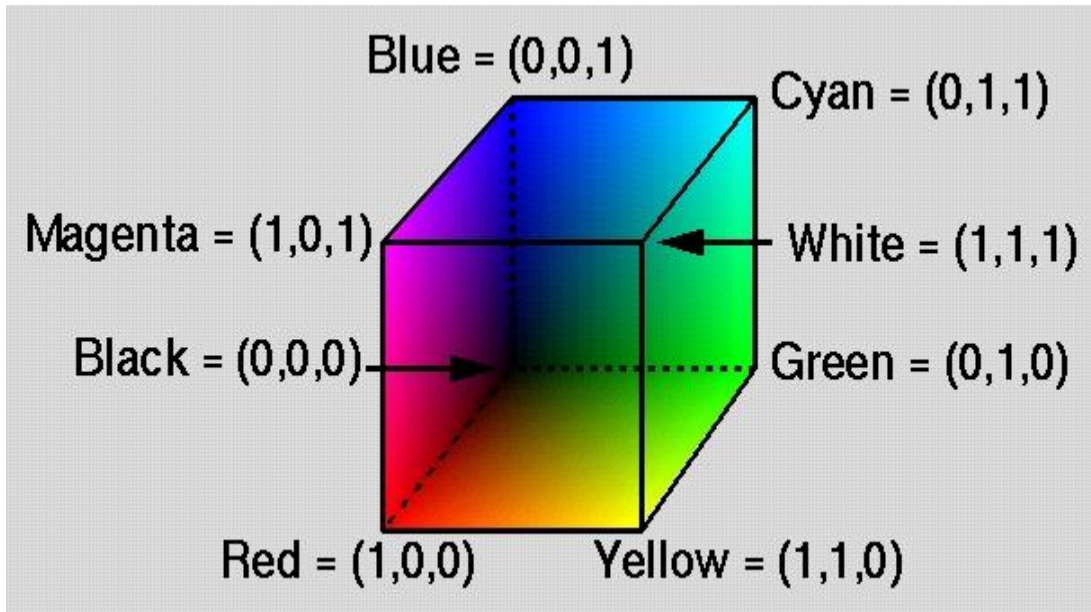
Figure 4.1: RGB colour cube, (R, G, B) vector represents a unique colour value [58].

Figure 4.1 shows a RGB colour cube in which R, G and B channels form the three dimensional vector space. In a 8-bit / byte word the minimum value of any RGB channel is represented by 0 and maximum by 255. The RGB colour space is also considered an additive colour space due to its ability to form various shades of colours by combining different intensities of the three primary colours i.e. R, G and B. In particular in the RGB colour space an all-zero vector represents a pixel of black colour and all-one vector represent a pixel of colour-white. For further details on the RGB colour space and their use in digital and print media, readers are referred to [57] and [59].

4.2.1.2 The HSV colour space.

HSV (Hue, Saturation and Value) colour space is mostly utilised in the fields of computer vision and computer graphics. Figure 4.2 illustrates the standard representation of the HSV colour space, where Figure 4.2(a) represents the HSV

colour gamut in which the H (Hue) component defines the fundamental colour of a pixel and its shades. Different shades and colours are defined and represented when moving anti clock wise from 0 degrees to 360 degrees. S (Saturation) defines and represents the shades of pixels available to represent a given colour. S increases towards the edge of a circular cross section of the cone and decreases towards the centre. 1 and 0 represent the highest and lowest saturations of a colour, respectively. V (Value) contains information related to the brightness or darkness, i.e., luminosity of a pixel. V increases when moving towards pixels with higher intensity colour values and reduces in the opposite direction. 1 and 0 represents the highest and lowest intensity values of a colour, respectively.

(a) (b)
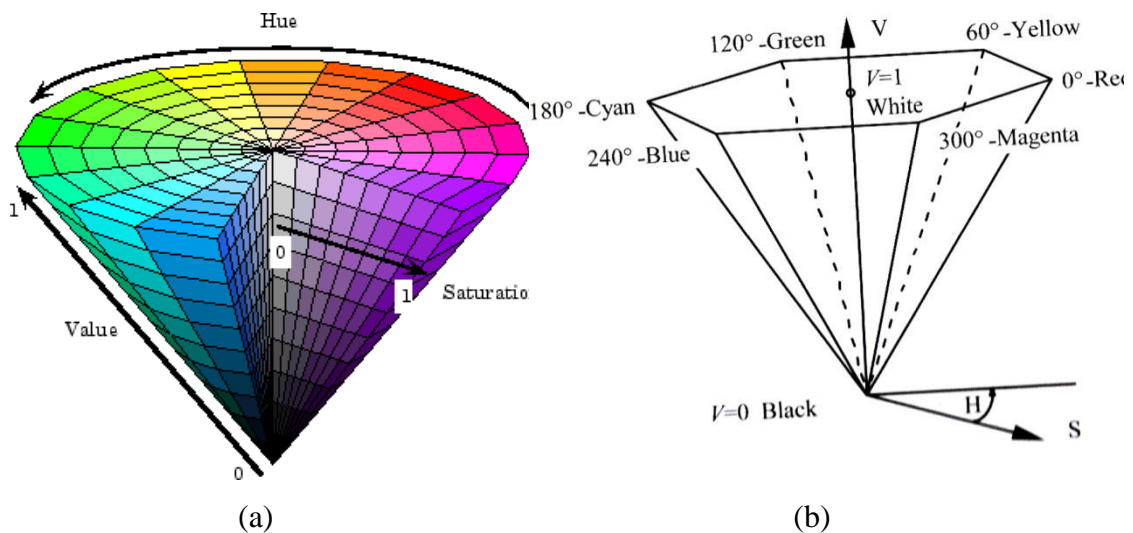
Figure 4. 2: HSV colour space, (a) HSV colour gamut [60] (b) HSV colour gamut representing angular values of different colours [57]

Figure 4.2 (b) illustrates how the H component, using angular values, define all colours that the HSV colour gamut can represent. Its circular gamut starts and ends at the same colour, which is the Red colour found at 0° and 360°. Moving anti clock wise in the gamut the colours, Yellow, Green, Cyan, Blue, Magenta are represented at 60°, 120°, 180°, 240° and 300° respectively.

4.2.1.3 Colour space conversion: From RGB to HSV.

An image represented in the RGB colour space can be converted to an image represented in the HSV colour space using the equations 4.2, 4.3 and 4.4 below [61].

$$H = \cos^{-1}\left(\frac{0.5\,(R - G) + (R - B)}{\sqrt{(R - G)^2 + (R - B)(G - B)}}\right) \tag{4.2}$$

$$S = 1 - \left(\frac{3}{R + G + B}\right) min(R, G, B) \tag{4.3}$$

$$V = max(R, G, B) \tag{4.4}$$

There are inherent dependencies between the three HSV components. H component will have no significance when S or V are representing by the lowest value i.e. 0. The colour will be shown black if V component is represented by the lowest value. Pure white colour is obtained when the V component is represented by the highest value, i.e. 1 and S component is represented by the lowest value, i.e. 0. For further useful reading on the HSV colour space readers are referred to [57] and [59].

4.3 Proposed Method.

Evaluating the effectiveness of treatment of corneal ulcers requires the determination of the ratio between the total area occupied by the ulcers and the total area of the cornea. This requires the determination of both the boundary of the cornea and those of the ulcers.

The proposed system comprises of a number of stages of image processing and analysis as illustrated by the system block diagram of figure 4.3. Firstly a clear, well lit up image of the cornea is taken using a high resolution colour camera and a flash set up mounted on a traditional slit lamp. Subsequently the captured images are

digitally stored in a computer memory for further processing and analysis as described below.
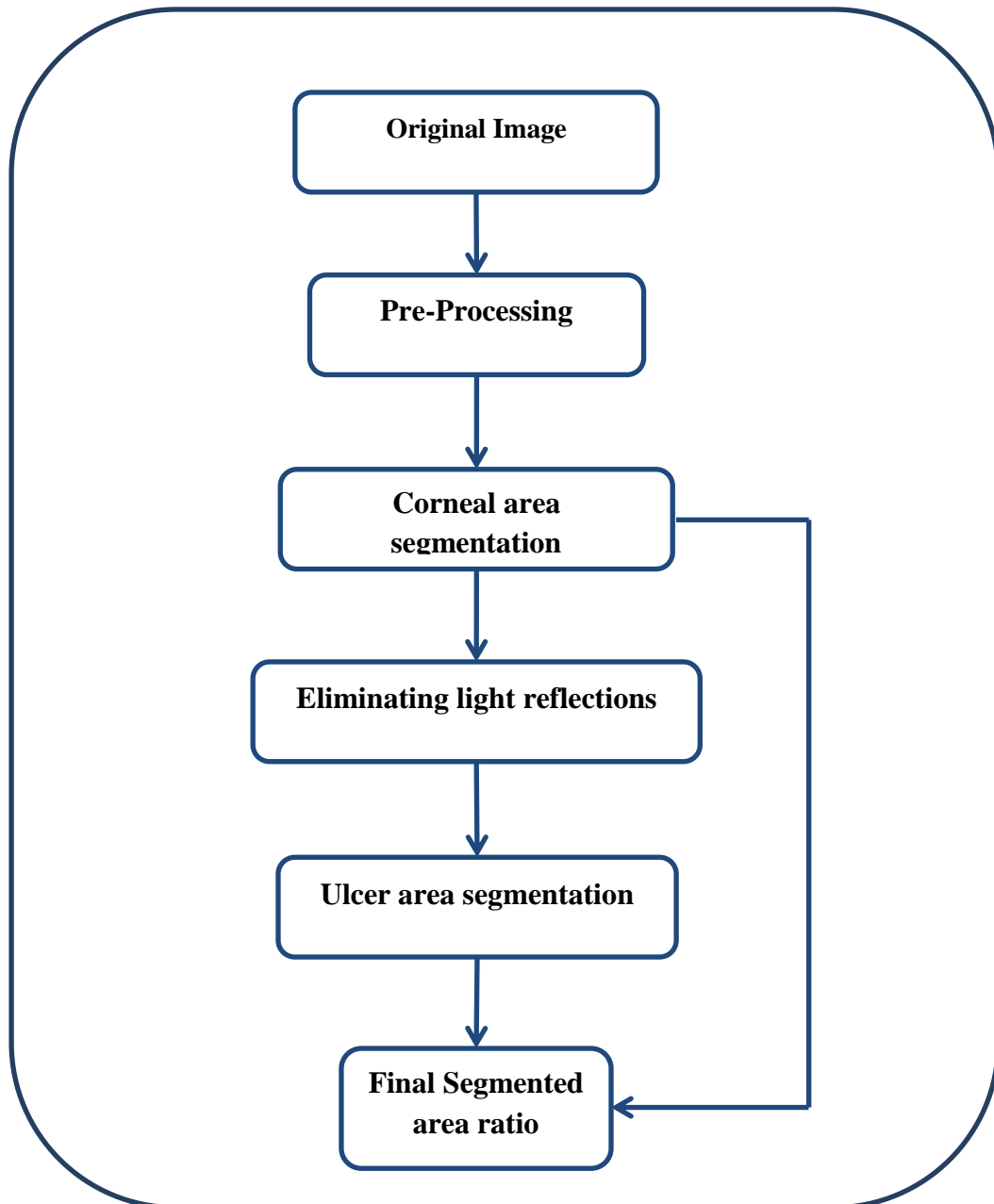
Figure 4.3: Proposed computer aided analysis approach.

4.3.1 Pre-Processing Stage.

In the pre-processing stage localised histogram equalisation [62] is used to bring back detail in any over or under exposed areas of the original corneal image. This is a vital stage given the nature of flash photography carried out on a naturally glossy surface of a human cornea. However in practical implementation of the proposed system this stage has been left as an optional stage that can be activated by the user if required rather than being a stage that is compulsory to be used. It is noted that flash photography on a shiny surface can lead to certain areas being over exposed to an extent that the above pre-processing stage will be deemed to be ineffective. The removal of such areas is handled by the process described in section 4.3.3, i.e., eliminating reflections.

4.3.2 Corneal Area Segmentation.

After the pre-processing stage, similar to the approach used in chapter-3, a semi-automated, accurate, corneal boundary segmentation approach (see figure 4.4) is used. In the initial stage an ellipse is drawn which has dimensions along the minor and major axes, approximately equal to half of the radius of circular edge (determined by a Canny edge detector with appropriate threshold settings) of the cornea. The system then allows the user to move the boundary and the entire elliptical shape, to enable its boundary's best alignment with that of the corneal boundary. Although this step requires manual intervention the process is easy and is worth the effort due to the difficulty of automatically detecting the accurate shape of a corneal boundary using any existing image processing approach.

It is noted here that once the corneal boundary is extracted the area outside it is ignored from being further processed or analysed based on the medical assumption that what is important is the determination of a given treatment process's impact on the ulcer area within the cornea. In other words this stage acts as a spatial, Region-of-Interest (ROI) based filtering stage.

<center>(a)   (b)</center>

<center>(e)</center>
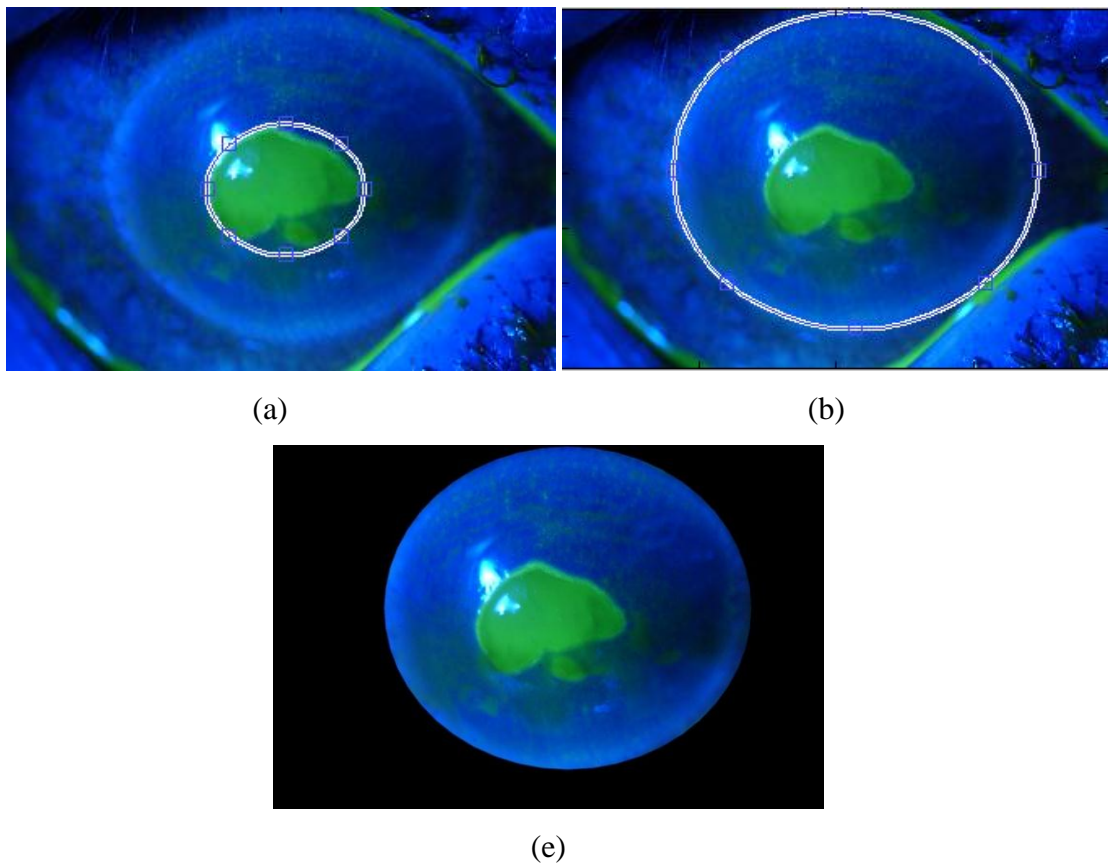
Figure 4.4: Semi-automated Segmentation of the Cornea (a) initial ellipse automatically has drawn within the cornea (b) manually adjusted ellipse to coincide with the corneal boundary (c) the final result after ignoring the area outside the corneal boundary.

4.3.3 Eliminating Light Reflections.

Section 4.3.4 will explain the colour based segmentation of corneal ulcer areas based of identifying areas that are 'green' in colour. It is noted that highlighted over exposed segments of the ulcer areas will not be detected as 'green' and hence will erroneously contribute towards ulcer area measurement (by not being inclusive) if not otherwise identified. We deal with the removal of potential reflections from the affected areas by making a logical comparison between the output results of the colour segmentation algorithm on corneal images taken from more than one view

direction, i.e., slightly different angles. Under viewpoint variation the position and the shape of the light reflection areas will change considerably as compared to the position and shape of the actual ulcer areas. It is noted that the potential normalised (i.e. after dividing by the area of the cornea) ulcer area will remain highest in pixel value in an image where the reflection area is outside the surface of the ulcer (see figure 4.5). The above rules are used to remove reflective areas from the ulcer area that is required to be accurately determined.

(a)

(b)
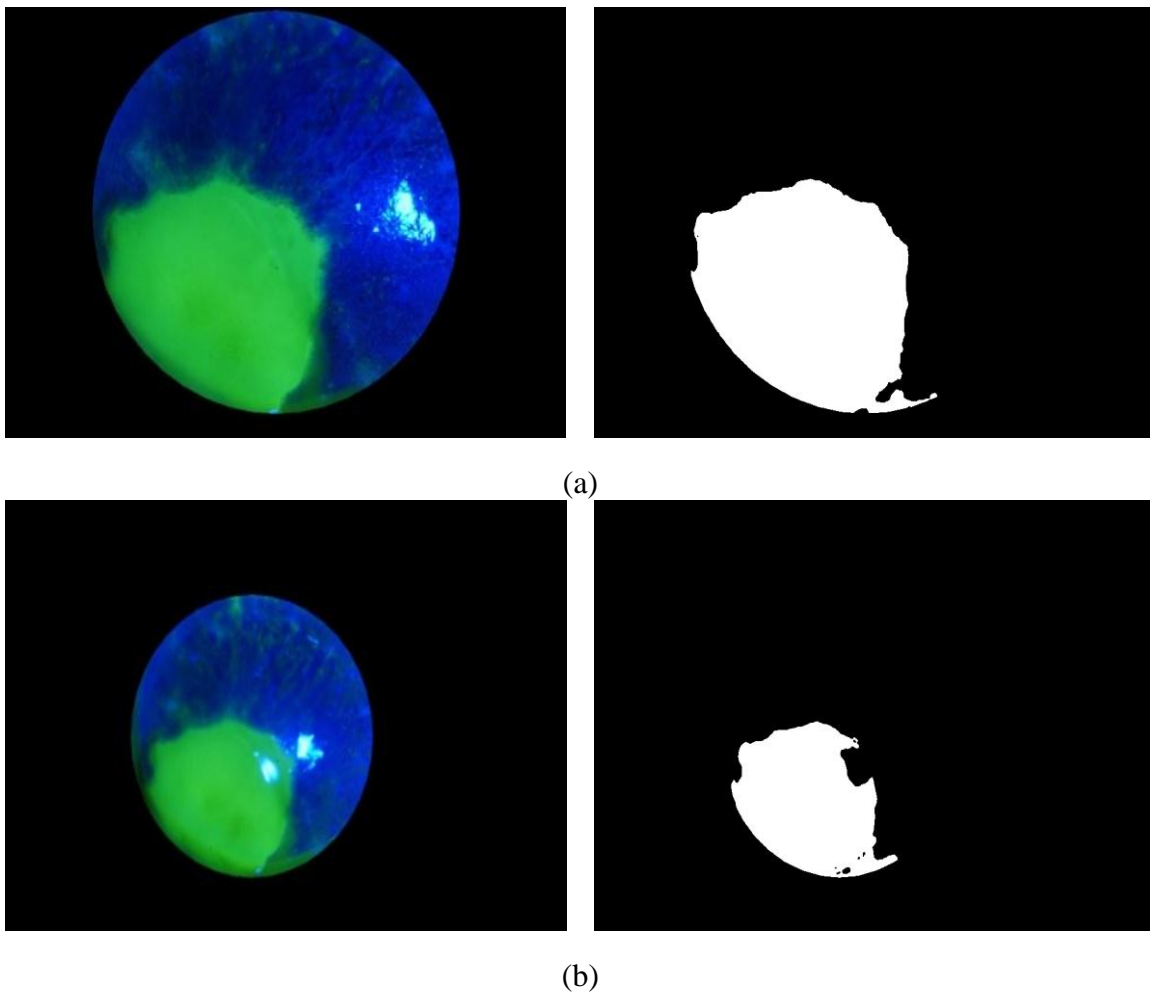
Figure 4.5: Illustrating the elimination of a reflective area within an ulcer area (a) view with the reflective area outside the ulcer area, (b) view with reflective area both within and outside the ulcer area.

4.3.4 Ulcer area segmentation and evaluation.

The output from stage 4.3.2 above is an image that segments the corneal area only (see figure 4.5(a) and 4(b)). In order to segment the ulcer area (the green pixels) a colour based segmentation process is proposed. Figure 4.6 illustrated the general steps of this stage.
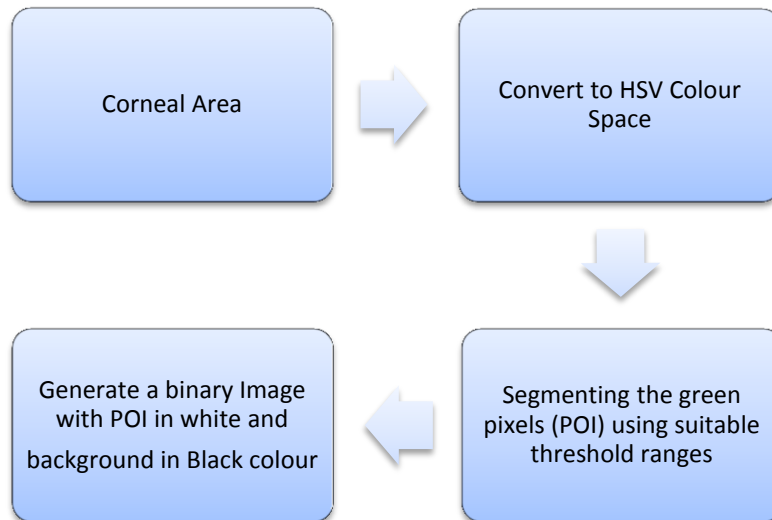
Figure 4.6: Colour based segmentation: The general process.

In this proposed algorithm we uses a colour based segmentation algorithm to segment the ulcer area instead of a feature based segmentation approach, as the ulcers areas have non-uniform shape and non-identifiable features. Further the images produced by the medical testing process are of two clear colours (ulcer area in green and the rest of the eye is blue) with different gradations, thus making colour based segmentation an accurate and more suitable approach to follow.

Due to the differences between light sources and the external influences on lighting we get a different gradation and variation in the illumination of the green colour (as defined by the RGB colour space) between test images. Therefore, we have used HSV colour space to segment the ulcer area due to its proven ability to enhance the

segmentation result [63]. RGB images taken from the normal camera are first transformed to the HSV colour space using equation 4.2, 4.3, 4.4 [64].

Where R,G and B represent the three channels of a RGB image. Ulcer area can be (green pixels) segmented using all three of the above components as shown in equations 4.2,4.3,4.4 i.e. H, S and V. H (Hue) component contains the original colour itself, while S (Saturation) generates different shades of a particular colour and V (Value) contains information related to brightness or darkness of the colour. Every colour in the H component of the HSV colour gamut has an angular value which varies according to the corresponding S and V components. If S and V components remain constant i.e. S = 100% and I = 100% then Green and Blue colours can be found at 120° and 240° respectively. These values are determined by taking the histogram of H, S and V components. [65], [66].

Subsequently the threshold values described in [63] is used to segment the green ulcer area. In doing so a binary image with white representing pixels values belonging to the corneal ulcer and black representing pixel values outside is created. Then a median filter is used on the binary image to remove holes.

Finally for each image the ratio between the total amount of pixels belonging to the entire corneal area and the total amount of pixels belonging to the ulcer area, is calculated. This ratio plays an important role in the analysis of the effectiveness of a treatment scheme adopted by medical professionals, i.e. the increase of the ratio means that the treatment is effective.

4.4 Experimental Results and analysis.

Experiments were performed on a set of five images with various sizes of corneal ulcers. The results are illustrated in Figures 4.7. The results illustrate the capability of the proposed approach to segment the ulcers irrespective of the gradation of the green colour in the images.

	Cornea Area	Ulcer Area	Ratio
Case1	232045	33204	%14
Case 2	248734	43227	%17.4
Case 3	241451	26997	%11.2
Case 4	258168	253901	%98
Case 5	315091	104475	%33

Table.4.1 segmentation results.

Figure 4.7 Experimental Results. (a) is the original colour images, (b) is the segmented corneal area, (c) is the colour based segmentation of ulcer areas, (d) is the binary images after filtering.

Case 1

(a)   (b)
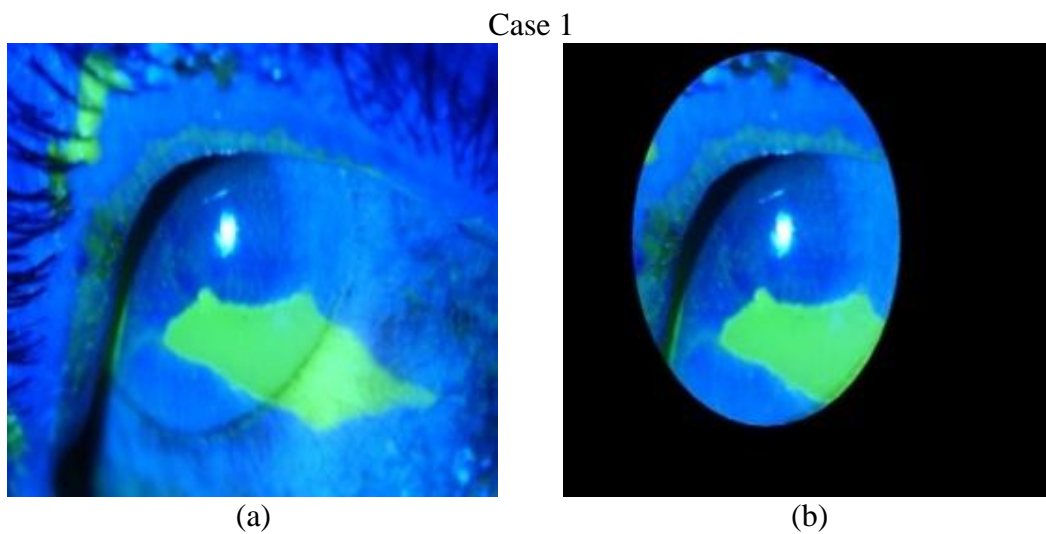
(c)

(d)

Case 2
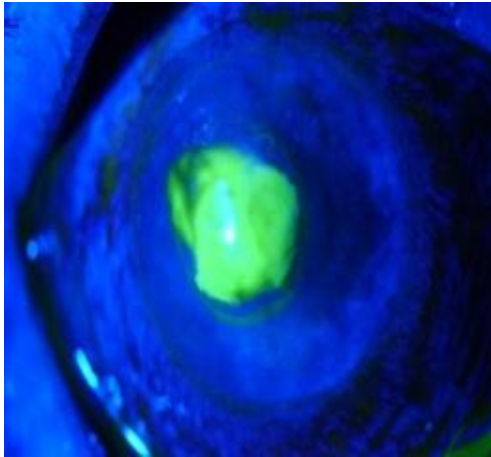
(a)
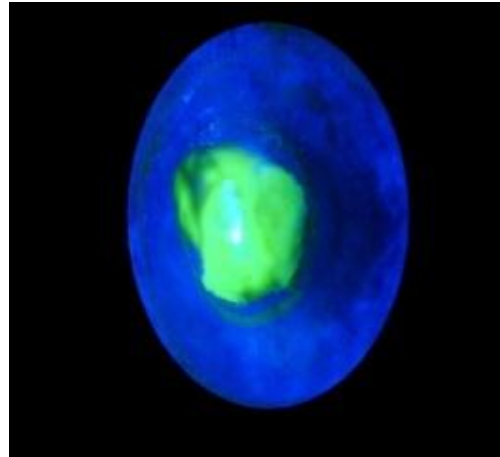
(b)

(c)
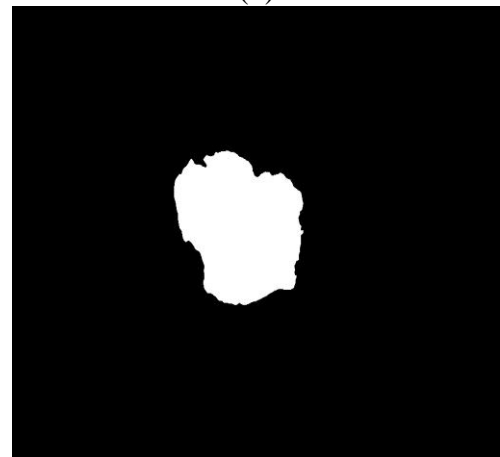
(d)

Case 3

(a)

(b)

(c)

(d)

Case 4

(a)

(b)

(c)

(d)

Case5
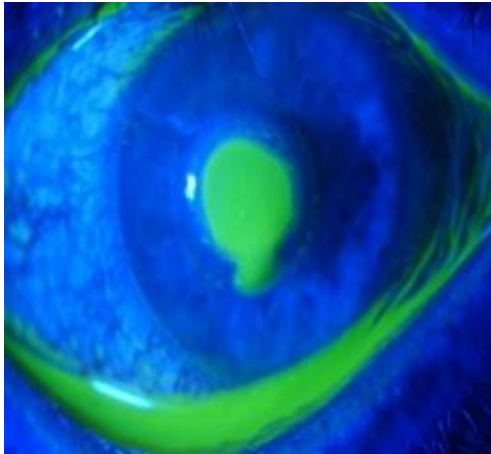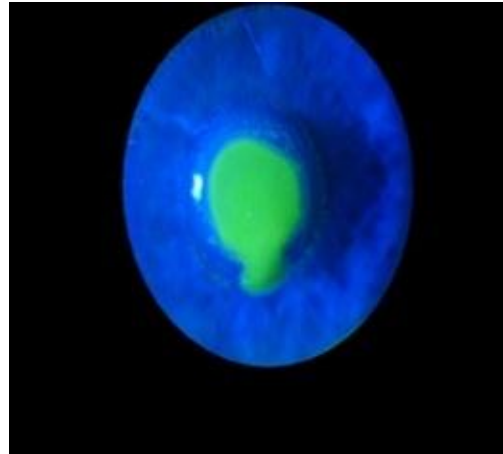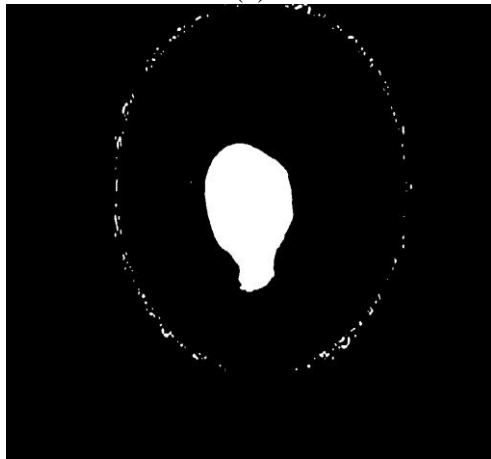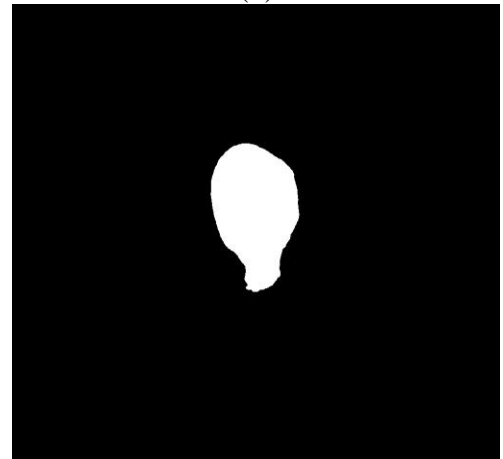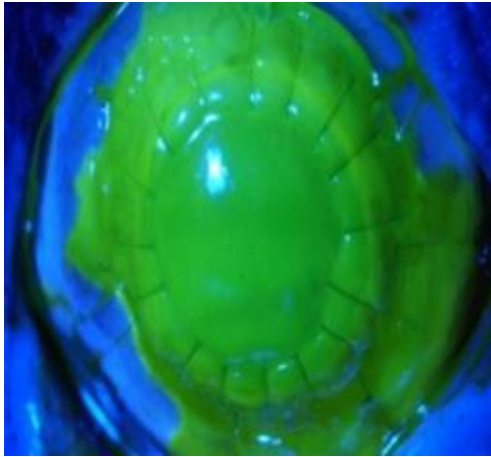
(a)   (b)
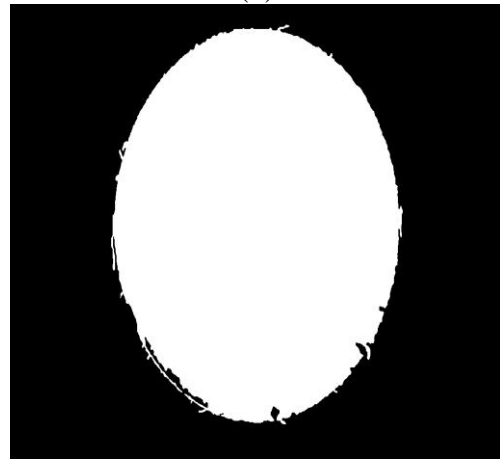
(c)   (d)
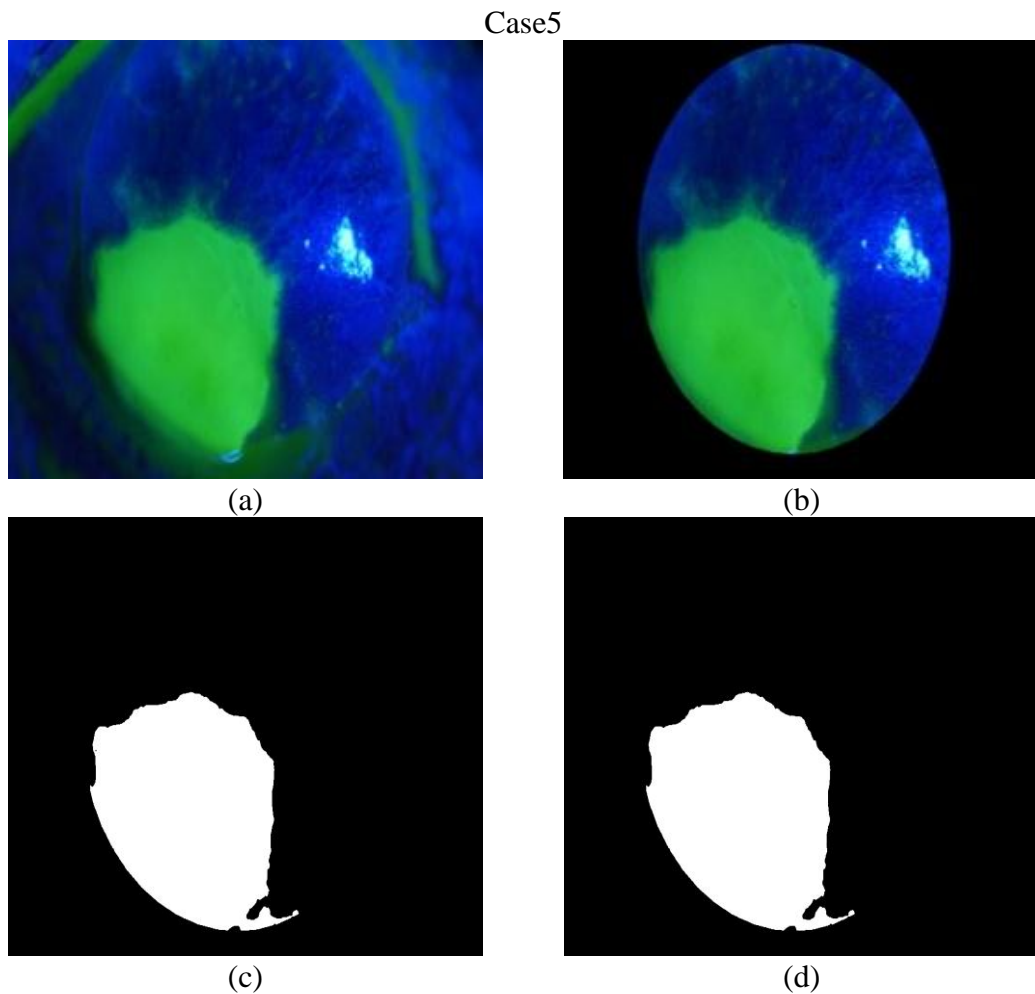
Figure 4.7: Experimental Results (a) original colour images (b) segmented corneal area (c) colour based segmentation of ulcer areas (d) binary images after filtering.

A closer investigation of the test images above shows that when the position of the light reflection is entirely confined within the ulcer area the median filtering stage applied subsequently removes reflective areas and replaces such areas with the background ulcer area, resulting in a correct outcome for the ratio being calculated. The thresholds used for colour based segmentation in the HSV colour space remains largely stable.

Figure 4.7 illustrates that the corneal area segmentation used before the ulcer area segmentation removes from the ulcer areas outside the corneal area from further investigation (see case-1 and case-3), as was required by the system that was being developed under the guidance of medical experts.

Figures 4.8, 4.9 and 4.10 illustrate cases of three different patients who had undergone treatment within a specified period of time, whose recovery process was recorded by the medical experts as new images taken on a monthly basis. Graphs in Charts 4.1, 4.2, 4.3 plot the corneal area change with respect to time, illustrating a clear recovery of the medical condition.

(a)   (b)
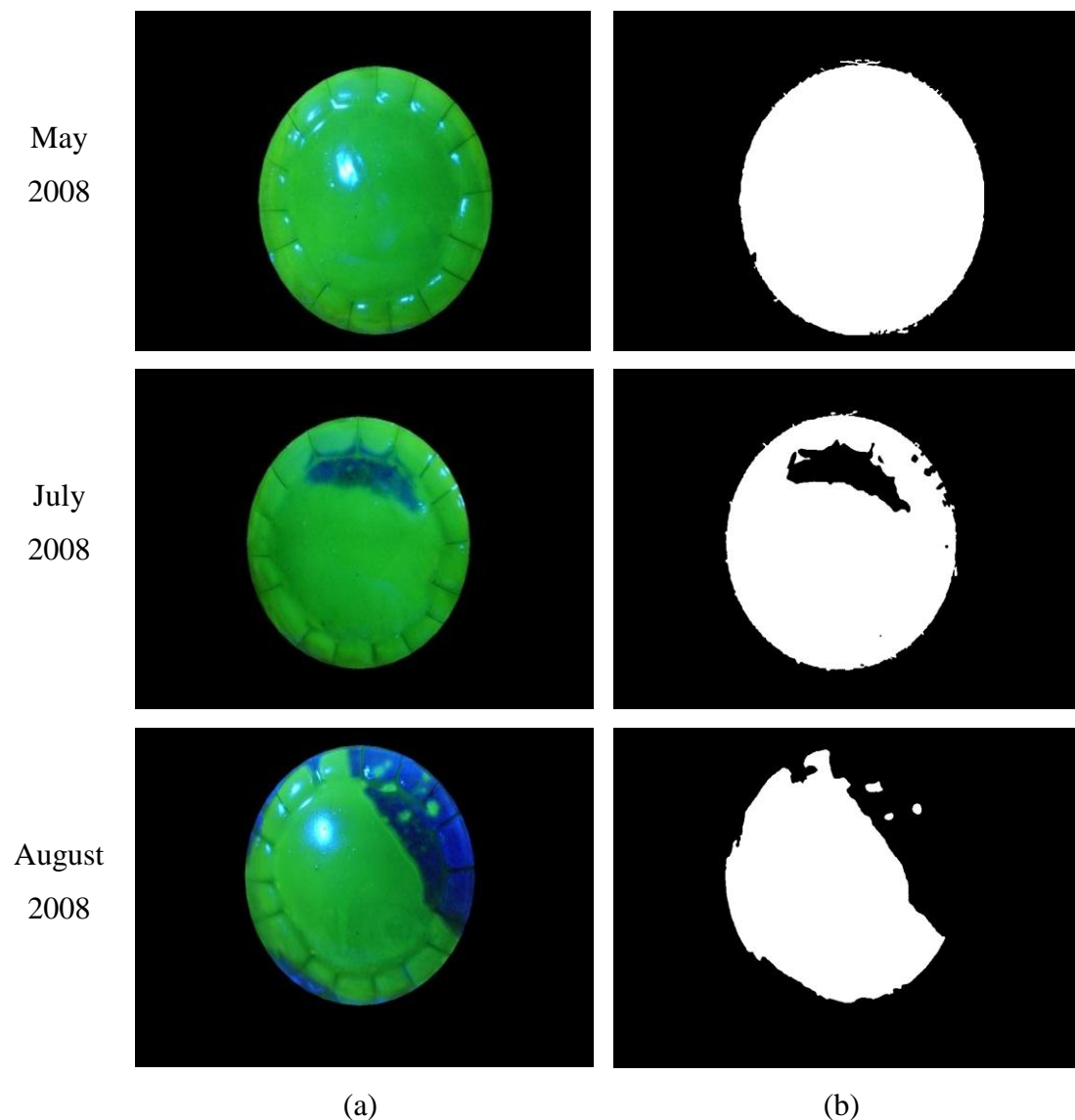
Figure 4.8: Results for the patient who has been undergoing medical treatment. (a) Original Images (b) binary images after segmentation.
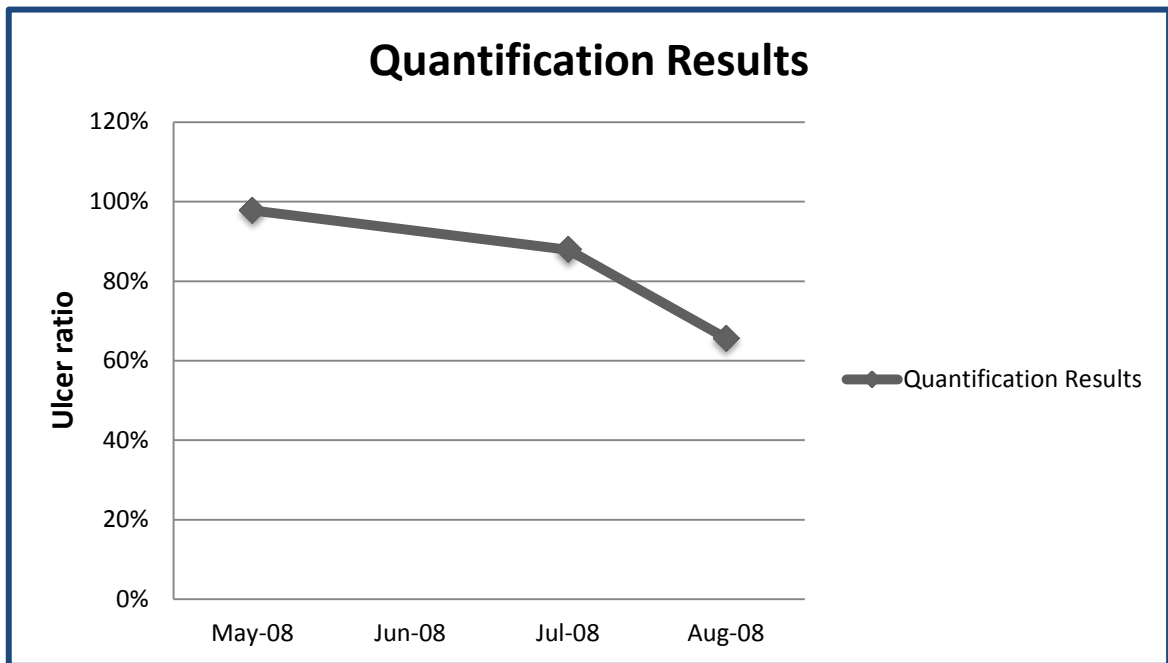
Chart 4.1: The healing progression of the cornea of the patient who had been undergoing medical treatment. Refer to table 4.1.

July
2008

(a)   (b)
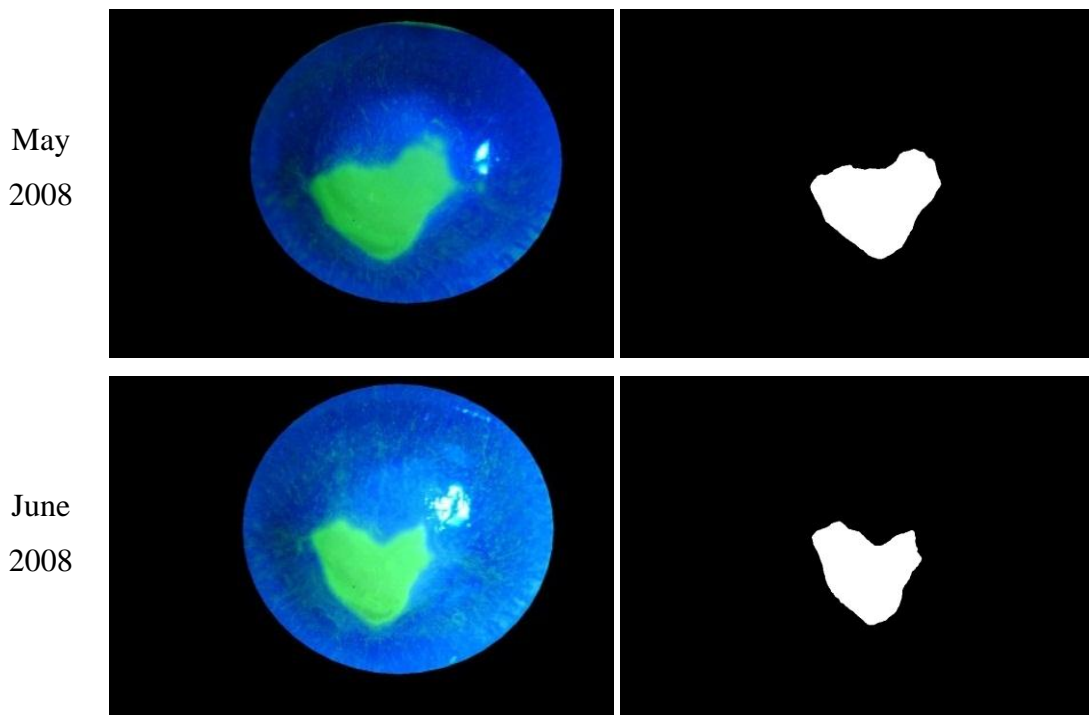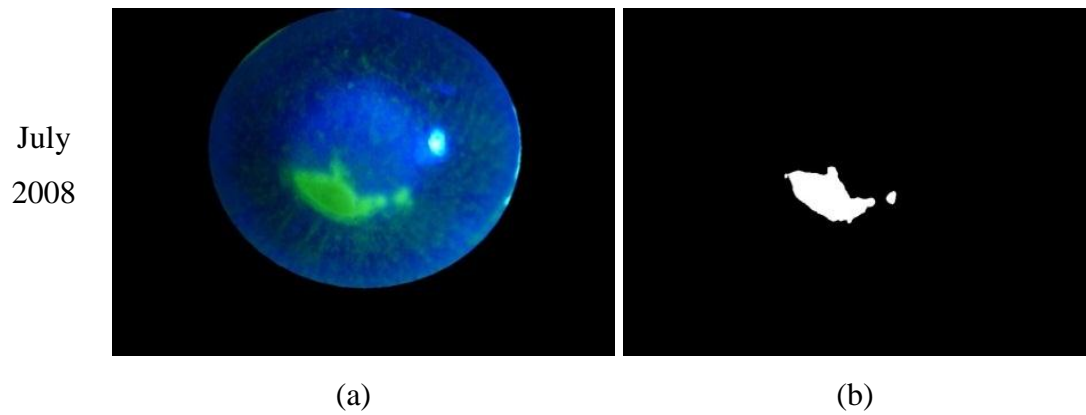
Figure 4.9: Results for the patient who has been undergoing medical treatment. (a) Original Images (b) binary images after segmentation.
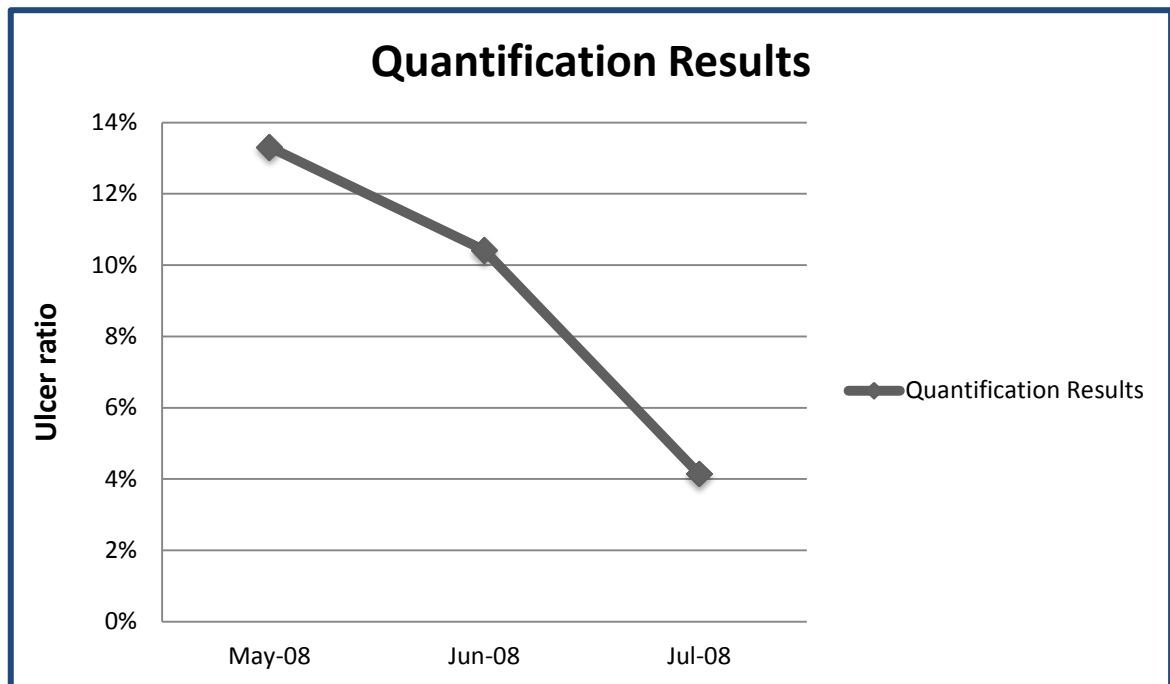
Chart 4.2: The healing progression of the cornea of the patient who had been undergoing medical treatment. Refer to table 4.1

November
2008

January
2009

March
2009

(a)   (b)
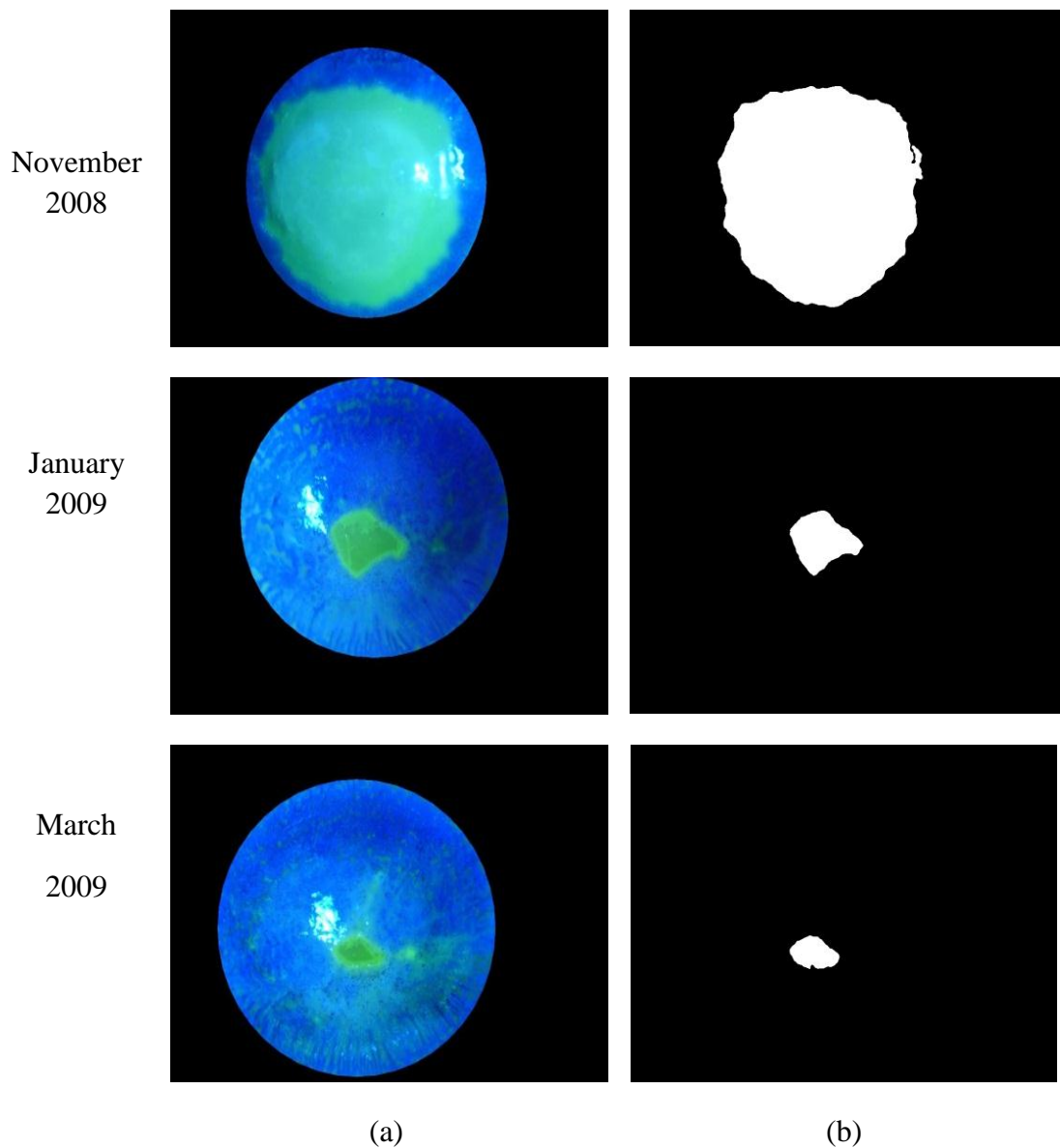
Figure 4.10**:** Results for the patient who has been undergoing medical treatment. (a) Original Images (b) binary images after segmentation.

It is noted that the fully automated selection of thresholds used for the segmentation of corneal area can be a challenging task given the fact that the dye's being used can appear in slightly different colours and the colour of the eye of a person can vary, resulting in slightly varying background colour for the segmentation algorithms to operate on. Hence in the practical system designed, implemented and tested we have made the thresholds variable from a pre-defined default value, enabling medical experts to vary them to obtain the best possible visual result of segmentation. This manual intervention does not undermine the

purpose of the system being designed as the idea is to obtain a method for the calculation of the ration of between the ulcer and corneal areas, which through existing methods is done at a very low level of accuracy using entirely manual processes prone to human error.
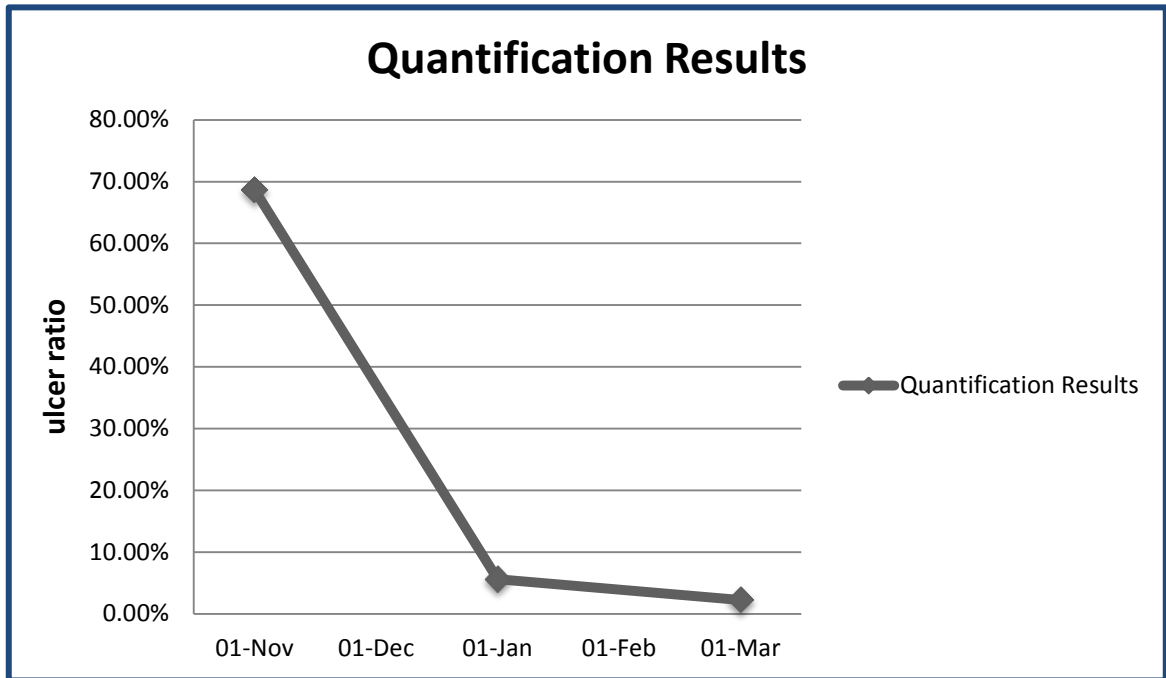
Chart 4.3**:** The healing progression of the cornea of the patient who had been undergoing medical treatment. Refer to table 4.1

4.5 Summery and Conclusion.

We have presented an efficient computer aided colour based segmentation approach to detect and segment corneal ulcers. We have provided experimental results on a sample of five corneal images with different sized ulcers. The performance of the proposed algorithms were analysed at various stages of the image processing pipeline to demonstrate the use of each stage. Further the approach was used to analyse the impact of a treatment process on a corneal ulcer by measuring the

change of the ratio corneal area to ulcer area over a given period of time, demonstrating its practical use in medical diagnostics.

It has been recognised that for making the proposed approach fully automatic, an efficient and robust approach to the determination of corneal boundary is required. In chapter-6 a detailed account of further research possible in this area will be presented.

CHAPTER 5

Total Hip Replacement

The hip is one of the body's largest joints. It is a ball-and-socket joint. The socket is formed by the acetabulum, which is part of the large pelvis bone. The ball is the femoral head, which is the upper end of the femur (thighbone). The most common cause of chronic hip pain and disability is arthritis. A number of diseases such as osteoarthritis, rheumatoid arthritis, and traumatic arthritis may result in damaged hip bones requiring surgery and replacement.

Total hip replacement is a surgical procedure in which both the thigh bone (Femur) and the socket are replaced with implant prosthesis. Hip replacement surgery is often required to be medically monitored to keep track of any possible cases of failure. This will result in early corrective action being possible thus avoiding likely acute pain for the patient.

Dislocation and misalignment are two important causes of hip replacement failure (see figure 5.1). Traumatology services spend a substantial amount of time on the pursuit of patients with prosthesis in order to check the state and feasible dislocation or misalignment of total hip replacement implants. This prognosis process is based on frequently manually inspecting a series of X-ray images that are gathered for a patient who has undergone total hip replacement surgery. In some cases the prosthesis may move fractionally resulting in traumatology services failing to detect a possible failure. This could be a significant issue that may lead to traumatic pain for the patient [67][68].

(a)   (b)
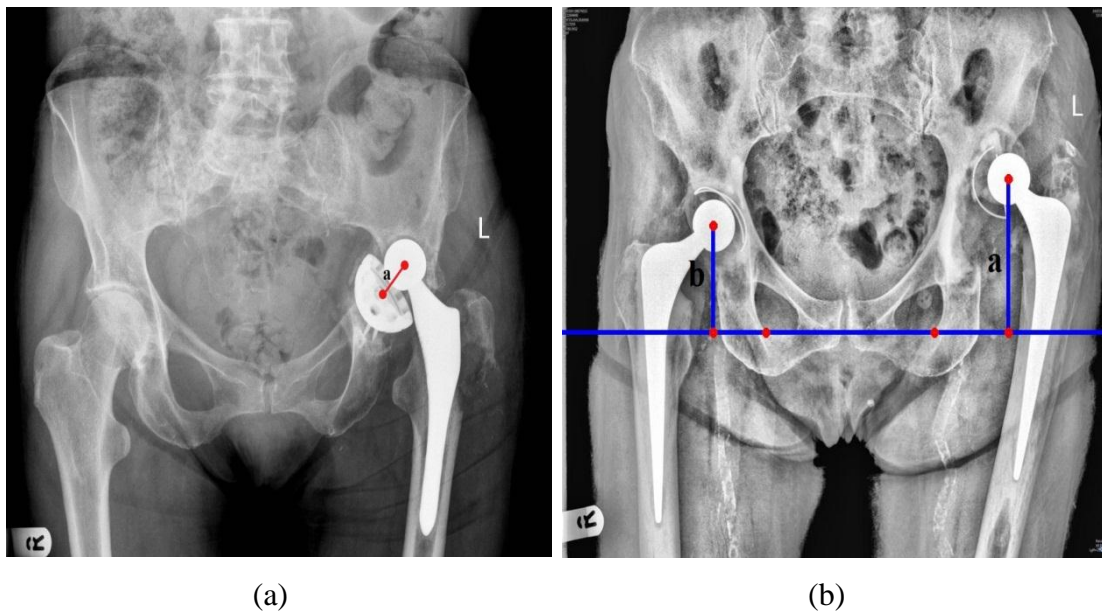
Figure 5.1: (a) Dislocation - a> threshold
(b) Misalignment - |b-a|>threshold.

A solution exists in using automated and/or semi-automated computer vision approaches to carry out this task leading to the possibility of reducing risks due to human error. The literature review presented in chapter 2 revealed a number of attempts [38-42] that have been taken by researchers worldwide towards providing computer vision systems which assess radiographs of patients who have had total hip replacements as part of their post-operative monitoring with the aim of providing early identification of potential implant failure.

For clarity of presentation, this chapter is divided into 5 sections. In addition to this section that introduces total hip replacement and the importance of its treatment, Section 5.1 introduces the research problem and the need for a solution. Section 5.2 introduces the fundamental concepts, theories and techniques on which the proposed algorithms are based on and defines relevant terms used. Section 5.3 discusses the proposed method. Section 5.4 provides experimental results and a comprehensive analysis of the performance of the proposed method. Finally Section 5.5 summarises and concludes the chapter.

5.1 Introduction.

The first step of detecting dislocations and misalignments is to define the positions of the key points that can be used in measuring dislocations. As discussed in chapter 2, a number of automatic and semi-automatic algorithms have been proposed in the past to this effect [38-42].

This chapter presents a Hough Transform and Filtered Back Projection based approach to detect regions of possible failure in total hip replacement x-ray images. The novelty of this work is the use of an automated computer aided approach that helps medical practitioners in assessing possible failures in total hip replacement x-ray images.

5.2 Research Background.

The hip replacement x-ray image analysis algorithms proposed in this chapter attempts to overcome a number of limitations of existing approaches and provide practical solutions. This section will introduce the reader to the fundamental concepts, theories and techniques on which the proposed algorithms are based and define the relevant terms used.

5. 2.1 Histogram Equalisations.

The Histogram equalisation usually increases the global contrast of the images. This normally works when the pixel of the image is represented by close contrast values. Through this adjustment, the intensities can be better distributed on the histogram. By effectively spreading out the most frequent intensity values this will allow for the areas of lower local contrast to gain a higher contrast.[69][70]
Histogram equalisation is usually introduced using continuous, rather than discrete, process functions. An image contains continuous intensity levels (in the interval

[0,1]) and that the transformation function f which maps an input image $A(x, y)$ onto an output image $B(x, y)$ is continuous within this interval.

It is assumed that the intensity density levels, e.g. $D_B = f(D_A)$ (transfer law) is single valued and monotonic increasing. This defines the inverse law $D_A = f^{-1}(D_B)$. Figure 5.2 illustrates an example of such a transfer function.
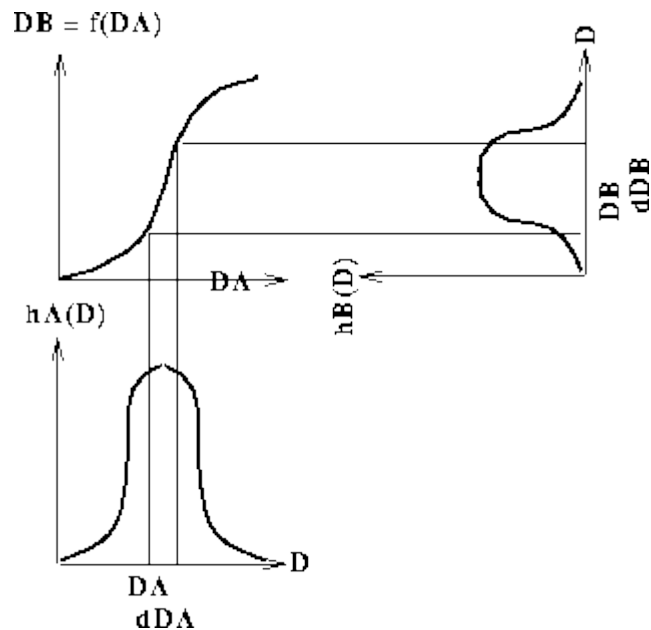
Figure 5.2: A histogram transformation function.[70]

All pixels in the input image with densities in the region D_A to $D_A + dD_A$ will have their pixel values re-assigned and the output pixels density value in range from

D_B to $D_B + dD_B$. The surface areas $h_A(D_A)dD_A$ and $h_B(D_B)dD_B$ will be equal, yielding:

$$h_B(D_B) = h_A(D_A) \div d(D_A) \tag{5.1}$$

Where

$$(\mathbf{x}) = \frac{\mathbf{df(x)}}{\mathbf{dx}} \qquad (5.2)$$

This transfers function (5.3) necessary to make the output densities equal to a fraction of the maximum number of intensity levels in the input image D_M.

$$d(D_A) = D_M * p_A(D_A) \qquad (5.3)$$

Therefore,

$$f(D_A) = D_M \int_v^{D_A} p_A(u)du = D_M * F_A(D_A) \qquad (5.4)$$

and the cumulative probability of the original image is $F_A(D_A)$.

A digital implementation of histogram equalization is usually performed by defining a transfer function of the form:

$$f(D_A) = max(0, round\left[D_M * \frac{n_k}{N^2}\right] - 1) \qquad (5.5)$$

where N is the number of image pixels and n_k is the number of pixels at intensity level k or less.

The output image will not necessarily be fully equalized and there may be unused intensity levels. These effects are likely to decrease as the number of pixels and intensity quantization levels in the input image are increased. [69][70][71].

In local histogram equalization (LHE) adopted as a pre-processing stage in the proposed approach to THR x-ray image analysis, Histogram Equalisation is used on small areas (given number of pixels) .

5.2.2 Hough transform

The Hough Transform is used in image analysis, computer vision, and digital image processing for feature extraction and shape analysis. Hough Transforms are widely used to classify objects according to their shapes. Often the first step the edge detector can be used as a pre-processing stage to detect the edges in the input image. This can be done by a simple edge detection filter such as a canny edge detector. In some cases this step is not necessary, as the algorithm can operate on the original grey level image. The classical Hough transform was concerned with the identification of lines in the images, but later the Hough transform has been extended to identifying positions of arbitrary shapes like circles and ellipse. [72][73]

The Hough transform can be described as a transformation of a point in the x,y-plane to the parameter space. The parameter space is defined according to the shape of the object of interest. In case of a linar transform for detecting straight lines, the straight line can in x,y-plane be described by: $y = ax + b$, where 'a' represents the slope and 'b' represents the intercept parameter.

The Hough transform for lines does not use the above representation of lines, since lines perpendicular to the x-axis will have a value of infinity. This will force the parameter space (a,b) to be infinite in size. Instead, a line is represented by its normal, which can be represented by an angel θ and a length r.

$$r = x\cos(\theta) + y\sin(\theta) \qquad\qquad (5.6)$$

The parameter r represents the distance between the line and the origin, while θ is the angle of the vector from the origin to this closest point see figure 5.3.
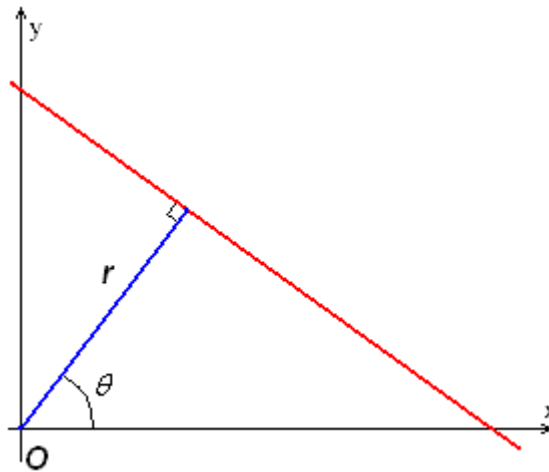
Figure 5.3: Parametric description of a straight line.[74]

In cases of detecting circular shape it is noted that a circle is much simpler to represent in parameter space. The equation of a circle is:

$$(x - a)^2 + (y - b)^2 = r^2 \qquad (5.7)$$

In the process of finding circles in an image, after finding all edges in the image, at each edge point we draw a circle with centre at the point and the desired radius. This circle is drawn in the parameter space at the coordinates which belong to the edge of the drawn circle. We increment the value in the accumulator matrix which essentially has a size equal to the number of the parameters in space. This way it sweeps over every edge point in the input image drawing circles with the desired radii and incrementing the values in the accumulator. When every edge point and every desired radius is used, we can look to the accumulator. The accumulator will now contain numbers corresponding to the number of circles passing through the individual coordinates. Thus the highest numbers correspond to the centre of the circles in the image. [72][74][75].
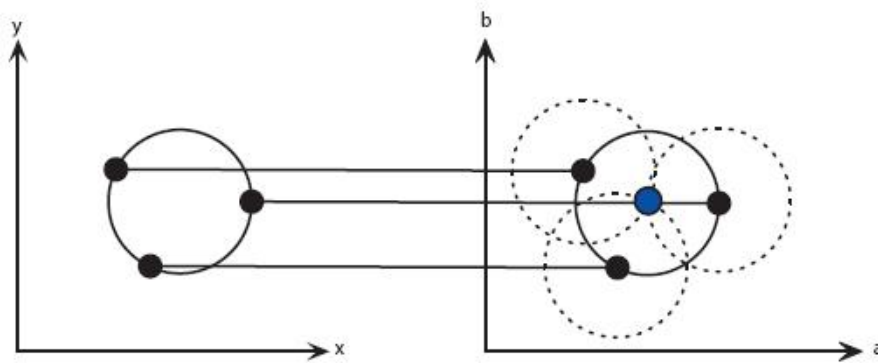
Figure 5.4: A Circular Hough transform from the x,y-space (left) to the parameter space (right) [note: this example is for a constant radius] [75]

5.2.3 Filtered Back Projection

Back Projection is an analytic reconstruction method used in image projections that has several drawbacks in obtaining a rough approximation to the original. However the improved, Filtered Back Projection algorithms [76][77][78] are an efficient (fast) and elegant alternative, which has extensively being used in reconstructing x-ray CT images and most SPECT and PET reconstructions work, until recently. The basic idea behind back projection is to simply run the projections back through the image to obtain a rough approximation to the original. [76] [77]

This equation calls for the filtered data to be back projected over the (x, y) plane. For parallel beam tomography the projections can be expressed as the Radon transform of the object that is to be reconstructed. The Radon transform is defined as:

$$g(s, \theta) = R(f) = \int_{-x}^{x} \int_{-x}^{x} f(x,y)\delta(c \cos \theta + y \sin \theta - s)dxdy. \tag{5.8}$$

the line integral along a line (a tomography beam) at an angle θ from the y-axis and at a distance $|s|$ from the origin. By rotating the coordinate system,

$$s = x \cos \theta + y \sin \theta \tag{5.9}$$

$$u = -x \sin \theta + y \cos \theta$$

or

$$x = s \cos \theta - u \sin \theta \tag{5.10}$$

$$y = -s \sin \theta + u \cos \theta$$

$g(s, \theta)$ can be expressed as

$$g(s, \theta) = \int_{-x}^{x} f(s \cos \theta - u \sin \theta, s \sin \theta + u \cos \theta) \, du \tag{5.11}$$

Filtered Back Projection is adopted in the proposed approach to determine the key point of the tearbone (see figure 5.9) in THR x-ray image analysis (see section 5.3.3).
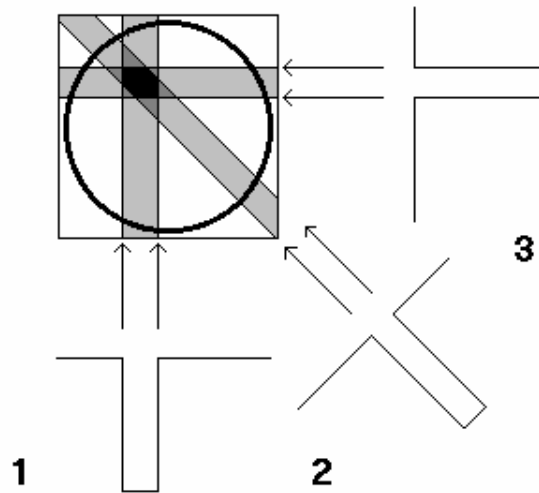
Figure 5.5: Example of back projection [78].

5.3 Proposed Method.
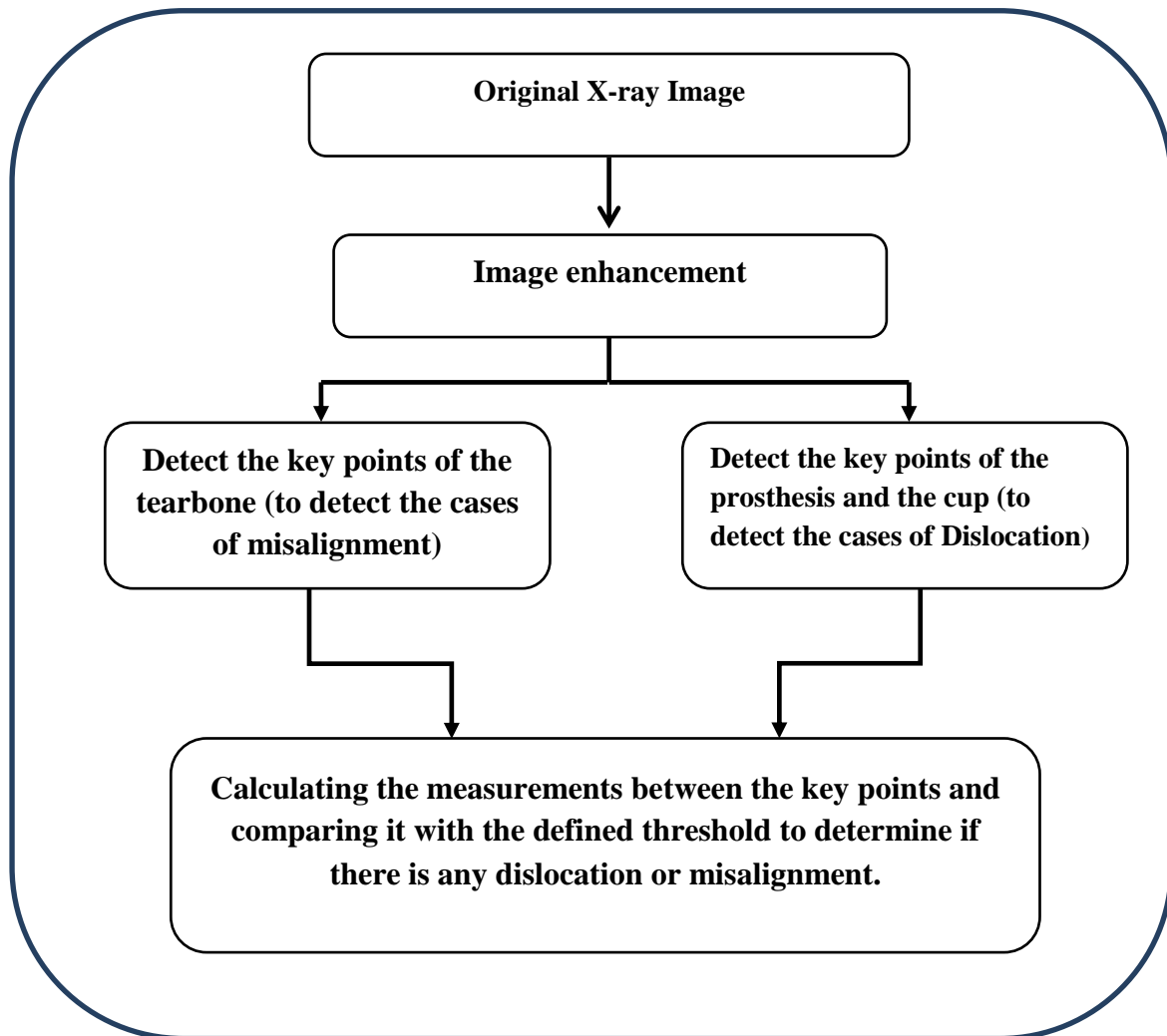
Figure 5.6: Proposed computer aided analysis approach.

Assessing total hip replacement x-ray images to determine the presence of possible imperfections such as dislocations, miss-alignments and miss-positioning, initially requires the identification of key points of interest in the human anatomy, as these points can be used as fixed reference points against which complications named above can be measured. This section proposes a computer vision based system that can be used to automatically determine the presence of above imperfections.

The proposed system comprises of a number of image processing stages as illustrated by the system block diagram of figure 5.6. Assuming that an X-ray image covering the region of interest as specified by the medical experts is available, the proposed algorithm works through a number of image processing stages to achieve the detection of possible imperfections

5.3.1 Image Enhancement.

In the image enhancement stage localised histogram equalisation [62] is used to bring back detail in any over or under exposed areas of the original x-ray image. Figure 5.7 illustrates the result of this stage.

(a)   (b)
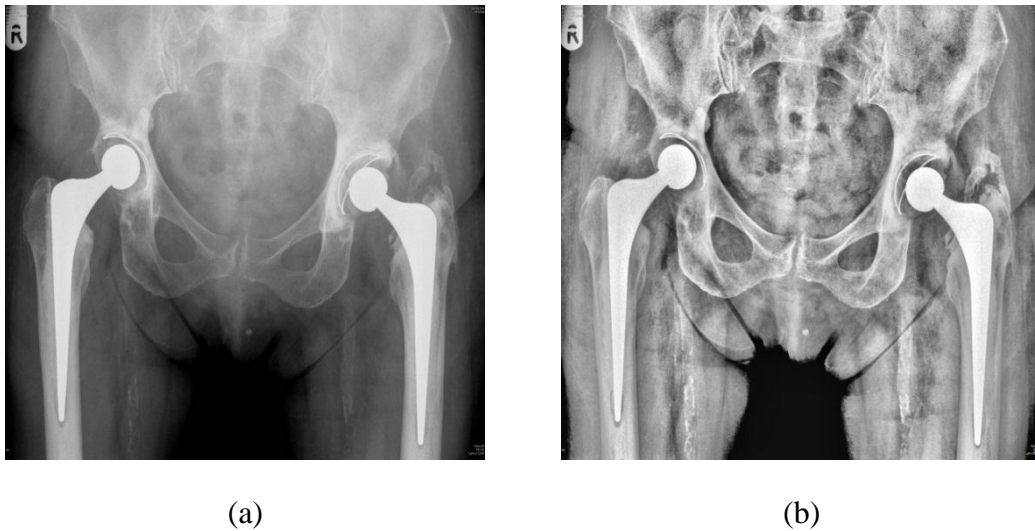
Figure 5.7: Illustrating the result of the enhancement stage (a) the original image, (b) the enhanced image.

Figure 5.7 illustrates that the enhanced images show an increased contrast and clearer edge definitions, thus increasing the chances of successful operation of the subsequent stages. In particular enhancing the edge definitions in and around the tearbone is a vital improvement that will enable the reference points on the tearbone to be located accurately for analysis of possible mis-alignment.

5.3.2 Detecting key points on the prosthesis and the cup.

The aim of this stage is to detect possible cases of dislocation of the head of the prosthesis from being within the cup, i.e. not being co-centred. To quantify dislocation we measure the distance between the centre points of the prosthesis's head (femoral head) and that of the cup (Acetabulum (Socket)). Ideally this measurement should be zero. However in practice medical experts will leave a tolerance (that defines a threshold value for our comparisons) within which the risk to the patient will be assumed to be Minimum.

First keypoint of interest is the centre point of the prosthesis's head (femoral head) and the second is the centre point of the cup (Acetabulum, i.e. the socket). In the proposed approach circular Hough Transform are used to detect these keypoints.

However before applying the Hough transform the Canny edge detection algorithm is used to detect the edges in the input image. Subsequently the algorithm searches for the presence of 2 circles (with two different radius values). Thus the proposed algorithm depends on defining a range of values for the radius of circles to be located and the number of circles being searched for. Figure 5.8 illustrates the results of applying the circular Hough Transforms.
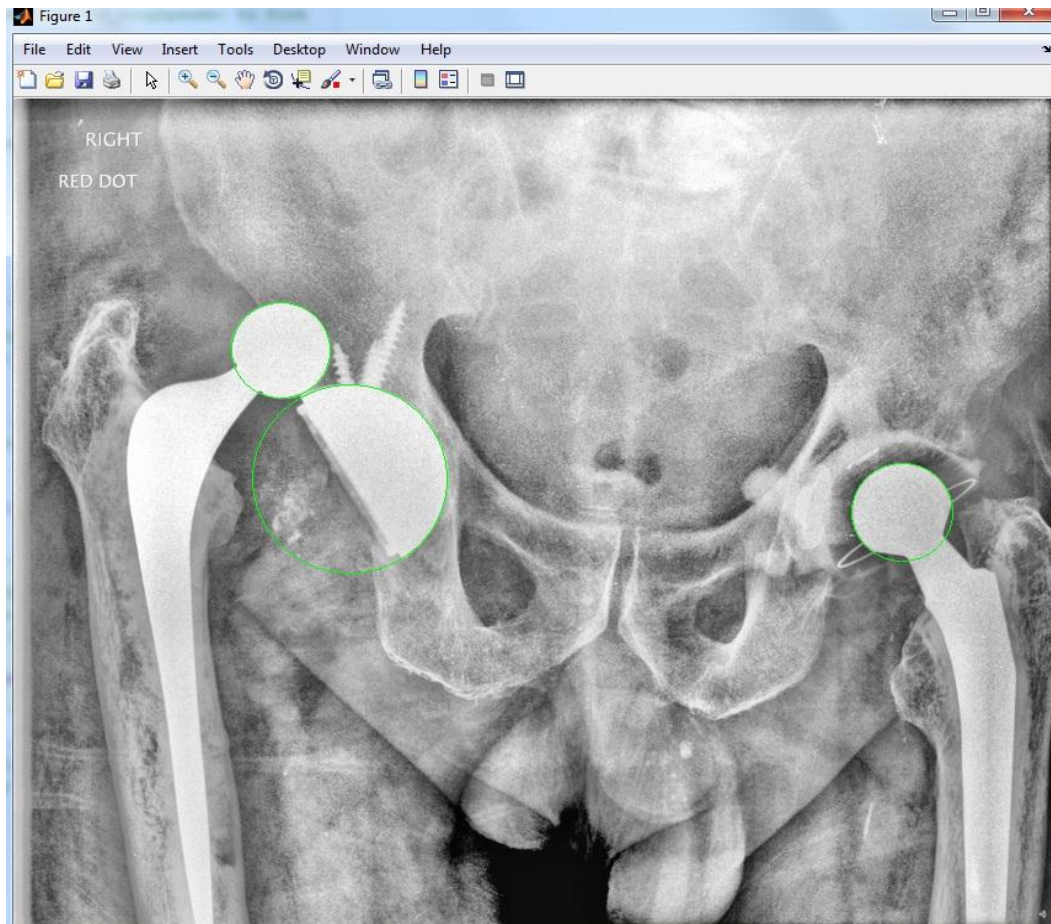
Figure5.8.The results of applying the circular Hough Transforms.

5.3.3 Defining the key points of the tearbone (to detect the misalignment cases).

In this stage we aim at detecting the cases of misalignment. This requires the calculation of the distance from centre of the prosthesis's head (femoral head) to a

straight line that passes across two reference points on the tearbone (see figure 5.1). This distance for both sides should be equal bilaterally if no misalignment has occurred.

Once the centre point of the prosthesis's head (femoral head) is known this information can be used predict the Region of Interest (ROI) in which the tearbone is located. Subsequently as illustrated by figure 5.9 the ROI can be extracted to limit the processing space in which the next stage of the approach is applied to. We adopt this approach to limit the occurrence of false positives in the subsequent stage.

Figure 5.9: The ROI that contains the tearbone.

As illustrated in figure 5.9, the tearbone area has a different texture and greylevel distribution as compared to other areas in the image. Therefore, this area can be extracted by setting a threshold range value that would work with the entire set of test images. The result is illustrated in figure 5.10.

The reference point on the tearbone area through which the reference line is drawn is obtained by calculating the curvature of points along the boundary of its shape. (See figure 5.10). The Filtered Back Projection approach (see section 5.2.3) was

used on each side of the tearbone to obtain the point at which the curvature shows a significant change on the appropriate corner of the shape.
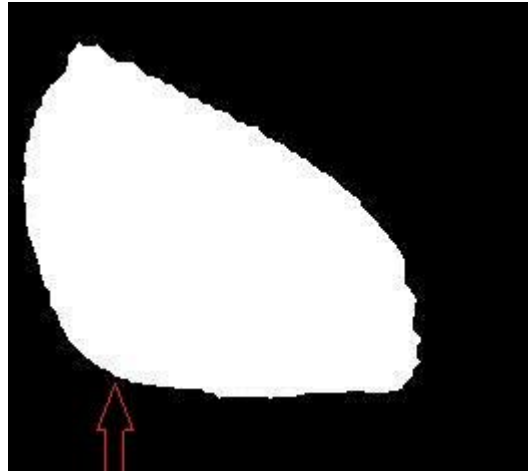
Figure 5.10: Key point of the tearbone.

In a small number of cases due to the threshold setting that was used obtaining the keypoints using the above approach was difficult. In such cases we assumed that the lowest point of the shapes selected to be the reference point (see figure 5.11).
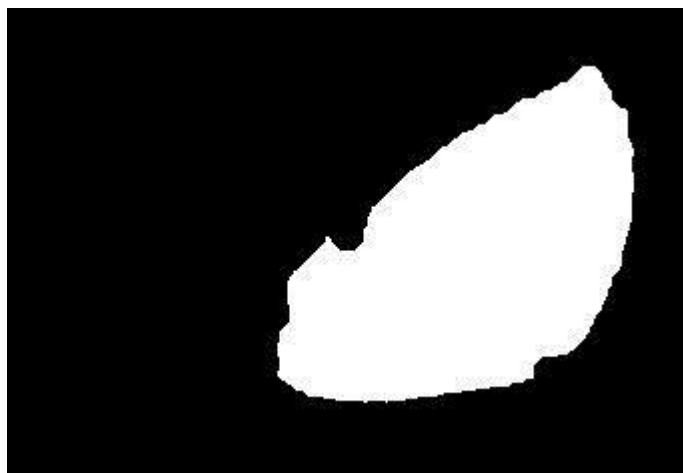
(a)
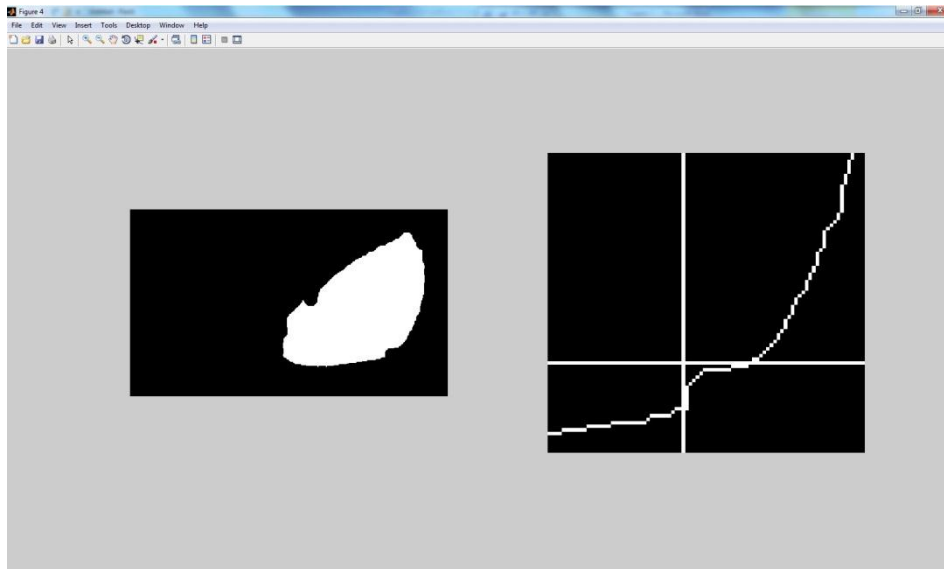
(b)

Figure 5.11: Example of a failure (a) The binary output image from the thresholding stage (b) Result of the Projections based approach showing two keypoints being picked up rather than one.

5.3.4 Determining the presence of Dislocation and/or Misalignment.

In the case of determining whether there is dislocation the distance between the centre point of the prosthesis head and the centre point of the cup is calculated and is compared with the threshold derived by the tolerance figure provided by the medical experts. (See figure 5.1 (a)). In the case of determining whether there is misalignment the difference in length between the two perpendiculars drawn from the centre point of the each prosthesis head to the straight line that connects the two key points defined on the tearbone is measured and compared with the threshold derived by the tolerance figure provided by the medical experts. (See figure 5.1(b)).

5.4 Experimental Results and analysis.

Experiments were performed on a set of images with various degrees of dislocation and misalignment. All algorithms were implemented in MATLAB. The results for four test images are illustrated in figure 5.12 and figure 5.13. The results illustrate

the capability of the proposed approach to determine the key points and detecting the cases of dislocation and misalignment in the THR X-ray images.

Dislocation Case 1

(a)
(b)
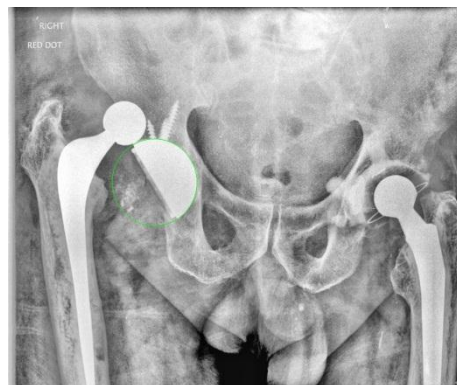
(c)
(d)
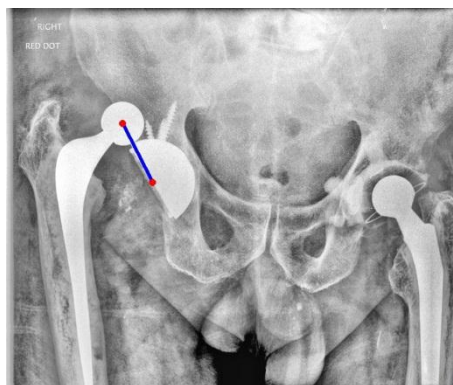
(e)

Dislocation Case 2

(a)

(b)

(c)

(d)

(e)
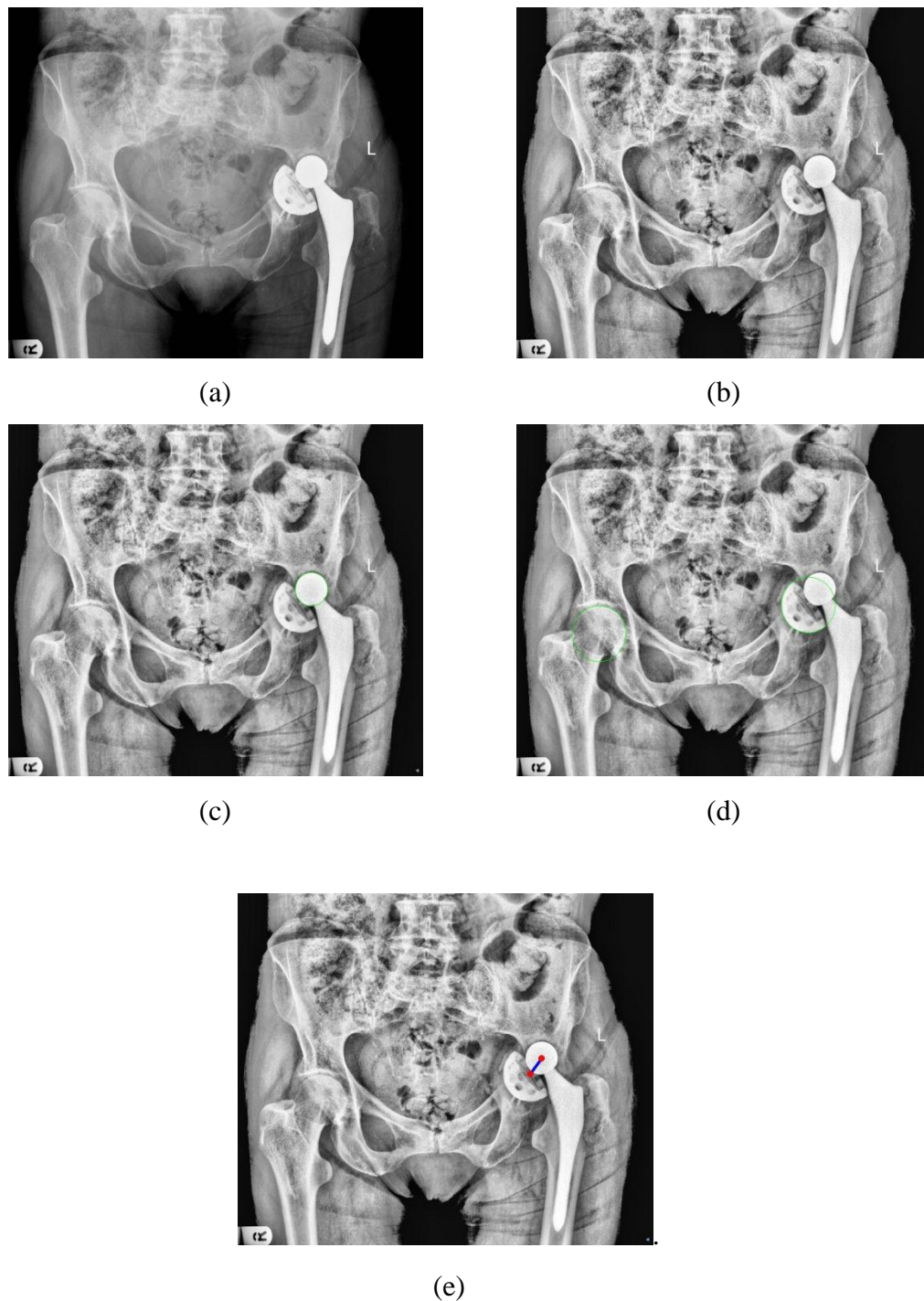
Figure5.12: Experimental Results (a) original X-ray images (b) Enhanced Image (c) Hough transform result to determine the centre point f prosthesis (d) Hough transform result to determine the centre point of the cup (e) The final result, the distance between the two centres.

Mislignment Case 1

(a)

(b)

(c)

(d)

(e)

Mislignment Case 2

(a)

(b)

(c)

(d)

(e)
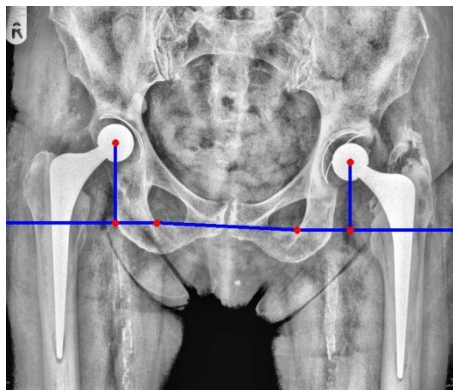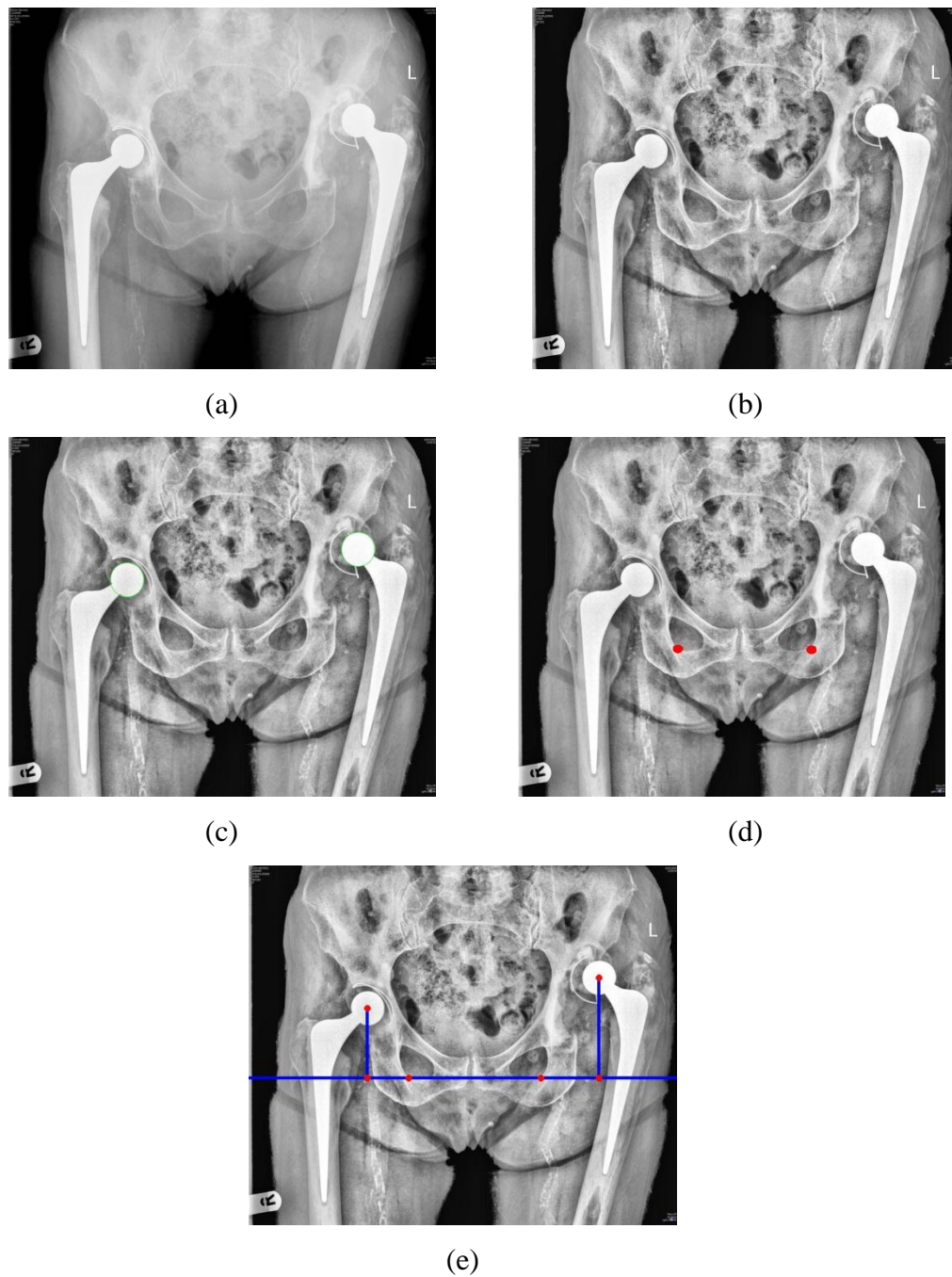
Figure5.13: Experimental Results (a) original X-ray images (b) Enhanced Image (c) Hough transform result to determine the two centre points of prosthesis head (d) Filtered Back Projection to determine the key points of the tearbone (e) The final result.

5.5 Summary and Conclusion.

We have proposed an efficient computer aided approach that can be used to automatically detect possible dislocations and misalignments in THR X-ray images. A detailed literature review carried out by us and feedback from medical specialists indicated that at present there are no such methods that are able to carry out this task fully automatically. Nevertheless such a computer aided tool can provide medical experts a valuable tool that can be used to minimise human error and to increase the level of accuracy of measurements that are normally carried out manually by such specialists by inspecting THR X-ray images.

The proposed approaches are based initially on the use of local histogram equalization to enhance the X-ray images to increase the chances or more accurately locating points and regions of interest in X-ray images which are normally low in contrast and noisy. Subsequently specific key points that are used to determine the presence of the above medical complications are located using a number of image segmentation and processing approaches. Thereafter, measurements are taken to compare the possible dislocations and misalignments and compare them with acceptable tolerances provided by the medical specialists. If the values are larger than the tolerances provided the cases are marked as positive.

Experimental results on a number of test images revealed that the proposed algorithms are capable of fully automatically detecting the presence of dislocations and misalignments. This is a contribution that originates from using computer vision and image analysis theory on supporting the medical profession resulting the possible saving of painful experiences to patients. In Chapter-6 we propose possible future improvements to this work.

CHAPTER 6

Conclusions

6.1 INTRODUCTION

This chapter summarizes the key ideas presented in chapters 3, 4 and 5, draws conclusions and emphasizes the important contributions made by the research presented in this thesis. It also gives an insight into possible future directions of research, particularly with the intention of further extending the functionality and efficiency of the proposed algorithms.

The main motivation to the research presented in this thesis originated from a number of requests that were made by medical practitioners working in the areas of Ophthalmology and treatment of complications that arise from THR surgery. This lead to a detailed review of literature that concluded that the application of computer vision algorithms in designing and developing medical imaging tools to aid the above areas are still in their infancy. Therefore the research presented in this thesis focused on providing effective and efficient solutions to some of the open research problems/challenges in the above medical areas namely, quantification of corneal neovascularization, measurement and monitoring the treatment process of corneal ulcers and detecting faults on total hip replacement x-ray images (i.e. dislocations and misalignments). In particular one key design issue of the proposed systems was providing solutions that can deal with a number of discrepancies normally present on medical images, such as noise, non-uniform illumination and reflections.

Chapters 3-5 presented the novel solutions and focused on the three key contributions of this thesis. Each chapter presented the research motivation, existing

solutions, research motivation, methodology adopted by the novel system, experimental results and a detailed analysis of the results when tested on real, medical images obtained via collaborations established with medical professionals. These chapters lead to the following conclusions.

6.2 CONCLUSION OF THE THESIS

The first contribution presented in Chapter 3, focused on using Contourlet Transforms for the quantification of corneal neovascularization. This approach has been previously successfully used in retinal blood vessels quantification. However investigations carried out within the research context of this thesis indicated that corneal images are significantly different and of a significantly lower quality when compared to retinal images, which are captured under more controlled environments, using high resolution, and high dynamic range cameras. Therefore modifications were required at pre-processing, post-processing stages and in the application stage of Contourlet Transforms to meet these challenges. Especially the presence of noise, non-uniform illumination and reflections that make the quantification process more difficult, was successfully addressed. The motivation behind the use of Contourlet Transforms was the capability to enhance the blood vessels before their segmentation is carried out as Contourlet Transforms provide multi-scale and multi-directional contour like features of images that can be utilised to this effect. Investigations revealed that the results obtained when Contourlet Transforms was applied to enhance the images before segmenting the blood vessels were more accurate than segmenting the blood vessels without applying the Contourlet transform. Experimental results on a number of real cases were presented to evaluate the effectiveness of the proposed tool in particular for monitoring the progress of treatment processes for corneal neovascularization, conducted over a period of time. The results were evaluated and compared with the opinion of collaborating medical experts who confirmed the validity of results.

Chapter 4 presented a medical imaging and analysis tool that can be effectively used

in monitoring the treatment process of corneal ulcers by segmenting and quantifying the variation of the size of ulcers over a period of time. A colour based approach was used to initially segment the ulcer area, due to the luminance liquid used in the process of medical diagnosis. However due to the practical nature of the image capture systems used to capture images of corneal ulcers and the surface reflectance of cornea itself, a number of additional complications had to be addressed, namely reflections, non-uniform illumination, image noise, under and over exposed areas etc. The proposed colour based segmentation algorithm that was developed in the HVS colour space had to be made robust to cater for all these needs. Experiments were performed on a number of real test images provided by medical experts. The results demonstrated the proposed tools ability to cater for all practical complications and to provide a useful tool for the segmentation and measurement (and hence monitoring) of corneal ulcers.

Finally Chapter 5 presented a novel algorithm to detect the dislocations and misalignments that can originate in total hip replacements. The detection of dislocations and misalignments required the determination of fixed reference points in the normal bone structure and certain identifiable key points on the steal and plastic components used in THR. The determination of these key points and reference points were based on the use of Hough Transforms and Projection based techniques. By comparing the distances between the keypoints with those figures specified by the medical experts, within valid tolerances, the proposed algorithms were able to conclude the presence of dislocations and misalignments. Experiments were conducted on a set of real THR images obtained from patients with a known prognosis. It was concluded that the proposed techniques were able to determine all cases of misalignments and dislocations, successfully.

6.3 FUTURE WORK

Although a number of novel contributions to the state-of-the-art in corneal neovascularization, corneal ulcers and total hip replacement areas have been

proposed in this thesis it is possible to extend the work to further improve recognition rates and functionality of the algorithms.

All implementations of the proposed algorithms have been carried out using MATLAB. One desirable task is to implement the proposed systems in languages such as C or C++ that will increase speed of quantifying, segmenting and detecting up to real-time rates. The conversion of the MATLAB implementation to C/C++ has the ability to increase the speed and to use them within systems supported by a wide range of software platforms and hardware systems.

In chapter 3 and 4, the algorithm proposed to segment the corneal area is semi-automatic as this approach is more accurate and is trusted by medical experts as compared to using an automated approach. It is suggested that further research be carried out in identifying an automatic approach to segment the corneal area that is robust against presence of image noise, making the proposed approach fully automatic. This will require the design of an efficient and robust approach to the determination of thresholding values used in the final stage of segmentation process.

The research in chapters 3 and 4 has resulted in the design and production of a hardware unit supported by software that implements the proposed computer vision algorithms. This unit is to enter clinical trials and will be tested for the analysis of corneal ulcers and quantification of corneal neovascularization. This device consists of an optical imaging pipeline that includes lenses, special filters and lighting that minimises reflections from the surface of the cornea. This hardware based approach to solving one of the challenges in corneal ulcers will result in an improved accuracy of segmentation when the proposed algorithms are utilised in practice.

References

[1]AJ. Huang, BD. Watson, E. Hernandez, SC. Tseng, Photothrombosis of corneal neovascularization by intravenous rose bengal and argon laser irradiation, *Arch Ophthalmol*,106:680-685, [PMID:2451909],1988.

[2]R. J. Epstein, R.L. Hendricks, D.M. Harris, Photodynamic therapy for corneal neovascularization, *Cornea*, 10:424-432, [PMID: 1834434], 1991.

[3]G. B. Primbs, R. Casey, K. Wamser, W.J. Snyder, D.H. Crean, Photodynamic therapy for corneal neovascularization, Ophthalmic Surg Lasers,29:832-838, [PMID:9793949] , 1998.

[4]K. Yoon, I. You, I. Kang, S. Im, J. Ahn, Y. Park, K. Y. Ahn, Photodynamic Therapy with Verteporfin for Corneal Neovascularization, *American Journal of Ophthalmology* ,144 (3), pp. 390–395,2007.

[5]I. Bahar, I. Kaiserman, P. McAllum, D. Rootman, , A. Slomovic, Subconjunctival Bevacizumab Injection for Corneal Neovascularization, *Lippincott Williams & Wilkins, Cornea* , Vol. 27, No 2, Feb 2008.

[6]O. M. Kirat, H. A. Al-Dhibi, Regression of aggressive corneal vascularization after photodynamic therapy, subconjunctival Avastin injections and topical cyclosporin-A 1% drops: A case report, Saudi Journal of Ophthalmology , 24, pp.151–154, 2010.

[7]M. Fossarello, E. Peiretti, I. Zucca, A. Serra, Photodynamic Therapy of Corneal Neovascularization with Verteporfin, *Cornea*, 22(5):485-488, Jul 2003.

[8]G. Corrent, T.J Roussel, S.C Tseng, B.D Watson, Promotion of graft survival by photothrombotic occlusion of corneal neovascularization, *Arch Ophthalmol*, 107:1501-1506, 1989.

[9]P. Feng , Y. Pan , B. Wei , W. Jin , D. Mi, Enhancing retinal image by the Contourlet transform, Pattern Recognition Letters, 28, 516–522, 2007.

[10]Q. Li, J. You, L .Zhang, P. Bhattacharya, Automated Retinal Vessel Segmentation Using Multiscale Analysis and Adaptive Thresholding, *IEEE Image Analysis and Interpretation,* pp.139-143, 2006.

[11]L. Espona, M. Carreira, M. Penedo, M. Ortega, Retinal Vessel Tree Segmentation using a Deformable Contour Model, *IEEE Pattern Recognition 19th International Conference*, pp. 1-4, Dec. 2008.

[12]B. S. Y. Lam and H. Yan, A Novel Vessel Segmentation Algorithm for Pathological Retina Images Based on the Divergence of Vector Fields, *IEEE Transaction on Medical Imaging*, Vol. 27, No. 2, Feb.2008.

[13]S. Chaudhuri, S. Chatterjee, N. Katz, M. Nelson, M. Goldbaum, Detection of

blood vessels in retinal images using two-dimensional matched filters*, IEEE Transactions on Medical Imaging*, 8 (3), pp. 263-269, Sept. 1989.

[14]C. Cursiefen, F. Bock, F. K. Horn, F. E. Kruse, B. Seitz, V. Borderie, B. Früh, M. A. Thiel, F. Wilhelm, B. Geudelin, I. Descohand, K. Steuhl, A. Hahn, D. Meller, GS-101 Antisense Oligonucleotide Eye Drops Inhibit Corneal Neovascularization, *American Academy of Ophthalmology*, Vol.116, No.9, 2009.

[15]F. Bock, J. Onderka, D. Hos, F. Horn, P. Martus, C. Cursiefen, Improved semiautomatic method for morphometry of angiogenesis and lymphangiogenesis in corneal flatmounts*, Experimental Eye Research*, Vol. 87, No. 5,pp.462–470, Nov. 2008.

[16]A. D. Proia, D. B. Chandler, W. L. Haynes, Quantitation of corneal neovascularization using computerized image analysis, *a Journal of Technical Methods and Pathology*, 58(4):473-479, 1988.

[17]D. R. Anijeet, Y. Zheng, A. Tey, M. Hodson, H. Sueke, S. B. Kaye , Imaging and Evaluation of Corneal Vascularization Using Fluorescein and Indocyanine Green Angiography, Investigative Ophthalmology & Visual Science, Vol.53, No.2, Feb. 2012.

[18]S. Amano, R. Rohan, M. Kuroki, M. Tolentino , A. P. Adamis , Requirement for Vascular Endothelial Growth Factor in Wound- and Inflammation-Related Corneal Neovascularization, Investigative Ophthalmology & Visual Science, Vol.39, No.1, Jan. 1998.

[19]M. P. Holzer, K. D. Solomon, D. T. Vroman, H. P. Sandoval, P. Margaron , T. J. Kasper , C. E. Crosson , Photodynamic Therapy with Verteporfin in a Rabbit Model of Corneal Neovascularization, Investigative Ophthalmology & Visual Science, Vol.44, No.7, Jul 2003.

[20]NIH Image tool, [Internet] available from *<http://rsb.info.nih.gov/nih-image/about.html>* [Accessed: Jul. 28, 2012].

[21]S. E. Umbaugh, R. H. Moss, W. V. Stoecker, Automatic Color Segmentation of Images with Application to Detection of Variegated Coloring in Skin Tumors, *IEEE ENGINEERING IN MEDICINE AND BIOLOGY MAGAZINE*, Dec. 1989.

[22]G. L. Hansen, E. M. Sparrow, J. Y. Kokate, K. J. Leland, P. A. Iaizzo, Wound Status Evaluation Using Color Image Processing, *IEEE TRANSACTIONS ON MEDICAL IMAGING*, Vol.16, No.1, Feb. 1997.

[23]M. Galushka, H. Zheng, D. Patterson, L. Bradley, Case-Based Tissue Classification for Monitoring Leg Ulcer Healing, *18th IEEE Symposium on Computer-Based Medical Systems (CBMS'05),* 2005.

[24]D. H. Chung, G. Sapiro, Segmenting Skin Lesions with Partial-Differential-Equations-Based Image Processing Algorithms, IEEE TRANSACTIONS ON MEDICAL IMAGING, Vol.19, No.7, Jul. 2000.

[25]H. Oduncu, A. Hoppe, M. Clark, R. J. Williams , K. G. Harding, Analysis of Skin Wound Images Using Digital Color Image Processing: A Preliminary Communication, *International Journal of Lower Extremity Wounds,* 3:151, 2004.

[26]M. Kolesnik, A. Fexa, Segmentation of Wounds in the Combined Color Texture Feature Space, *Medical Imaging, Image Processing, Proceedings of SPIE*, Vol.5370, 2004.

[27]B. Acha, C. Serrano, J. I. Acha, Segmentation and classification of burn images by color and texture information, *Journal of Biomedical Optics*, 10(3), May. 2005.

[28]A. E. Yahya and M. J. Nordin, Accurate Iris Segmentation Method for Non-Cooperative Iris Recognition System, *Journal of Computer Science*, 6 (5): 527-532, 2010.

[29]Chan-Vese Algorithm, [internet] Available from < http://math.arizona.edu/~rcrandall/ECE532_ProjectPaper.pdf > [Accessed: Aug. 9 2012].

[30]M. M. Oliveira, B. Bowen, R, McKenna, Y. Chang, Fast Digital Image Inpainting, *International Conference on Visualization, Imaging and Image Processing (VIIP),* Sep. 2001.

[31]M. Bertalmio, G. Sapiro, V. Caselles , C. Ballester, Image Inpainting, [internet] Available from *<http://www.tecgraf.puc-rio.br/~scuri/inf1378/pub/bertalmi.pdf>* [Accessed: Aug. 9 2012].

[32]Z. He, T. Tan, Z. Sun, Topology modeling for Adaboost-cascade based object detection, *Pattern Recognition Letters*, Jan. 2010.

[33]P. Viola, M. Jones, Rapid Object Detection using a Boosted Cascade of Simple Features, *Conference on Computer Vision and Pattern Recognition,* 2001.

[34]G. Annapoorani, R. Krishnamoorthi, P. G. Jeya, S. Petchiammal, Accurate and Fast Iris Segmentation, International Journal of Engineering Science and Technology, Vol. 2(6), 1492-1499, 2010.

[35]A. Zaim, Automatic Segmentation of Iris Images for the Purpose of Identification, *IEEE International Conference Image Processing* , vol.3, pp.11-14, Sept. 2005 .

[36]P. Yao, J. Li, X. Ye, Z. Zhuang , B. Li , Iris Recognition Algorithm Using Modified Log-Gabor Filters, *The 18th International Conference on Pattern Recognition (ICPR'06)* ,Vol.4,pp. 461–464, 2006.

[37]Log-Gabor filter , [Internet], available from ,*<http://www.csse.uwa.edu.au/~pk/research/matlabfns/PhaseCongruency/Docs/convexpl.html>* [Accessed: Jul.29, 2012]

[38]A. Oprea, C. Vertan:A Quantitative Evaluation of the Hip Prosthesis Segmentation Quality in X-ray Image, *International Symposium in Signals, Circuits and Systems, ISSCS*, vol.1,pp.1-4, Jul. 2007.

[39]L. Florea and C. Vertan, AUTOMATIC HIP PROSTHESIS FIT ESTIMATION BY COOPERATIVE X-RAY IMAGE SEGMENTATION, *U.P.B. Sci. Bull., Series C*, Vol.71, No.4, 2009.

[40]M. Komeno, M. Hasegawa, A.Sudo, A. Uchida, Computed Tomographic Evaluation of Component Position on Dislocation After Total Hip Arthroplasty, *Healio Orthopedics*, Vol.29, No.12, Dec. 2006.

[41]T. M. Barker, W. J. Donnelly, Automated image analysis technique for measurement of femoral component subsidence in total hip joint replacement, *Medical Engineering & Physics*,Vol.25, No.2,pp.91–97, Mar 2003.

[42]R. Smith and K. Najarian, Automated Segmentation of Pelvic Bone Structure in X-Ray Radiographs Using Active Shape Models and Directed Hough Transform, Bioinformatics and Biomeidcine Workshops, IEEE International Conference, pp.56-63 , Nov. 2008.

[43]M. N. Do and M. Vetterli, The Contourlet Transform: An Efficient Directional Multi-resolution Image Representation, *IEEE Transactions Image on Processing*, 14(12), pp.2091-2106, Dec. 2005.

[44]P. J. Burt, E. H. Adelson, The Laplacian pyramid as a compact image code, *IEEE Trans on Communications*, vol.31, no.4, pp.532–540, Apr. 1983.

[45]R. H. Bamberger, M. J. T. Smith, A filter bank for the directional decomposition of images: Theory and design, *IEEE Transactions on Signal Processing*, vol.40, no.4, pp.882-893, Apr. 1992.

[46]M. Vetterli, Multidimensional Subband Coding: Some Theory and Algorithms, *Signal Process*, 6(2), pp.97–112, Feb. 1984.

[47]Y. Wiseman, E. Fredj, contour Extraction of Compressed JPEG Images, *Journal of Graphic Tools*, Vol.6 (3), pp.37-43, 2001.

[48]Z. Zhao, J. Yuan, Q. Gao, Y. Kong, Wavelet Image De-noising Method Based on Noise Standard Deviation Estimation, *International Conference on Wavelet Analysis and Pattern Recognition*,Vol.4**, pp.**1910-1914, 2007.

[49]J. Immerker, Fast Noise Variance Estimation, *Computer Vision and Image Understanding*, Vol.64, No.2, 1996.

[50]Unsharp filtering, [Internet] available from *<http://www.scribd.com/itssiraj/d/26538465-An-Introduction-to-Digital-Image-Processing-With-Matlab>,* [Accessed: Jun.13, 2012].

[51]Unsharp filtering, [Internet] available from *<http://www.mathworks.co.uk/help /toolbox/images/ref/fspecial.html>,* [Accessed: Jun 13, 2012].

[52]L. Lam, S. Lee, C. Y. Suen, Thinning Methodologies-A Comprehensive Survey, *IEEE Transactions on Pattern Analysis and Machine Intelligence*, Vol.14, No.9, Sep. 1992.

[53]T. Y. Zhang, C. Y. Suen, A fast parallel algorithm for thinning digital patterns, *Communications of the ACM*, vol.27, no.3, pp. 236-239, 1984.

[54]Z.Guo, R.W.Hall, parallel thinning with two-subiteration algorithms, *Communications of the ACM*, Vol.32, no.3, pp.359-373, 1989.

[55]A.Deshpande., "Corneal Ulcer" 28 July 2010 http://www.buzzle.com/articles/corneal-ulcer.html (10 march 2012).

[56]P. Garg, G. N. Rao. , "Corneal Ulcer:Diagnosis and Management," Journal of Community Eye Health International Centre for Eye Health, London. Papers 12(30), 21–23 (1999).

[57]A. Koschan, M. A. Abidi, *Digital Color Image Processing*, ISBN 978-0-470-14708-5.

[58]RGB Colour Space, [Internet] Available from *<http://prosjekt.ffi.no/unik-4660/lectures04/chapters/Introduction.html>* [Accessed: Jul. 05 2012].

[59]D. Travis, *Effective Color Displays Theory and Practice. Academic Press*, ISBN 0-12-697690-2, 1991.

[60]HSI / HSV Colour gamut, [Internet] Available from *<http://www.mathworks.com/access/helpdesk/help/toolbox/images/hsvcone.gif>* [Accessed: Jul. 05, 2012].

[61]M. Tkalcic, J. Tasic, Colour spaces - perceptual, historical and applicational background, *In The IEEE Region 8 EUROCON 2003 proceedings* ,pp.304-308, 2003.

[62]C. Tsai, A Fast Dynamic Range Compression with Local Contrast Preservation Algorithm and its Application to Real-Time Video Enhancement, *Multimedia, IEEE Transactions*, Vol.14, No.44.

[63]U. Zakir, A. N. J. Leonce , E. A. Edirisinghe, Road sign segmentation based on colour spaces: A Comparative Study, *the 11th Iasted International Conference on Computer Graphics and Imgaing*, 679, 567-583, 2010.

[64]M. Tkalcic, J. F. Tasic, Colour Spaces – perceptual, historical and applicational background, *Eurocon Computer as a Tool*, Vol.1, pp.304-308, Sept. 2003.

[65]A.Ford, A. Roberts, Colour Space Conversions, Aug. 1998.

[66]N. Koren, HSL/HSV Colour gamut, [Internet] Available from *<http://www.normankoren.com/light_color.html> [Accessed :March. 09*, 2012].

[67]Total hip replacement [Internet] available from *<http://orthoinfo.aaos.org/topic.cfm?topic=a00377>* [Accessed: October 13, 2012].

[68]Total hip arthroplasty [Internet] available from *<http://www.radiologyassistant.nl/en/p431c8258e7ac3/hip-total-hip arthroplasty.html>* [Accessed: October 13, 2012].

[69]Histogram equalization [Internet] available from < *http://en.wikipedia.org/wiki/Histogram_equalization>* [Accessed: October 15, 2012].

[70]Local Histogram equalization [Internet] available from < *http://homepages.inf.ed.ac.uk/rbf/HIPR2/histeq.htm>* [Accessed: October 15, 2012].

[71]Local Histogram equalization [Internet] available from < *http://fourier.eng.hmc.edu/e161/lectures/HistogramEqualization.pdf.>* [Accessed: October 15, 2012].

[72]Hough Transform [Internet] Available from *<http://homepages.inf.ed.ac.uk/rbf/HIPR2/hough.htm>* [Accessed: September 28, 2012]

[73]M. Wohlfart, Hough transform applications in Computer Graphics (with focus on medical visualization), 2003.

[74]Hough Transform [Internet] Available from
<*http://en.wikipedia.org/wiki/Hough_transform*> [Accessed: September 28, 2012]

[75]S. J. K. Pedersen, Circular Hough Transform, *Vision, Graphics, and Interactive Systems,* Nov 2007.

[76]G.L. Zeng, Image reconstruction Ð a *tutorial,Computerized Medical Imaging and Graphics,* 25, 97-103, 2001.

[77]Filtered Back Projection [Internet] available from <
http://www.owlnet.rice.edu/~elec539/Projects97/cult/node2.html> [Accessed: October 16, 2012].

[78]M. C. Villa Uriol, Reconstruction from Projections, *Computational Imaging Lab lecture.*

[79]N. A. Otoum and E. A. Edirisinghe, A Computer Vision Approach to Quantification of Corneal Neovascularization ,*Proceeding of the IASTED International Symposia,(737) Imaging and Signal Processing in Healthcare and Technology – 2011, Washington*, 10.2316/P.2011.737-048

[80]N. A. Otoum, E .A. Edirisinghe, Quantification of Corneal Neovascularization via Contourlet Transform based Segmentation of Blood Vessels, *the International Conference on Information and Communication Systems (ICICS 2011), Irbid, Jordan*, Paper 13, pages 28-33,ISBN: 978-1-4507-8208-1-90000.

[81]N. A. Otoum, E. A. Edirisinghe, H. Dua and L. Faraj, Evaluating the effectiveness of treatment of corneal ulcers via computer-based automatic image analysis, *Optics, Photonics, and Digital Technologies for Multimedia Applications II, SPIE* , 8436, 84360D (2012).

[82]N. A. Otoum, E. A. Edirisinghe, Quantification of Corneal Neovascularization via Contourlet Transform based Segmentation of Blood Vessels. *Ubiquitous Computing and Communication Journal*, vol.7, no.5, pp.1297-1308, ISSN 1992-8424

APPENDIX-A

Scholarly Contributions

The work presented in this thesis has resulted in a number of paper submissions/acceptances. The details are as follows.

REFEREED CONFERENCE PUBLICATIONS

A1-N. A. Otoum and E. A. Edirisinghe, A Computer Vision Approach to Quantification of Corneal Neovascularization ,Proceeding of the IASTED International Symposia,(737) Imaging and Signal Processing in Healthcare and Technology – 2011, Washington, 10.2316/P.2011.737-048

A2-N. A. Otoum, E. A. Edirisinghe, Quantification of Corneal Neovascularization via Contourlet Transform based Segmentation of Blood Vessels, In Proceedings of the International Conference on Information and Communication Systems (ICICS 2011), Irbid, Jordan, Paper 13, pages 28-33,ISBN: 978-1-4507-8208-1-90000.

A3-N. A. Otoum, E. A. Edirisinghe, H. Dua and L. Faraj, Evaluating the effectiveness of treatment of corneal ulcers via computer-based automatic image analysis, Optics, Photonics, and Digital Technologies for Multimedia Applications II, SPIE, 8436, 84360D (2012).

A4-N. A. Otoum, E. A. Edirisinghe, Quantification of Corneal Neovascularization via Contourlet Transform based Segmentation of Blood Vessels. Ubiquitous Computing and Communication Journal, vol.7, no.5, pp.1297-1308, ISSN 1992-8424

CONFERENCE PAPERS TO BE SUBMITTED

A5-N. A. Otoum, E. A. Edirisinghe, an efficient computer aided approach to automatically detect possible dislocations and misalignments in THR X-ray images, to the 9th International Conference on Computer Vision Systems (ICVS) 2013.

JOURNAL PAPERS TO BE SUBMITTED

A6-N. A. Otoum, E. A. Edirisinghe, an efficient computer aided approach to automatically detect possible dislocations and misalignments in THR X-ray images, to SPIE Medical Imaging Journal